

Electronic Supplementary Information (ESI)

Towards catalytic redox-active Iridium polypyridyl complex by *in situ* photosubstitution

Yi Zhen Tan, Xiangyang Wu^a, Yunpeng Lu, Shunsuke Chiba and Edwin K. L. Yeow*

School of Chemistry, Chemical Engineering and Biotechnology, Nanyang Technological
University, 21 Nanyang Link, 636371, Singapore

E-mail: edwinyeow@ntu.edu.sg

Table of Content:

S1. Experimental Section:	Page
Materials	S3
<i>In situ</i> formation of modified iridium complexes	S3
Irradiation of 1	S4
Anion-exchange	S5
Preparation of <i>N</i> -Boc-Pro-OCs	S5
X-ray crystallography	S5
Steady-state spectroscopy	S7
Time-resolved spectroscopy	S8
Cyclic Voltammetry	S9
Hydrodehalogenation of aryl halides with 1 and 3	S9
Hydrodehalogenation of aryl halides with Ir-mod ($t_{\text{irra}} = 8$ h)	S10
Photochemical reaction quantum yield determination	S10
Light-On/Off experiment	S11
GC-FID analysis	S12
NMR spectroscopy	S12
Ir-mod/Ni dual-catalyzed decarboxylative cross-coupling of 2 and 4-bromobenzotrifluoride	S14
Computational studies	S15
Supplementary References	S15
S2. Supplementary Figures	
Fig. S1 - S24	S17-S30
GC Figures (Fig. S25 - S58)	S31-S47
NMR Figures (Fig. S59 - S87)	S47-S62
S3. Supplementary Tables	S63

S1. EXPERIMENTAL SECTION

Materials. $[\text{Ir}(\text{df}(\text{CF}_3)\text{ppy})_2(\text{bpy})]\text{PF}_6$ (**1**) was purchased from Sigma-Aldrich (MQ100) and ChemScene (> 95.0 %). Both HPLC and spectroscopic grade dimethylformamide (DMF) were purchased from TCI and TEDIA. 4-Bromobenzotrifluoride (99%), 4'-bromoacetophenone (98%), 4-bromoanisole (> 99.9%), 4-bromotoluene (98%), 4-bromobiphenyl (98%), 2-chlorobenzotrifluoride (99%), 4-chlorobenzonitrile (99%), α,α,α -trifluorotoluene (> 99%), 4-fluorotoluene (97%), acetophenone (> 98%), anisole (99%), toluene (ACS reagent, > 99.5%), biphenyl (> 99%), benzonitrile (99%), *N*-(*tert*-butoxycarbonyl)-proline (*N*-Boc proline) (> 99.0%), cesium carbonate (Cs_2CO_3) (99.9% trace metals basis) and 1,1,3,3-tetramethylguanidine (TMG) (99%) were purchased from Sigma-Aldrich. Ammonium acetate (97%) was purchased from Alfa Aesar. Ethanol (99.8%, analytical reagent grade) was purchased from Fisher Scientific. 1,8-Diazabicyclo[5.4.0]undec-7-ene (98+ %, DBU) was purchased from Alfa Aesar.

***In situ* formation of modified iridium complexes.** *N*-Boc proline (0.03 M), Cs_2CO_3 (0.03 M) and **1** (0.2 mM) were added into a 25 mL Schlenk tube containing DMF (10 mL). The reaction mixture was sealed with a PTFE stopcock and degassed by bubbling Ar for 30 min. The mixture was then irradiated with a 456-nm LED lamp (40 W, Kessil) placed ~3.5 cm away from the center of the tube for an irradiation time t_{irra} between 0.5 to 12 h. The reaction temperature was maintained at 30 °C using a standing fan. After light exposure, the mass spectrum of the solution was recorded using a mass spectrometer (Thermo Finnigan LCQ Fleet).

Ir complex **2** was purified with a C18 semi-preparative column fitted to a reversed-phase high performance liquid chromatography (HPLC)-photodiode array system (Waters). Briefly, a 30-min blue light irradiated mixture ($t_{\text{irra}} = 30$ min) was concentrated and injected into the HPLC.

The mobile phases used were acetonitrile and 10 mM ammonium acetate in Milli-Q water. A gradient system, shown in the table below, was used to separate the modified iridium complexes:

Time (min)	10 mM Ammonium acetate (%)	Acetonitrile (%)
0	15	85
70	20	80
120	15	85

To purify **Ir-mod**, the mixture after blue light irradiation for a prolonged time ($t_{\text{irra}} = 2, 4, 6, 8, 12$ and 14 h) was added to an equivalent volume of 0.01 mM of ammonium hexafluorophosphate. The mixture is left to stand for 15 min before it is transferred into a 1.5 mL centrifuge tube and centrifuged at 13000 rpm for 10 min. The supernatant is removed and the solid is dissolved in ethyl acetate. Purification of the complexes was achieved by flash column chromatography using hexane/ethyl acetate (2:1) as eluents on a silica gel column. The fractions were concentrated *via* rotary evaporation and subjected to the anion exchange procedure.

Irradiation of 1. MS experiment: **1** (0.2 mM) was added into a 25 mL Schlenk tube containing DMF (10 mL). The mixture was sealed with a PTFE stopcock and degassed by bubbling Ar for 30 min. The mixture was then irradiated with a 456 -nm LED lamp (40 W, Kessil) placed ~ 3.5 cm away from the center of the tube for an irradiation time t_{irra} of 6 h. The reaction temperature was maintained at 30 °C using a standing fan. After light exposure, the mass spectrum of the solution was recorded using a mass spectrometer (Thermo Finnigan LCQ Fleet).

Emission experiment: A 1.0 Schlenk arm quartz fluorescence cuvette was used, and **1** (30 μM) was prepared in DMF. The solution was degassed by bubbling Ar into the solution for 30 min. The solution was irradiated with a 456-nm LED lamp (40 W, Kessil) placed 3.5 cm away from the center of the cuvette and irradiated from 0 - 90 min. Emission spectra in DMF were measured on a fluorescence spectrometer (Varian Cary Eclipse). The emission spectrum was recorded using an excitation wavelength $\lambda_{\text{ex}} = 340$ nm.

Anion-exchange. Ammonium hexafluorophosphate (15 mg, 1 mM) was first added into Milli-Q water (10 mL), and the solution added into a DMF solution of the iridium complex (0.01 mM). The mixture was then left to sit for 15 min before centrifugation at 13000 rpm for 10 min. The supernatant was removed and the solid sediment washed with Milli-Q water (3×1 mL), centrifuged and dried in a desiccator.

Preparation of *N*-Boc-Pro-OCs. *N*-Boc proline (0.03 M) and Cs_2CO_3 (0.03 M) were added into an 8 mL vial containing ethanol (3 mL) and a stir bar. The solution was stirred overnight until it turned clear. The solution was then concentrated using a rotary evaporator and dried in a desiccator.

X-ray crystallography. X-ray-quality crystals of **2** were grown by the slow vapor diffusion method. Basically, the HPLC eluate collected between $t_r = 132$ and 147 min (Fig. S2†) was dissolved in dichloromethane. The solution was passed through a PTFE filter and added into an oven-dried 4 mL vial. The vial was covered with an aluminium foil, and punctured in the middle using a 22 G needle. The vial was placed inside a 25 mL vial and 2 mL of pentane was added into

the outer vial. The 25 mL vial was sealed with Parafilm and allowed to stand in the dark. Orange plate-like crystals were formed in the inner vial within 96 h. A similar procedure was also adopted for obtaining crystals of **1**.

Ir complex 2/Ir complex 1: A crystal of approximate dimensions (0.020 mm × 0.200 mm × 0.220 mm)/(0.005 mm × 0.010 mm × 0.100 mm) was used for the X-ray crystallographic analysis. The X-ray intensity data ($\lambda = 0.71073 \text{ \AA}$) was measured according to the data collection details in Table S4†/S13†.

A total of 383/420 frames were collected with a total exposure time of 0.64 h/0.93 h. The Bruker SAINT software package, using a narrow-frame algorithm, was used to integrate the frames. A total of 90199/141121 reflections to a maximum θ angle of $25.00^\circ/27.00^\circ$ ($0.84 \text{ \AA}/0.78 \text{ \AA}$ resolution) were yielded when the data was integrated using an orthorhombic unit cell. 10180/10989 reflections were independent (average redundancy 8.860/12.842, completeness = 99.9 %/99.9 %, $R_{\text{int}} = 7.61 \text{ \%}/14.30 \text{ \%}$, $R_{\text{sig}} = 4.05 \text{ \%}/5.72 \text{ \%}$) and 7328/7185 (71.98 %/65.38 %) reflections were greater than $2\sigma(F^2)$. Upon refinement of the XYZ-centroids of 9799/9927 reflections above $20 \sigma(I)$ with $4.77^\circ/4.547^\circ < 2\theta < 60.26^\circ/54.57^\circ$, we obtained the final cell constants of $a = 25.7591(5) \text{ \AA}/17.9150(8) \text{ \AA}$, $b = 19.7247(4) \text{ \AA}/22.4618(9) \text{ \AA}$, $c = 22.7912(4) \text{ \AA}/25.0531(8) \text{ \AA}$, and volume = $11580.0(4) \text{ \AA}^3/10081.4(7) \text{ \AA}^3$. The Multi-Scan method (SADABS) was used to correct the data for absorption effects. The minimum to maximum apparent transmission ratio was 0.733/0.727, and the calculated minimum and maximum transmission coefficients (based on crystal size) were 0.6220/0.7630 and 0.9540/0.9860.

The Bruker SHELXTL Software Package was used to solve the structure and for structure refinement using the space group $Pbcn/Pccn$, with $Z = 8$ for the formula unit, $C_{53}H_{52}F_{10}IrN_5O_4/C_{47.25}H_{43.50}Cl_{2.50}F_{10}IrN_4O_4$. The final anisotropic full-matrix least-squares refinement on F^2 with

728/795 variables converged at R1 = 7.38 %/4.77 % for the observed data and wR2 = 18.83 %/14.93 % for all data; the goodness-of-fit was 1.197/1.066. The largest peak in the final difference electron density synthesis was 2.556 e⁻ Å⁻³/1.828 e⁻ Å⁻³, largest hole was -4.613 e⁻ Å⁻³/-0.894 e⁻ Å⁻³ with an RMS deviation of 0.156 e⁻ Å⁻³/0.159 e⁻ Å⁻³, calculated density was 1.383 g cm⁻³/1.584 g cm⁻³ and F(000), 4832 e⁻/4772 e⁻. Characterization data are provided in the Supplementary Tables S4† – S19†.

Steady-state spectroscopy. UV-Vis absorption and emission spectra in DMF were measured on a UV-Vis spectrophotometer (Varian Cary 100 Bio) and fluorescence spectrometer (Varian Cary Eclipse), respectively. A 1.0 Schlenk arm quartz fluorescence cuvette was used, and **1** (30 μM), **2** and **Ir-mod** were prepared in DMF (spectroscopy grade). The absorbance of **2** and **Ir-mod** in DMF were matched at 340 nm to that of **1**. All samples were degassed prior to measurement by bubbling Ar for 20 min. For the Stern-Volmer analysis, various concentrations of *N*-Boc-Pro-OCs (*i.e.*, from 0.167 to 4.5 mM) were added into the solutions of **1** and **2**. The emission spectra were measured using an excitation wavelength $\lambda_{\text{ex}} = 340$ nm. Stern-Volmer analysis was also conducted for **Ir-mod** ($t_{\text{irra}} = 8$ h) with *N*-Boc-Pro-OCs concentration varying from 0.5 to 20 mM. At high concentrations of *N*-Boc-Pro-O-Cs, the emission of **Ir-mod** was corrected for the fraction of light absorbed by *N*-Boc-Pro-OCs using the following equation:

$$F_{\text{Ir-mod}} = \frac{A_{\text{Ir-mod}}}{A_{\text{Ir-mod}} + A_{\text{N-Boc-Pro-O-Cs}}} (1 - 10^{-(A_{\text{Ir-mod}} + A_{\text{N-Boc-Pro-O-Cs}})})$$

where $A_{\text{Ir-mod}}$ and $A_{\text{N-Boc-Pro-O-Cs}}$ are the absorbance of **Ir-mod** and *N*-Boc-Pro-OCs at 340 nm.

The emission quantum yields were determined as follows: **1** (30 μM) and **2** (50 μM) in degassed DMF and **1** in degassed acetonitrile (ACN) (absorbance at 400 nm matched to either that

of **1** or **2** in DMF) were prepared and the emission spectra recorded using an excitation wavelength $\lambda_{\text{ex}} = 400$ nm. The emission quantum yields of **1** and **2** in DMF (*i.e.*, $\phi_{f,1}$) were determined using the following equation $\frac{\phi_{f,1}}{\phi_{f,2}} = \frac{(1-10^{-A_2})n_1^2\alpha_1}{(1-10^{-A_1})n_2^2\alpha_2}$, where $\phi_{f,2}$ ($= 0.68$)^{S1} is the emission quantum yield of **1** in ACN, A_1 and A_2 are the absorbances at 400 nm for the samples in DMF and ACN, respectively, n_1 and n_2 are the refractive indices of DMF and ACN, respectively, and α_1 and α_2 are the areas under the emission spectra in DMF and ACN, respectively.

Time-resolved spectroscopy. Emission lifetime decay. The emission lifetime decays of the excited state of the iridium complexes were measured using a laser flash photolysis spectrometer (LKS.60, Applied Photophysics) equipped with a Q-Switched Nd:YAG laser (Brilliant B, Quantel) and a R928 photomultiplier. All samples were excited using a 355-nm light, and emission of **1/2** and **Ir-mod** monitored at 495 nm and 530 nm, respectively. In the first experiment, the lifetime decays of **1** (200 μM), **2** (200 μM) and **Ir-mod** ($t_{\text{irra}} = 8$ h, absorbance at 355 nm matched to that of 200 μM **1**) in degassed DMF were recorded. In the second experiment, Stern-Volmer analysis was conducted by separately adding different amounts of *N*-Boc-Pro-OCs (*i.e.*, 0.167 – 5 mM) into degassed DMF solutions of **1** (30 μM) and **2** (30 μM). In the third experiment, both the steady-state emission spectra and lifetime decays of degassed DMF solutions of **1** and isolated **Ir-mod** prepared after various light exposure times t_{irra} were measured in the absence and presence of 4.5 mM *N*-Boc-Pro-OCs. In this case, the absorbances of the **Ir-mod** solutions at 340 nm and 355 nm were matched to that of 30 μM **1** for the steady-state and time-resolved studies, respectively. In the fourth experiment, a degassed DMF solution of **1** (200 μM) and excess *N*-Boc-Pro-OCs (30 mM) was first exposed to blue light (456 nm lamp) for 8 h, and the lifetime decay of the resulting

solution containing modified iridium complexes (**Ir-mod**) immediately measured. The concentrations of **1** and *N*-Boc-Pro-OCs were the same as in the hydrodehalogenation experiments.

ns-Transient absorption spectroscopy. ns-Transient absorption (TA) spectroscopy was conducted using a laser flash photolysis spectrometer (LKS.60, Applied Photophysics), equipped with a Q-Switched Nd:YAG laser (Brilliant B, Quantel), 150 W Xe lamp and R928 photomultiplier, to record ns-difference absorption (ΔOD) spectra. The samples were excited at 355 nm. The sample solutions were prepared by degassing DMF solutions of **1** (200 μM), **2** (200 μM) and **Ir-mod** ($t_{\text{irra}} = 8$ h) (absorbance at 355 nm matched to that of 200 μM **1**) by bubbling Ar for 20 min.

Cyclic Voltammetry. A 3-electrode glass electrochemical cell with a Teflon cap and glassy carbon working electrode, platinum wire counter electrode and an Ag/AgCl reference electrode (RedoxMe) was used. Cyclic voltammetry (CV) was performed with a potentiostat (Metrohm Autolab PGSTAT204). For the measurements, **1**, **2**, **Ir-mod** ($t_{\text{irra}} = 8$ h), *N*-Boc proline and *N*-Boc pyrrolidine were dissolved in dry DMF or dry ACN with TBAPF₆ (0.1 M) as the electrolyte. The solutions were degassed by bubbling Ar for at least 30 min prior to measurements. Ferrocene (Fc) was used as a standard for conversion to vs. saturated calomel electrode (SCE) (*i.e.*, $E_{\text{Fc}^+/\text{Fc}} = +0.4$ V).

Hydrodehalogenation of aryl halides with 1 and 2. In a 10-mL Schlenk tube equipped with a magnetic stir bar, *N*-Boc proline (0.03 M), Cs₂CO₃ (0.03 M), aryl halide (0.02 M) and **1** or **2** (0.2 mM) were added into DMF (3 mL). The reaction mixture was sealed with a PTFE stopcock and degassed by bubbling Ar for 30 min. The reaction mixture was then irradiated for 24 h with a 456-

nm LED lamp (40 W, Kessil) placed 3.5 cm away from the centre of the tube. A standing fan was used to keep the reaction temperature at 30°C throughout the entire reaction. For the work up, the reaction mixture was diluted with a NaHCO₃ solution and extracted thrice with ethyl acetate. The organic solution was washed thrice with water before being dried over MgSO₄, filtered and concentrated *via* rotatory evaporation. GC was used to determine all product yields and ¹⁹F NMR was used to determine the product yields for the hydrodehalogenation reaction of aryl fluorides. An aliquot (1 mL) of the reaction mixture was injected into a gas chromatography spectrometer equipped with a SH-Rtx-5 column. Another 0.5 mL aliquot of the solution was added to an internal standard (4-fluorotoluene, 10 μL) and transferred into an NMR tube.

Hydrodehalogenation of aryl halides with Ir-mod ($t_{\text{irra}} = 8 \text{ h}$). In a 10-mL Schlenk tube equipped with a magnetic stir bar, *N*-Boc proline (0.03 M), Cs₂CO₃ (0.03 M), aryl halide (0.02 M) and **Ir-mod** ($t_{\text{irra}} = 8 \text{ h}$) (0.6 mM) were added into DMF (3 mL). The reaction mixture was sealed with a PTFE stopcock and degassed by bubbling Ar for 30 min. The reaction mixture was then irradiated for 24 h with a 456-nm LED lamp (40 W, Kessil) placed 3.5 cm away from the centre of the tube. A standing fan was used to keep the reaction temperature at 30°C throughout the entire reaction. For the work up, the reaction mixture was diluted with a NaHCO₃ solution and extracted thrice with ethyl acetate. The organic solution was washed thrice with water before being dried over MgSO₄, filtered and concentrated *via* rotatory evaporation. GC was used to determine all product yields and ¹⁹F NMR was used to determine the product yields for the hydrodehalogenation reaction of aryl fluorides. An aliquot (1 mL) of the reaction mixture was injected into a gas chromatography spectrometer equipped with a SH-Rtx-5 column. Another 0.5 mL aliquot of the

solution was added to an internal standard (4-fluorotoluene, 10 μ L) and transferred into an NMR tube.

Photochemical reaction quantum yield determination.^{S2} In a 1.0-cm Schlenk arm quartz fluorescence cuvette, *N*-Boc proline (0.03 M), Cs₂CO₃ (0.03 M), 4-bromobenzotrifluoride (0.02 M) and **1** (0.6 mM) were added into DMF (3 mL). The reaction mixture was degassed by bubbling Ar into the solution for 30 min. The UV-Vis absorption spectrum of the reaction mixture at 456 nm was recorded with the UV-Visible spectrophotometer (Varian Cary 100 Bio). The illumination intensity of the Kessil lamp at 456 nm was recorded with a power meter (FieldMate, Coherent, USA) equipped with a sensor (PM150-50XC). The solution was irradiated for 2 h with a 456-nm LED lamp (40 W, Kessil) placed 3.5 cm away from the center of the tube. A standing fan was used to keep the reaction temperature at 30°C throughout the entire reaction. An internal standard (4-fluorotoluene, 0.02 mL) and the reaction mixture (0.5 mL) were added into an NMR tube and ¹⁹F NMR was used to determine the yield. The reaction quantum yield was obtained with the following

equation $\phi = \frac{nN_A}{fES\lambda} \frac{t}{hc}$ where N_A is the Avogadro number, t is the reaction time, f is the absorption factor ($f = 1 - 10^{-A}$) of the reaction solution absorbance at 456 nm, E is the illumination intensity, S is the area of the irradiated solution, λ is the wavelength of the Kessil lamp, h is Planck's constant and c is the velocity of light.

Light-On/Off experiment. In a 10-mL Schlenk tube equipped with a magnetic stir bar, *N*-Boc proline (0.03 M), Cs₂CO₃ (0.03 M), 4-bromobenzotrifluoride (0.02 M) and **1** (0.6 mM) were added into DMF (3 mL). The reaction mixture was degassed by bubbling Ar into the solution for 30 min. The reaction was stirred and irradiated with a 456-nm LED lamp (40 W, Kessil) placed 3.5 cm

away from the center of the tube. Light-on (90 min) and light-off (90 min) cycles were conducted. To determine the product yield after each light-on or light-off event, a 0.2 mL aliquot of the solution was extracted under Ar and quenched upon addition of CDCl_3 (0.3 mL) and an internal standard (4-fluorotoluene, 0.02 mL). The mixture was then transferred into an NMR tube and ^{19}F NMR was used to determine the product yield.

GC-FID analysis. Gas chromatography (GC) with flame ionization detection (FID) was performed using capillary columns (length: 30 m; inner diam.: 0.25 mm; film: 0.25 μm) using He gas as carrier. GC-FID spectra were measured using a GC spectrometer (Shimadzu, GC-2010). The column temperature was programmed at 60 °C for the first 10 minutes and then 0.50 °C min^{-1} from 60 °C to 65 °C, and then 7 °C min^{-1} from 65 °C to 168 °C, and then 15 °C min^{-1} from 168 °C to 260 °C. Peak integration and retention time of the GC chromatograms were obtained using the LabSolutions software from Shimadzu. Product yields were determined by comparing the peak area of the chromatogram against the calibration curve. Calibration curves and GC chromatograms are given in Fig. S25† - S58†.

NMR spectroscopy. ^1H and ^{19}F NMR spectra were recorded on a NMR spectrometer (400 MHz, JEOL) in either d-benzene or CDCl_3 with an internal solvent signal as reference (d-benzene: δH 7.26; CDCl_3 : δH 7.26). ^{19}F NMR was also conducted in DMF solvent with 4-fluorotoluene as the reference (δF -120.0 ppm). NMR data are reported as: chemical shift (ppm), multiplicity (s = singlet, d = doublet, t = triplet, q = quartet, m = multiplet), coupling constants (Hz), number of protons and assignment of proton, if indicated. NMR spectra are given in Fig S5†, S6† and S59† - S87†.

1: ^1H NMR (400 MHz, acetone- d_6) (refer to Fig. 1): δ 8.93 (d, 2 H, $J = 2$ Hz, $\text{dF}(\text{CF}_3)\text{ppy}$, pyridyl- H^5), 8.61 (dd, 2 H, $J = 9$ Hz, 2 Hz, dtbbpy- H^6), 8.40 (dd, 2 H, $J = 9$ Hz, 2 Hz, dtbbpy- H^8), 8.18 (d, 2 H, $J = 6$ Hz, $\text{dF}(\text{CF}_3)\text{ppy}$, pyridyl- H^4), 7.69 (m, 4 H, dtbbpy- H^7 and $\text{dF}(\text{CF}_3)\text{ppy}$, pyridyl- H^3), 6.86 (td, 2 H, $J = 9$ Hz, 2 Hz, $\text{dF}(\text{CF}_3)\text{ppy}$, phenyl- H^2), 5.97 (dd, 2 H, $J = 9$ Hz, 2 Hz, $\text{dF}(\text{CF}_3)\text{ppy}$, phenyl- H^1), 1.47 (s, 18 H); ^{13}C (400 MHz, acetone d_6): δ 168.0, 165.5, 156.1, 155.8, 151.2, 145.8, 137.3, 126.9, 126.2, 125.2, 124.1, 122.7, 120.9, 114.6, 114.4, 99.3, 35.8, 29.5.^{S1}

2: ^1H NMR (400 MHz, acetone- d_6): δ 8.84 (s, 1 H), 8.72 (s, 1 H), 8.64 (t, 2 H, $J = 9$ Hz), 8.42 (t, 2 H, $J = 9$ Hz), 8.17 (d, 1 H, $J = 6$ Hz), 7.85 (s, 1 H), 7.81 (s, 2 H), 7.57 (s, 1 H), 7.00 (t, 1 H, $J = 11$ Hz), 6.86 (t, 1 H, $J = 11$ Hz), 6.05 (d, 1 H, $J = 9$ Hz), 5.92 (d, 1 H, $J = 9$ Hz), 5.54 (d, 1 H, $J = 9$ Hz), 3.33 (m, 2 H), 2.38 (t, 2 H, $J = 8$ Hz), 1.82 (m, 2 H), 1.42 (s, 9 H), 1.33 (s, 9 H), 1.29 (s, 9 H).

Acetophenone: ^1H NMR (400 MHz, CDCl_3): δ 7.86 – 7.83 (m, 2 H), 7.46 – 7.42 (m, 1 H), 7.36 – 7.32 (m, 2 H), 2.47 (s, 3 H).

Anisole: ^1H NMR (400 MHz, CDCl_3): δ 7.40 – 7.35 (m, 2 H), 7.06 – 7.03 (m, 1 H), 7.01 – 6.98 (m, 2 H), 3.87 (s, 3 H).

Benzotrifluoride: ^1H NMR (400 MHz, CDCl_3): δ 7.66 – 7.64 (m, 2 H), 7.58 – 7.55 (m, 1 H), 7.51 – 7.47 (m, 2 H).

Toluene: ^1H NMR (400 MHz, CDCl_3): δ 7.22 – 7.11 (m, 5 H), 2.30 (s, 3 H).

Biphenyl: ^1H NMR (400 MHz, CDCl_3): δ 7.61 – 7.60 (m, 2 H), 7.47 – 7.43 (m, 2 H), 7.36 (dd, $J = 7, 2$ Hz, 1 H).

Benzonitrile: ^1H NMR (400 MHz, CDCl_3): δ 7.62 – 7.57 (m, 3 H), 7.48 – 7.44 (m, 2 H). ^{19}F NMR (400 MHz, 4-Fluorotoluene): δ 62.9

4-Bromoacetophenone: ^1H NMR (400 MHz, CDCl_3): δ 7.81 (dt, $J = 11, 2$ Hz, 2 H), 7.60 (dt, $J = 11, 2$ Hz, 2 H), 2.58 (s, 3 H).

4-Bromoanisole: ^1H NMR (400 MHz, CDCl_3): δ 7.38 (dt, $J = 4, 9$ Hz, 2 H), 6.79 (dt, $J = 4, 9$ Hz, 2 H), 3.78 (s, 3 H).

4-Bromobenzotrifluoride: ^1H NMR (400 MHz, CDCl_3): δ 7.63 (d, $J = 8$ Hz, 2 H), 7.49 (d, $J = 8$ Hz, 2 H). ^{19}F NMR (400 MHz, DMF, 4-fluorotoluene as internal standard): δ 62.9

4-Bromotoluene: ^1H NMR (400 MHz, CDCl_3): δ 7.37 (d, $J = 8$ Hz, 2 H), 7.05 (d, $J = 8$ Hz, 2 H), 2.31 (s, 3 H).

4-Bromobiphenyl: ^1H NMR (400 MHz, CDCl_3): δ 7.59 – 7.56 (m, 4 H), 7.49 – 7.43 (m, 4 H), 7.40 – 7.36 (m, 1 H).

2-Chlorobenzotrifluoride: ^1H NMR (400 MHz, CDCl_3): δ 7.70 (d, $J = 8$ Hz, 1 H), 7.52 – 7.46 (m, 2 H), 7.37 (t, $J = 8$ Hz, 1 H). ^{19}F NMR (400 MHz, DMF, 4-Fluorotoluene as internal standard): δ 62.7

4-Chlorobenzonitrile: ^1H NMR (400 MHz, CDCl_3): δ 7.60 (dt, $J = 4, 8$ Hz, 2 H), 7.46 (dt, $J = 4, 8$ Hz, 2 H).

Ir-mod/Ni dual-catalyzed decarboxylative cross-coupling of *N*-Boc proline and 4-bromobenzotrifluoride. In a 10-mL Schlenk tube equipped with a magnetic stir bar, *N*-Boc proline (0.03 M), Cs_2CO_3 (0.03 M), $\text{NiCl}_2 \bullet \text{glyme}$ (2 mM), 4,4'-di-*tert*-butyl-2,2'-bipyridyl (3 mM), 4-bromobenzotrifluoride (0.02 M) and **Ir-mod** ($t_{\text{irra}} = 8$ h) (0.6 mM) were added into DMF (3 mL). The reaction mixture was sealed with a PTFE stopcock and deoxygenated by bubbling Ar for 30 min. The reaction mixture was then irradiated for 72 h with a 456-nm LED lamp (40 W, Kessil) placed 3.5 cm away from the centre of the tube. A standing fan was used to keep the reaction temperature at 30°C throughout the entire reaction. For the work up, the reaction mixture was diluted with a NaHCO_3 solution and extracted thrice with ethyl acetate. The organic solution

was washed thrice with water before being dried over MgSO₄, filtered and concentrated *via* rotatory evaporation.

¹H NMR spectra were recorded on a JEOL ECA400 spectrometer in CDCl₃ (TMS peak, δ = 7.26 ppm was used as an internal peak standard) (Fig. S87†). 1,1,2,2-tetrachloroethane (0.19 mmol, 20 μ L) was used as an internal standard, NMR yield: 88%. ¹H NMR (400 MHz, CDCl₃) rotameric mixture: δ 7.56 (d, J = 8.0 Hz, 2H), 7.29 (d, J = 8.0 Hz, 2H), 4.98 and 4.81 (2 brs, 1H, rotamer), 3.64 (m, 2H), 2.32 (m, 1H), 1.90-1.87 (m, 1H), 1.83-1.81 (m, 2H), 1.39 (s, 3H), 1.18 (s, 6H).

Computational studies. All geometries were optimized with Gaussian 09, Revision E.01.^{S3} The density functional B3LYP was used in the geometry optimizations and time-dependent density functional calculations for singlet-singlet transition.^{S4,S5} The basis set chosen in the calculations were: def2-svp for H, C, N, O, F, and def2-tzvp for Ir atom with def2-tzvp pseudo potential.^{S6,S7} The solvent effect is modelled with PCM model in the DMF solution.^{S8}

SUPPLEMENTARY REFERENCES

- S1. Lowry, M. S.; Goldsmith, J. I.; Slinker, J. D.; Rohl, R.; Pascal, Jr., R. A.; Malliaras, G. G.; Bernhard, S. Single-Layer Electroluminescence Devices and Photoinduced Hydrogen Production from an Ionic Iridium(III) Complex. *Chem. Mater.* **2005**, *17*, 5712-5719.
- S2. Li, H.; Tang, X.; Pang, J. H.; Yeow, E. K. L.; Wu, J.; Chiba, S. Polysulfide Anions as Visible Light Photoredox Catalysts for Aryl Cross-Coupling. *J. Am. Chem. Soc.* **2021**, *143*, 481-487.
- S3. Gaussian 09, Revision E.01, Frisch, M. J.; et al. Gaussian, Inc., Wallingford CT, 2016.

- S4. Becke, A. D. Density-Functional Thermochemistry. III. The Role of Exact Exchange. *J. Chem. Phys.* **1993**, *98*, 5648-52.
- S5. Lee, C.; Yang, W.; Parr, R. G. Development of the Colle-Salvetti Correlation-Energy Formula Into a Functional of the Electron Density. *Phys. Rev. B* **1998**, *37*, 785-89.
- S6. Weigend, F.; Ahlrichs, R. Balanced Basis Sets of Split Valence, Triple Zeta Valence and Quadruple Zeta Valence Quality for H to Rn: Design and Assessment of Accuracy. *Phys. Chem. Chem. Phys.* **2005**, *7*, 3297-3305.
- S7. Weigend, F. Accurate Coulomb-Fitting Basis Sets For H to Rn. *Phys. Chem. Chem. Phys.* **2006**, *8*, 1057-1065.
- S8. Scalmani, G.; Frisch, M. J. Continuous Surface Charge Polarizable Continuum Models of Solvation. I. General Formalism. *J. Chem. Phys.* **2010**, *132*, 114110.

S2. SUPPLEMENTARY FIGURES

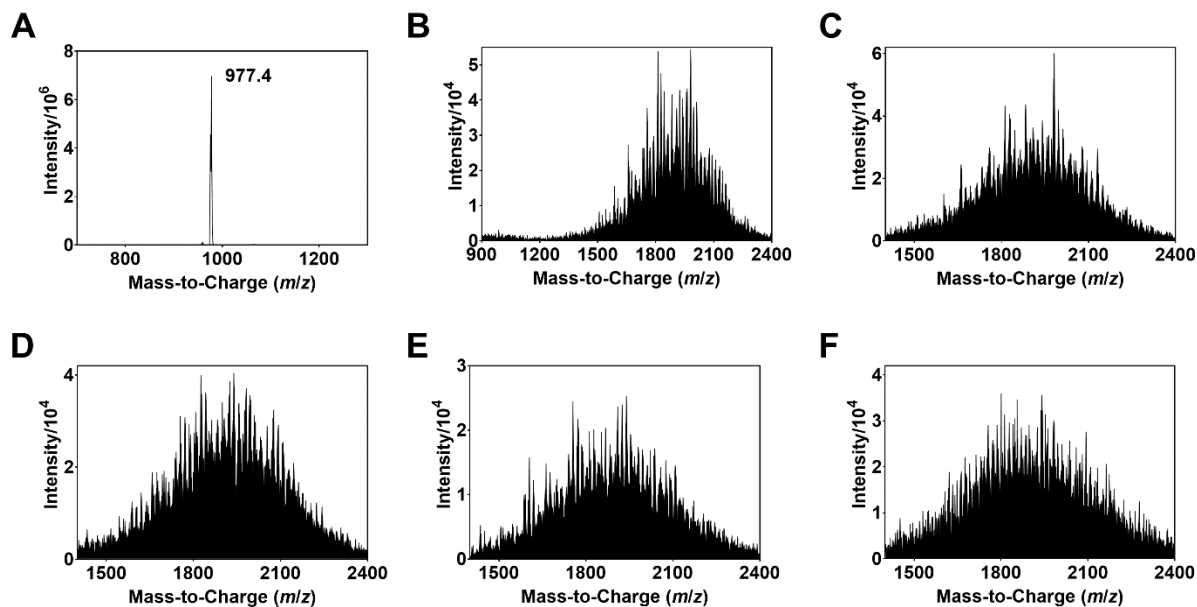


Fig. S1 ESI-MS spectra of (A) non-irradiated **1**, and samples of **1** and *N*-Boc-Pro-OCs exposed to blue light for (B) 2 h (inset: m/z 783.78 peak), (C) 4 h, (D) 6 h, (E) 12 h and (F) 14 h.

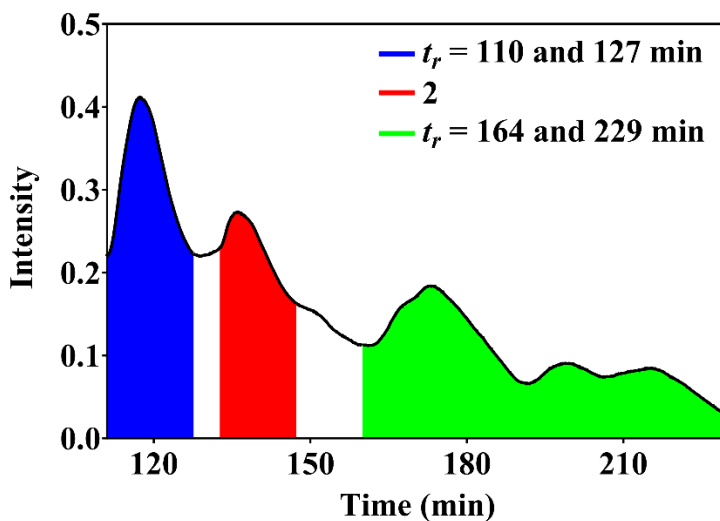


Fig. S2 HPLC chromatogram. Solute eluted between retention times $t_r = 110$ and 127 min, $t_r = 132$ and 147 min (Ir complex **2**), and $t_r = 164$ and 229 min.

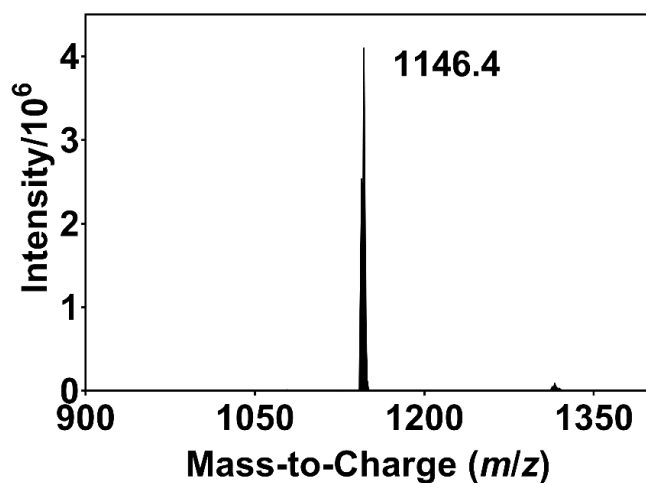


Fig. S3 ESI-MS spectrum of isolated **2**.

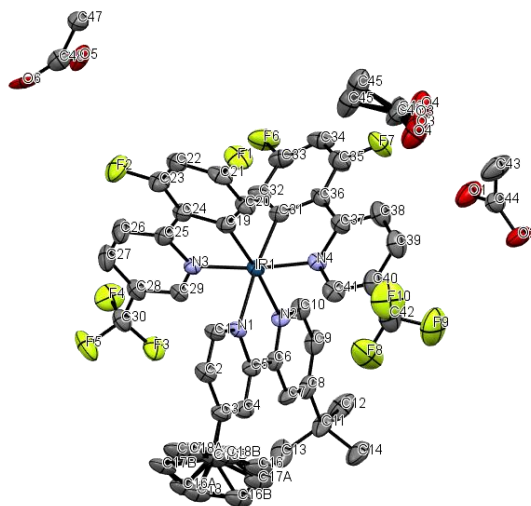


Fig. S4 Structure and numbering scheme of **1**. Some disorder is observed in the *t*-Bu group of the bipyridine ligand. Acetate counter anions are shown, however, hydrogen atoms and dichloromethane (used during crystallization) were removed for clarity. See Supplementary Table S10 – S16 for additional data.

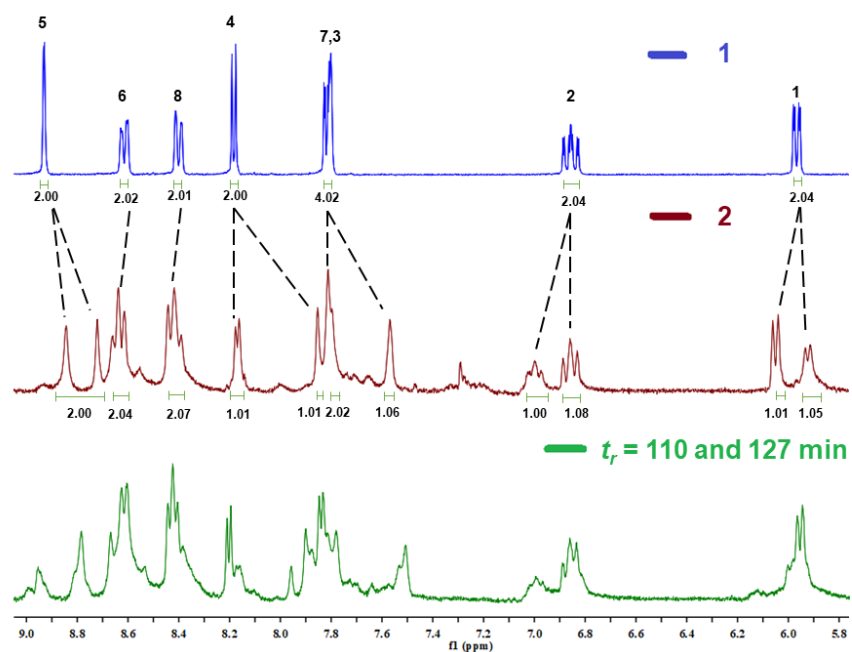


Fig S5 ^1H NMR spectrum (400 MHz, acetone- d_6) of **1**, **2** and the solute collected between $t_r = 110$ and 127 min (Fig. S2†).

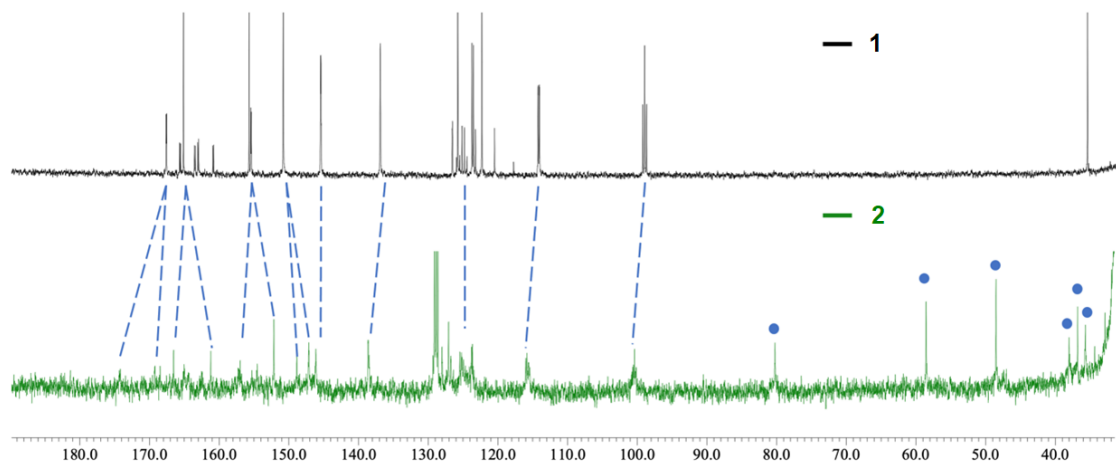


Fig. S6 Partial ^{13}C NMR (400 MHz, acetone- d_6) of **1** and **2**, showing splitting and shifting of aromatic carbons due to the asymmetrical structure. New peaks are seen in the upfield region of **2** due to the covalently bonded NBP molecule on the Ir complex.

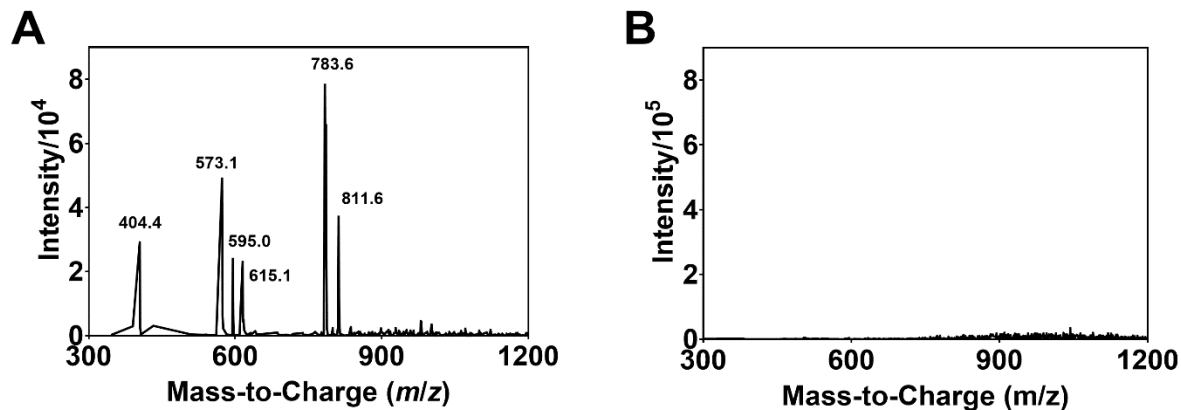


Fig. S7 ESI-MS spectra after irradiating a degassed DMF solution of **1**, *N*-Boc proline and Cs₂CO₃ with blue light (456 nm, 40 W) (A) before and (B) after purification with flash column chromatography. Only the 300 < *m/z* < 1200 region is shown.

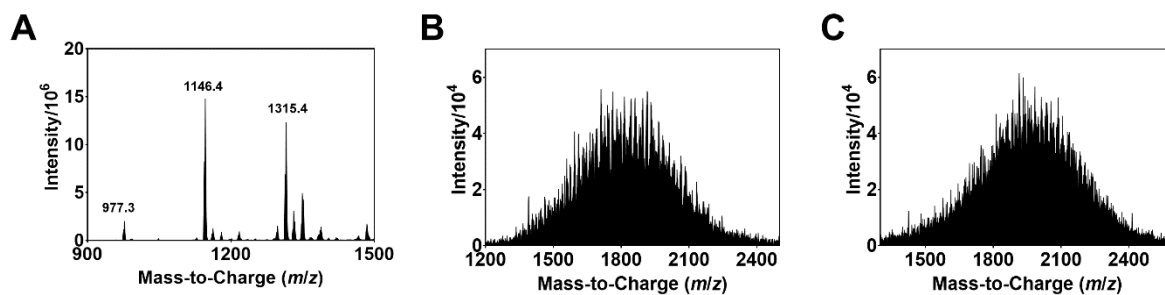


Fig. S8 ESI-MS spectra of the modified complexes formed after irradiating a degassed DMF solution of **1**, *N*-Boc proline, Cs₂CO₃ and 4-bromobenzotrifluoride with blue light (456 nm, 40 W) for (A) 0.5 h, (B) 2 h and (C) 8 h.

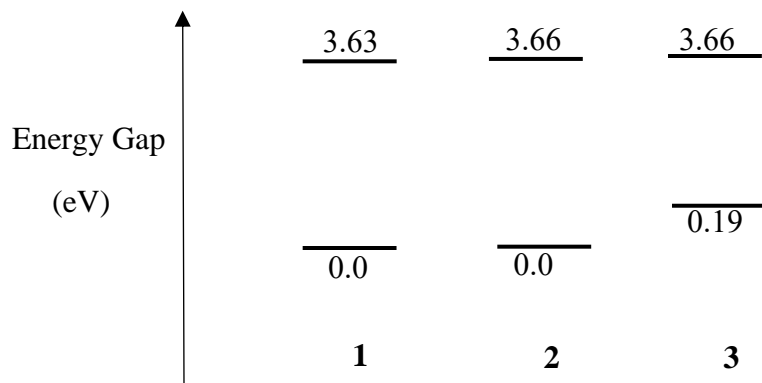


Fig. S9 Energy diagram of the HOMO and LUMO of **1**, **2** and **3**.

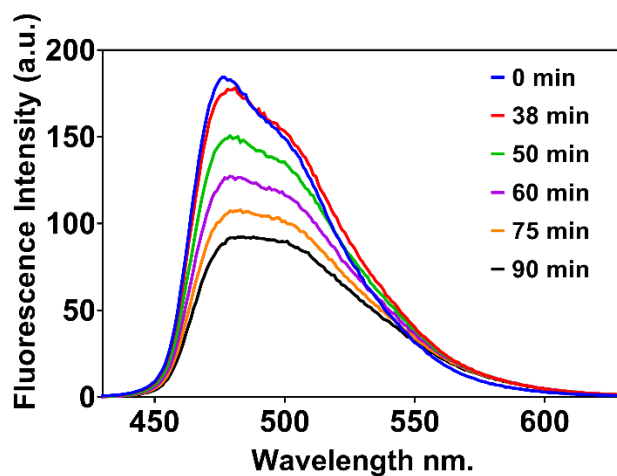


Fig. S10 Emission spectra of a degassed DMF solution of **1** after different irradiation times with a 456-nm light.

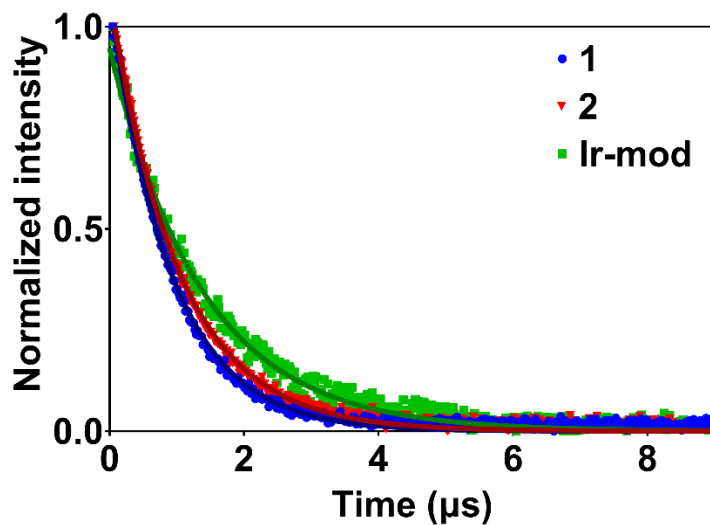


Fig. S11 Normalized emission lifetime decay profiles of degassed DMF solutions of **1** (200 μM), **2** (200 μM), and **Ir-mod** ($t_{\text{irra}} = 8$ h) with absorbance matched to that of **1** at 355 nm. The excitation wavelength is $\lambda_{\text{ex}} = 355$ nm for all samples. The emission is monitored at $\lambda_{\text{em}} = 495$ nm for **1** and **2**, and $\lambda_{\text{em}} = 530$ nm for **Ir-mod**. The decays are described using a mono-exponential decay function.

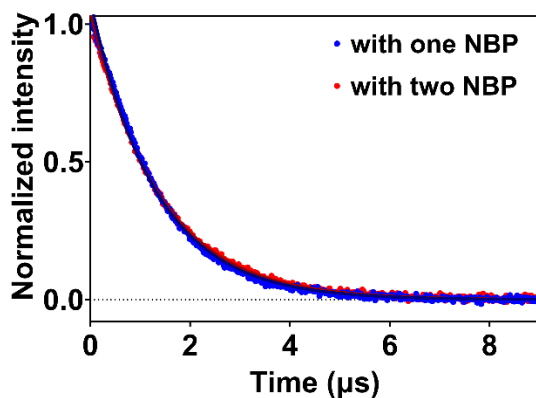


Fig. S12 Normalized emission lifetime decay profiles of degassed DMF solutions of Ir(III) complex with one NBP unit substituted at a different position compared to **3** (*i.e.*, m/z 1146 solute collected between $t_{\text{R}} = 110$ and 127 min in Fig S2†) and Ir(III) complexes with two NBP substituents (m/z 1315.4 solute). The excitation wavelength is $\lambda_{\text{ex}} = 355$ nm and emission monitored at $\lambda_{\text{em}} = 495$ nm. The decays are described by a mono-exponential decay function.

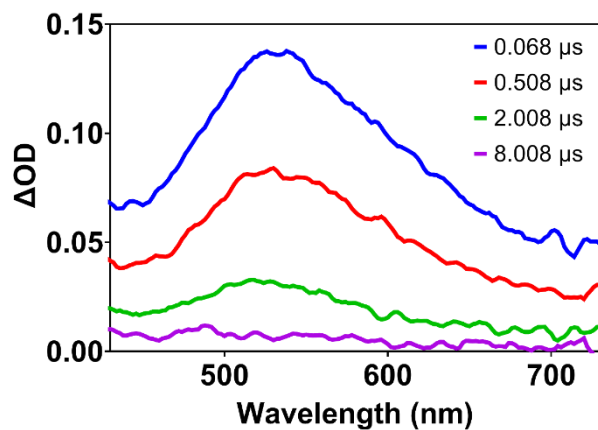


Fig. S13 ns-Transient absorption spectra of a degassed DMF solution of **Ir-mod** ($t_{\text{irra}} = 8$ h) at various delay times. The absorbance of **Ir-mod** was matched to that of 200 μM **1** at 355 nm, and the sample was excited at 355 nm.

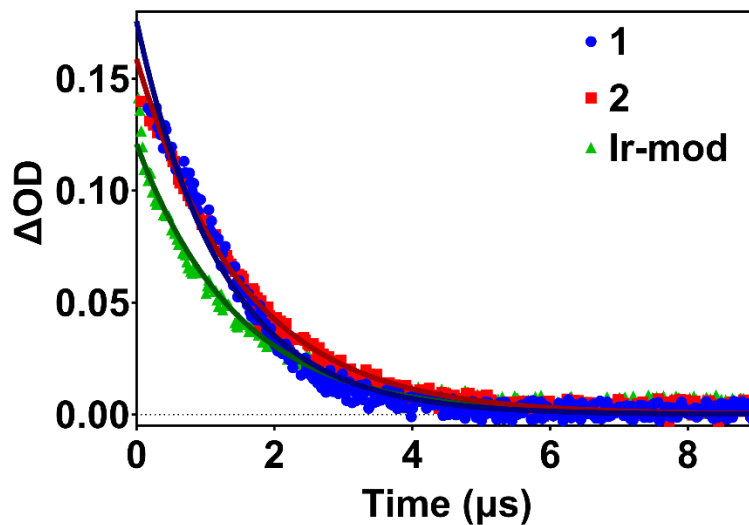


Fig. S14 The kinetic traces of **1** (200 μM), **2** (200 μM) probed at 494 nm, and **Ir-mod** ($t_{\text{irra}} = 8$ h) probed at 530 nm. The traces are described using a mono-exponential decay function

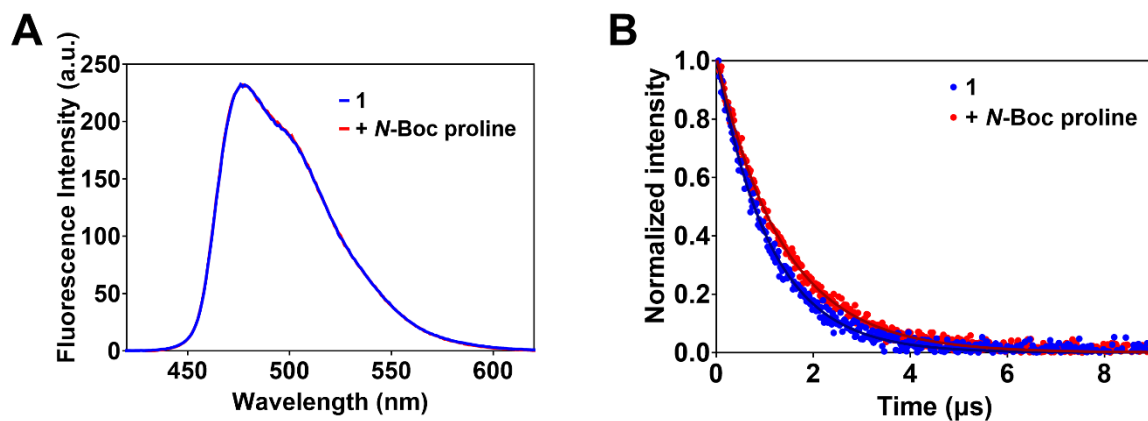


Fig. S15 (A) Emission spectra of degassed DMF solutions of **1** in the absence and presence of *N*-Boc proline (4.5 mM). The absorbance of the solutions are kept similar at the excitation wavelength $\lambda_{\text{ex}} = 340$ nm. (B) Corresponding emission lifetime decay profiles obtained using an excitation wavelength $\lambda_{\text{ex}} = 355$ nm and monitoring emission at 495 nm. The lifetime decays are described using a mono-exponential decay function with a lifetime component of 1.09 and 1.35 μs in the absence and presence of *N*-Boc proline, respectively. The results indicate that **1** is not quenched by *N*-Boc proline.

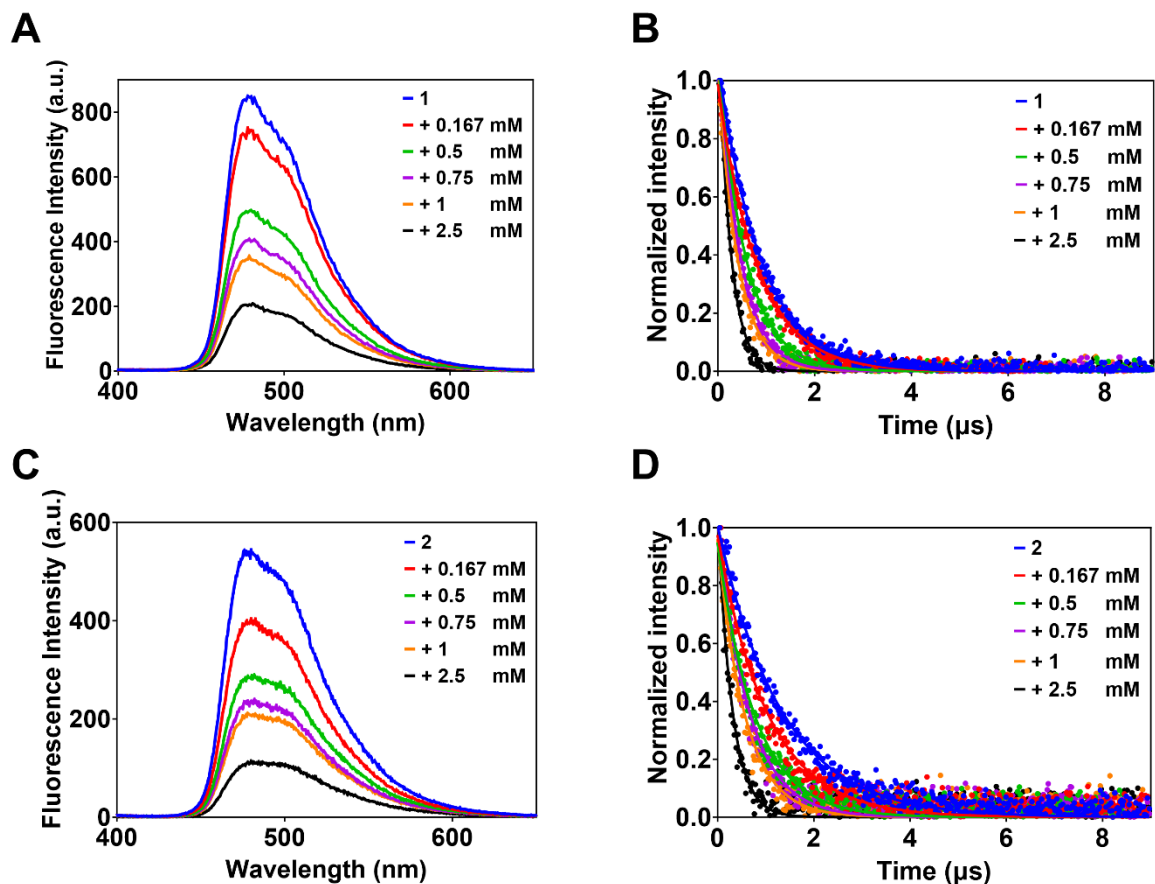


Fig. S16 Emission spectra of (A) **1** (30 μM) and (C) **2** (30 μM) in the absence and presence of various concentrations of *N*-Boc-Pro-OCs (0.167 – 5 mM) in degassed DMF. The absorbance of the solutions are kept similar at the excitation wavelength $\lambda_{\text{ex}} = 340$ nm. Emission lifetime decay profiles of (B) **1** (30 μM) and (D) **2** (30 μM) in the absence and presence of various concentrations of *N*-Boc-Pro-OCs (0.167 – 5 mM) in degassed DMF. The excitation wavelength $\lambda_{\text{ex}} = 355$ nm and emission monitored at $\lambda_{\text{em}} = 495$ nm. The lifetime decays are described by a mono-exponential decay function.

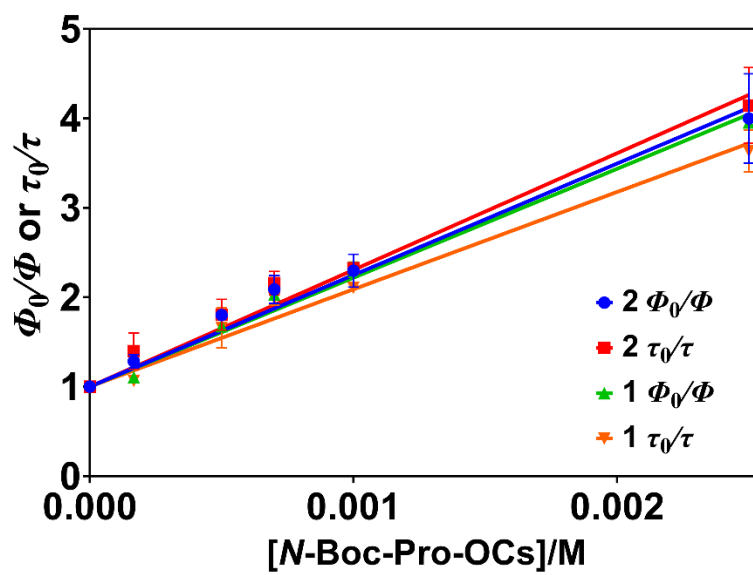


Fig. S17 Stern-Volmer plots for **1** and **2** in the presence of *N*-Boc-Pro-OCs (0.167 – 5 mM) based on the data presented in Fig. S16†.

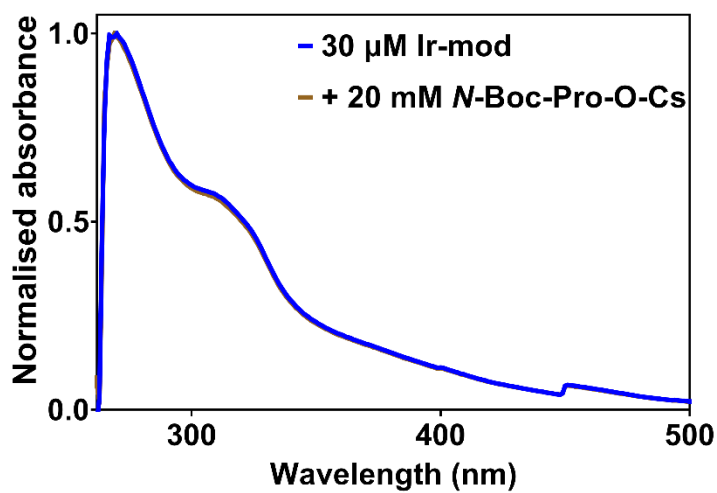


Fig. S18 Normalized absorption spectra of **Ir-mod** ($t_{\text{irra}} = 8$ h) in the absence of presence of 20 mM *N*-Boc-Pro-OCs. Solvent is DMF.

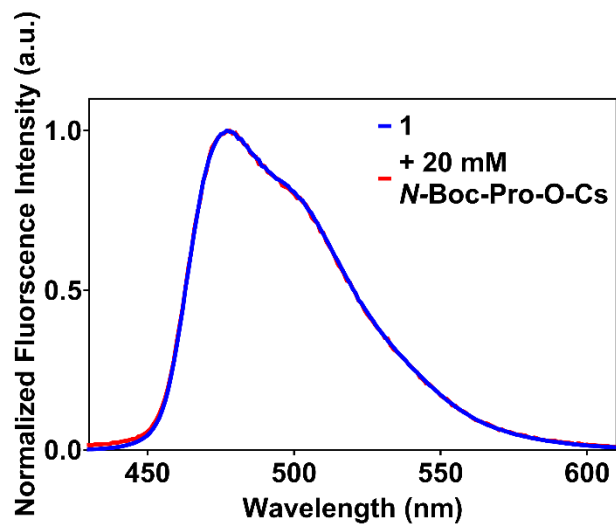


Fig. S19 Normalized emission spectra of **1** in the absence of presence of 20 mM *N*-Boc-Pro-OCs. Solvent is degassed DMF and $\lambda_{\text{ex}} = 340$ nm.

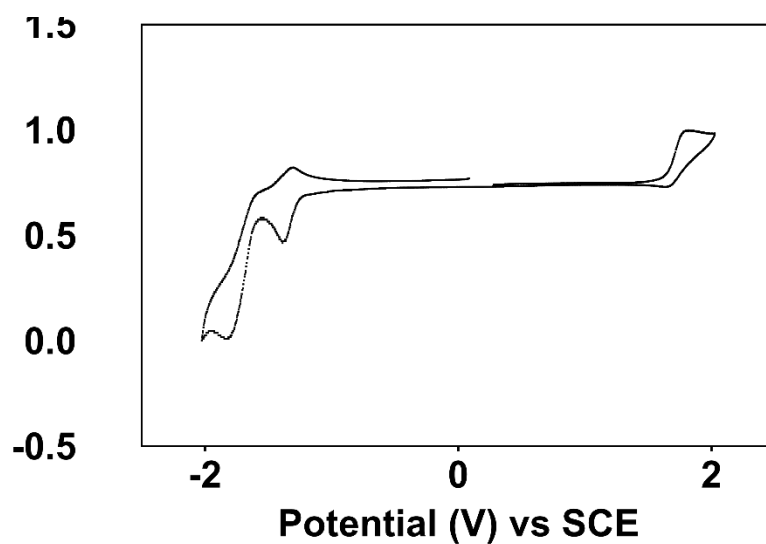


Fig. S20 Cyclic voltammetry of **1** in degassed ACN. $E_{1/2}(\text{ox}) = +1.71$ V vs. SCE and $E_{1/2}(\text{red}) = -1.35$ and -1.73 V vs. SCE.

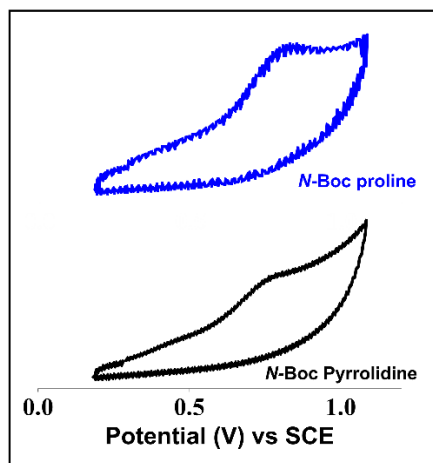


Fig. S21 Cyclic voltammetry of *N*-Boc proline and *N*-Boc pyrrolidine in DMF with $E_{1/2}(\text{ox}) = +0.82$ V vs. SCE and $+0.77$ V vs. SCE, respectively.

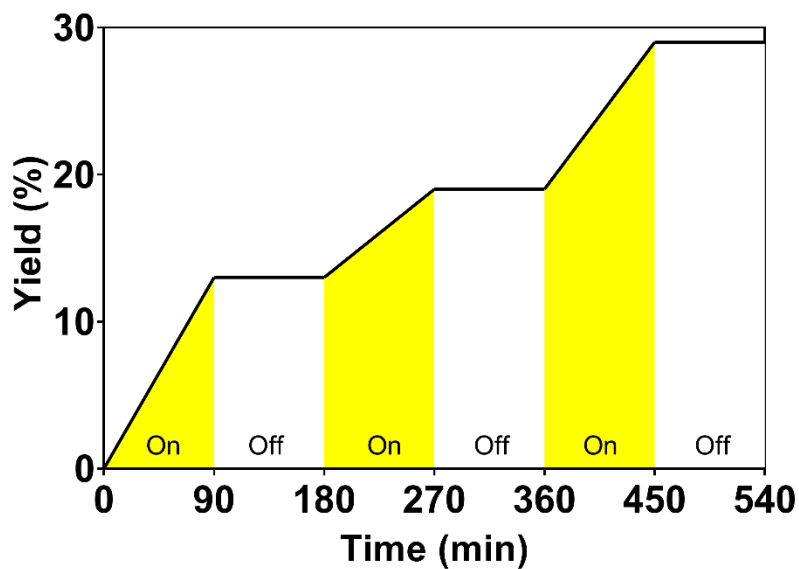


Fig. S22 Plot of product yield (%) vs. time for the light on-off experiment. The product yield of the reaction after turning on and off a 456-nm lamp (40 W) that is used to irradiate a degassed DMF solution of 4-bromobenzotrifluoride, **1**, *N*-Boc proline and Cs_2CO_3 is obtained from ^{19}F NMR.

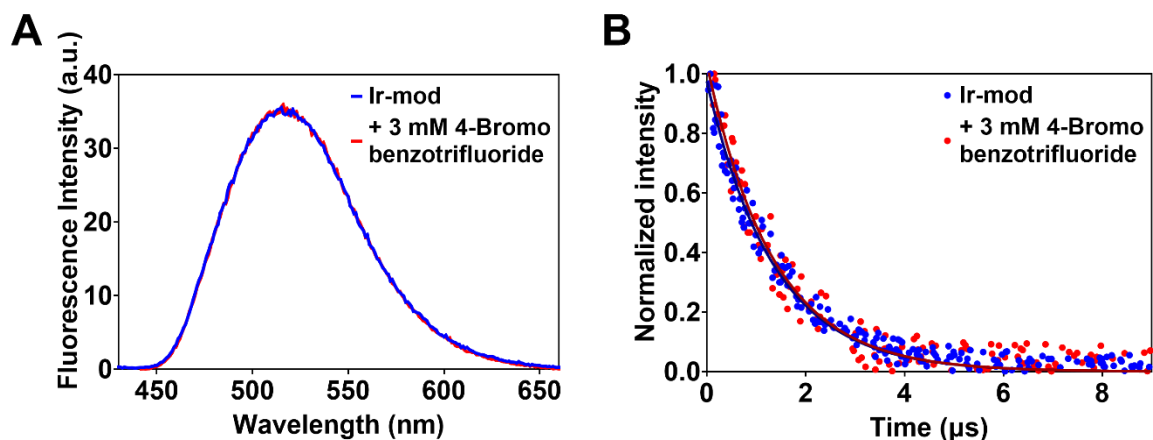


Fig. S23 (A) Emission spectra of degassed DMF solutions of **Ir-mod** ($t_{\text{irra}} = 8$ h) in the absence and presence of 4-bromobenzotrifluoride (3 mM). The absorbance of the solutions are kept similar at the excitation wavelength $\lambda_{\text{ex}} = 340$ nm. (B) Corresponding emission lifetime decay profiles. Excitation wavelength is 355 nm and emission monitored at 530 nm. The lifetime decays are described using a mono-exponential decay function with a lifetime component of 1.35 μs for both in the absence and presence of 4-bromobenzotrifluoride (3 mM). The results indicate that **Ir-mod** is not quenched by 4-bromobenzotrifluoride.

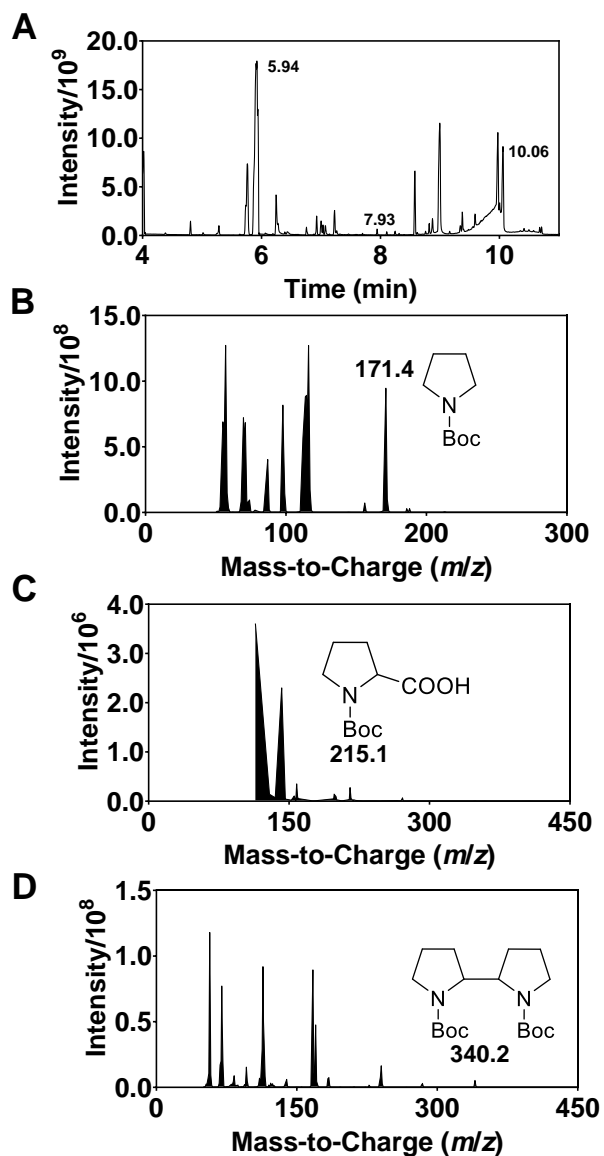


Fig. S24 (A) GC-MS chromatogram of the crude reaction mixture of the hydrodehalogenation reaction of 4-bromoanisole in the presence of **1**, *N*-Boc proline, Cs_2CO_3 and 456-nm light irradiation for 24 h. The peaks at 5.94, 7.93 and 10.06 min correspond to the mass spectra of *N*-Boc pyrrolidine ($m/z = 171.4$) (B), *N*-Boc proline ($m/z = 215.1$) (C) and dimeric *N*-Boc pyrrolidine ($m/z = 340.2$) (D).

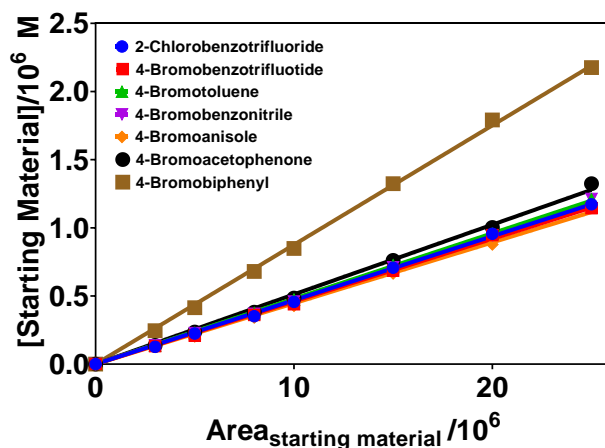


Fig. S25 GC-FID calibration graphs for standard aryl halides used in this study. The gradients (R^2) from a linear fit are 0.0469 (0.999), 0.0511 (0.999), 0.0460 (0.999), 0.0446 (0.999), 0.0476 (0.999), 0.0480 (0.997) and 0.0876 (0.999) for 2-chlorobenzotrifluoride, 4-bromoacetophenone, 4-bromobenzotrifluoride, 4-bromoanisole, 4-bromobenzonitrile, 4-bromotoluene and 4-bromobiphenyl, respectively

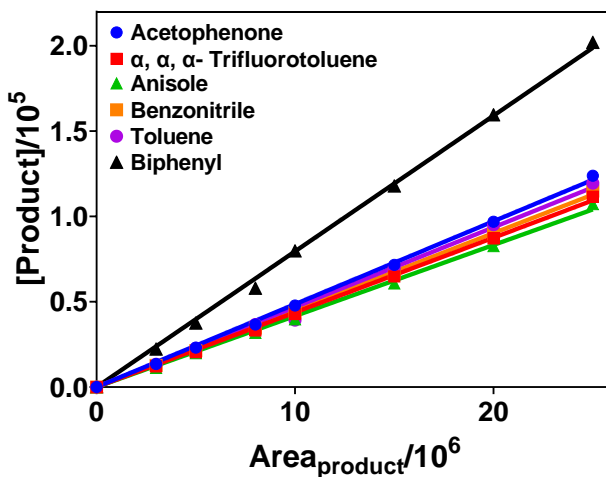


Fig. S26 GC-FID calibration graphs for the standard hydrodehalogenation products. The gradients (R^2) from a linear fit are 0.0486 (0.999), 0.0438 (0.999), 0.0416 (0.998), 0.0451 (0.999), 0.0468 (0.997) and 0.0795 (0.999) for acetophenone, α, α, α -trifluorotoluene, anisole, benzonitrile, toluene and biphenyl, respectively.

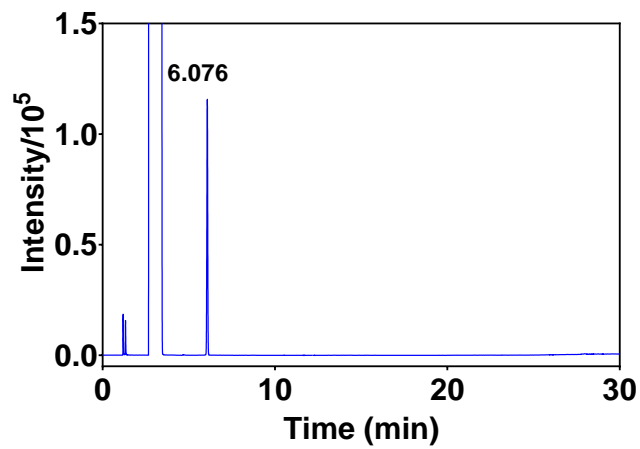


Fig. S27 GC chromatogram of a standard 4-bromobenzotrifluoride (6.076 min).

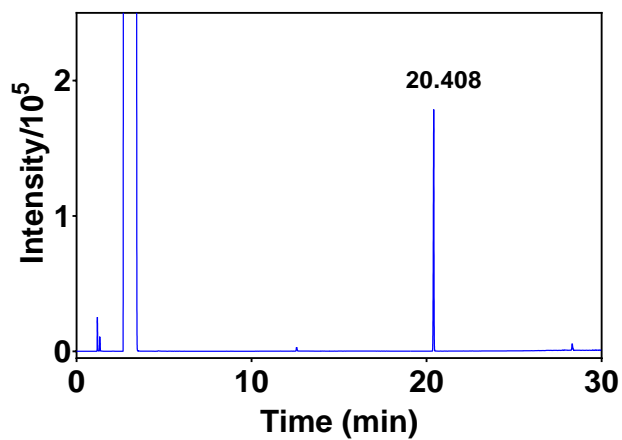


Fig. S28 GC chromatogram of a standard 4-bromoacetophenone (20.408 min).

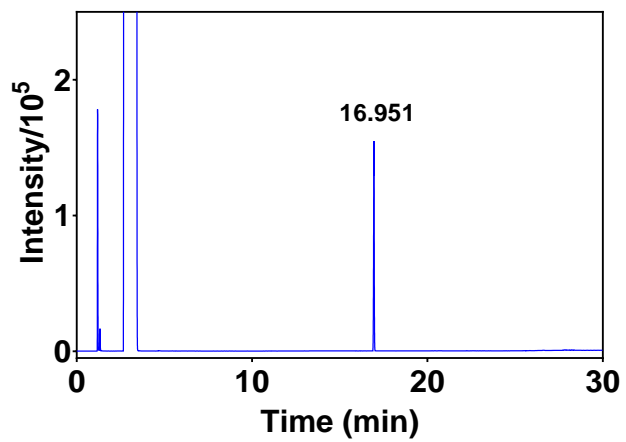


Fig. S29 GC chromatogram of a standard 4-bromoanisole (16.951 min).

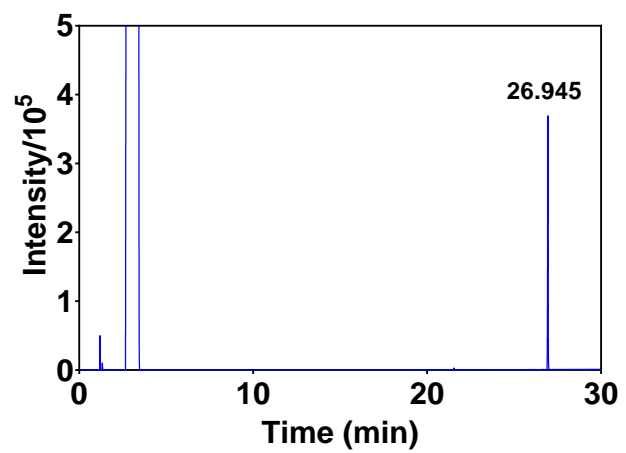


Fig. S30 GC chromatogram of a standard 4-bromobiphenyl (26.945 min).

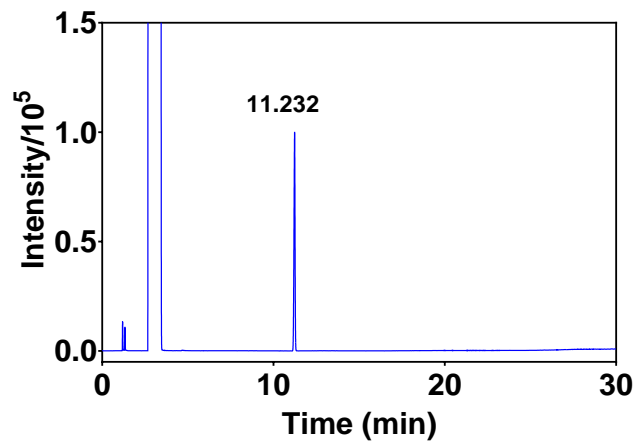


Fig. S31 GC chromatogram of a standard 4-bromotoluene (11.232 min).

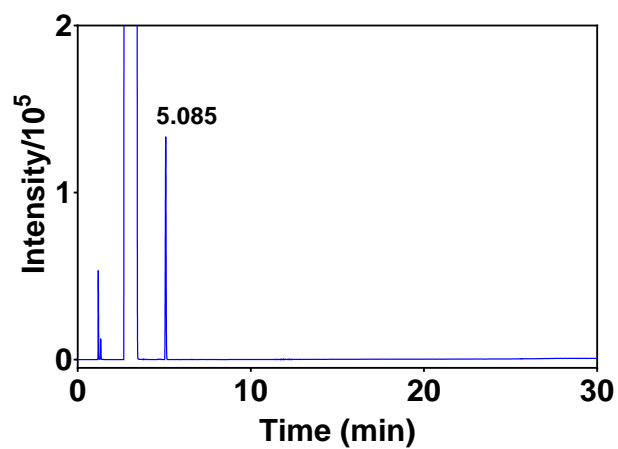


Fig. S32 GC chromatogram of a standard 2-chlorobenzotrifluoride (5.085 min).

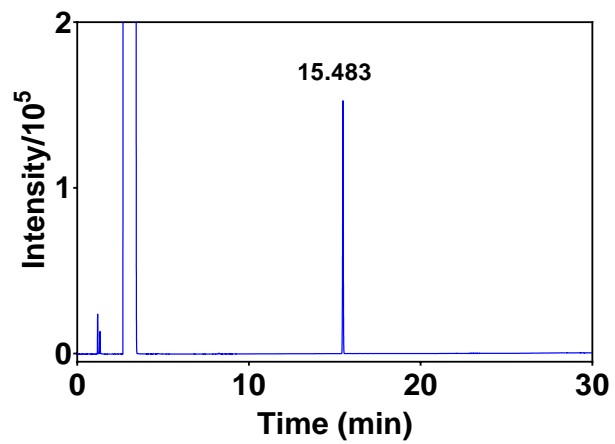


Fig. S33 GC chromatogram of a standard 4-chlorobenzonitrile (15.483 min).

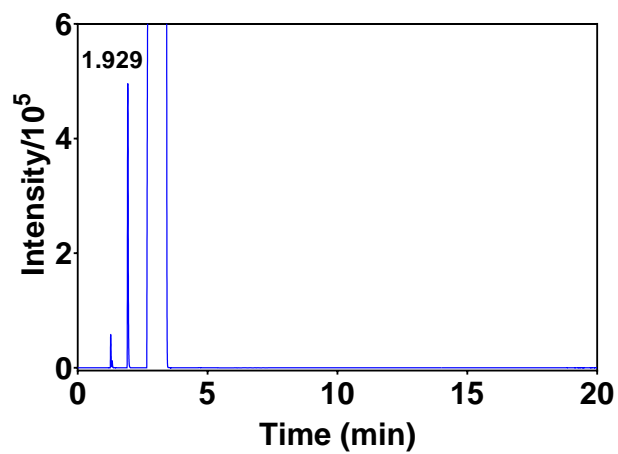


Fig. S34 GC chromatogram of a standard α,α,α -trifluorotoluene (1.929 min).

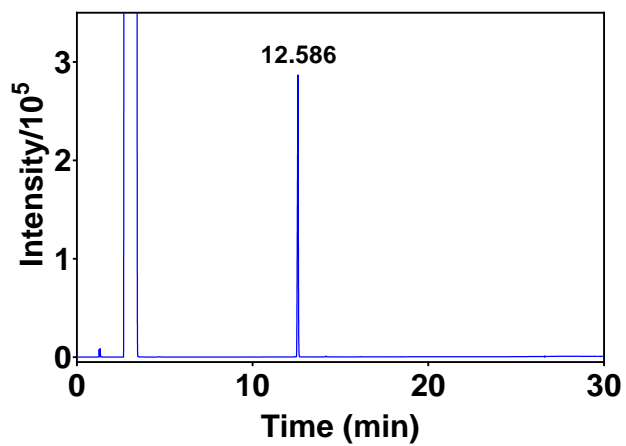


Fig. S35 GC chromatogram of a standard acetophenone (12.586 min).

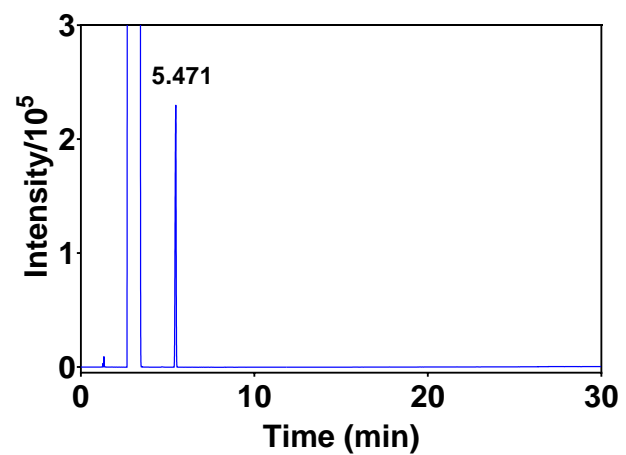


Fig. S36 GC chromatogram of a standard anisole (5.471 min).

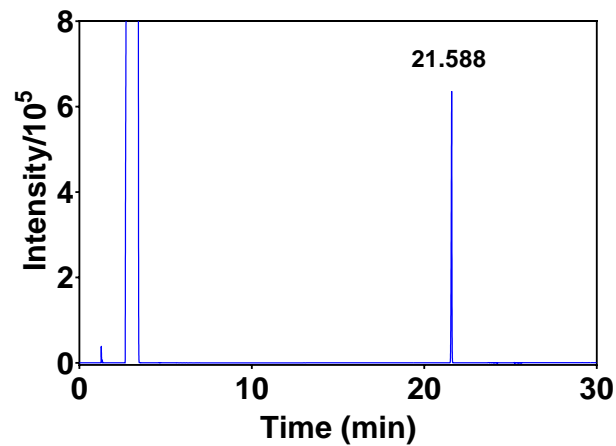


Fig. S37 GC chromatogram of a standard biphenyl (21.588 min).

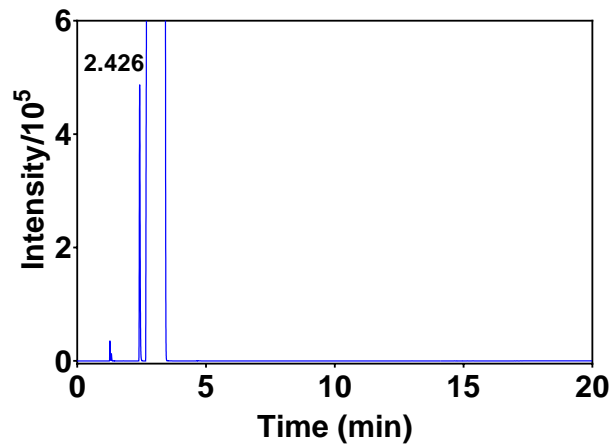


Fig. S38 GC chromatogram of a standard toluene (2.426 min).

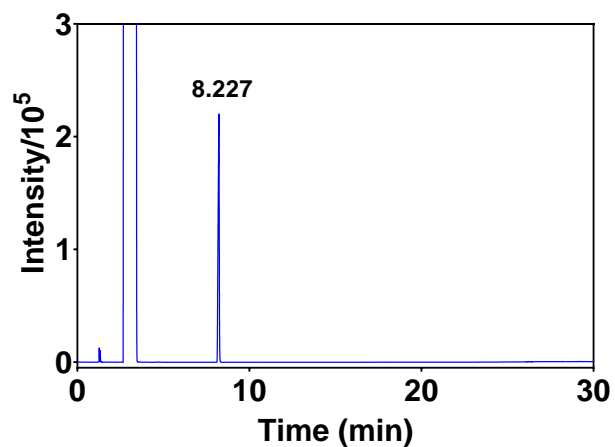


Fig. S39 GC chromatogram of a standard benzonitrile (8.227 min).

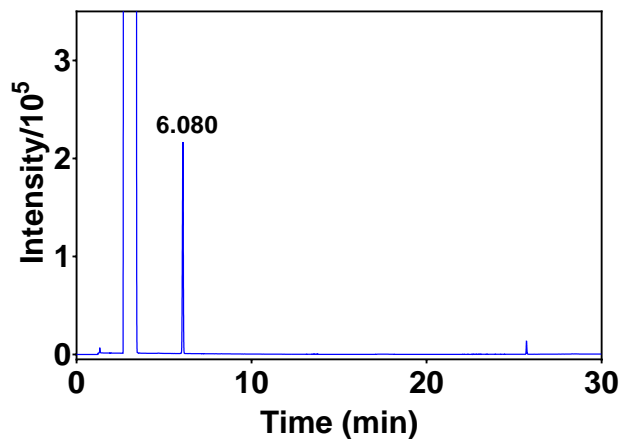


Fig. S40 GC chromatogram of the hydrodehalogenation reaction of 4-bromobenzotrifluoride in the absence of iridium complex and *N*-Boc proline, and presence of Cs₂CO₃ and 456-nm light irradiation for 24 h (entry 1, Table 3). The peak at 6.080 min corresponds to 4-bromobenzotrifluoride.

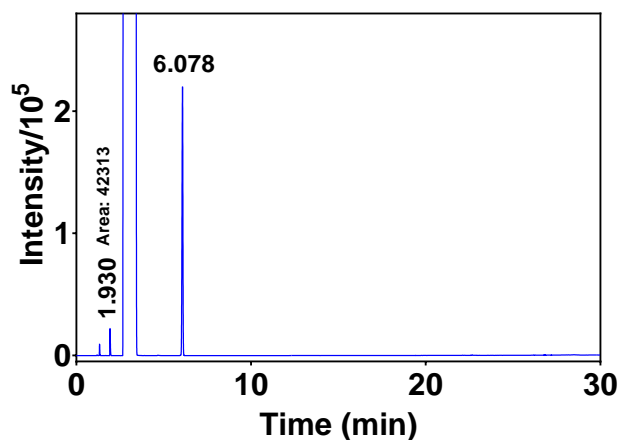


Fig. S41 GC chromatogram of the hydrodehalogenation reaction of 4-bromobenzotrifluoride in the presence of **1**, Cs₂CO₃ and 456-nm light irradiation for 24 h, and absence of *N*-Boc proline (entry 2, Table 3). The peaks at 1.930 and 6.078 min corresponds to α,α,α -trifluorotoluene and 4-bromobenzotrifluoride, respectively.

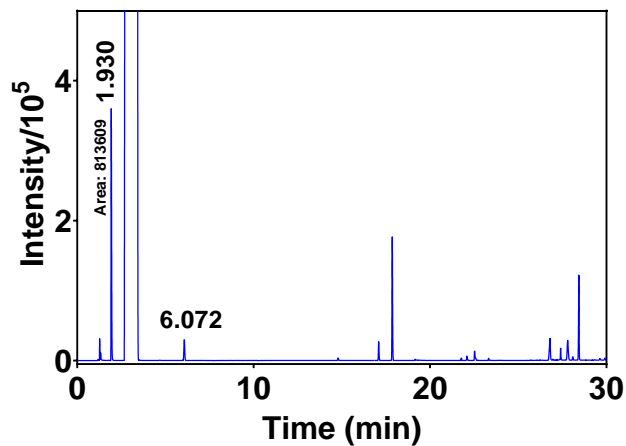


Fig. S42 GC chromatogram of the hydrodehalogenation reaction of 4-bromobenzotrifluoride in the presence of **1**, *N*-Boc proline, Cs_2CO_3 and 456-nm light irradiation for 24 h (entry 3, Table 3). The peak at 1.930 and 6.072 min corresponds to α,α,α -trifluorotoluene and 4-bromobenzotrifluoride, respectively.

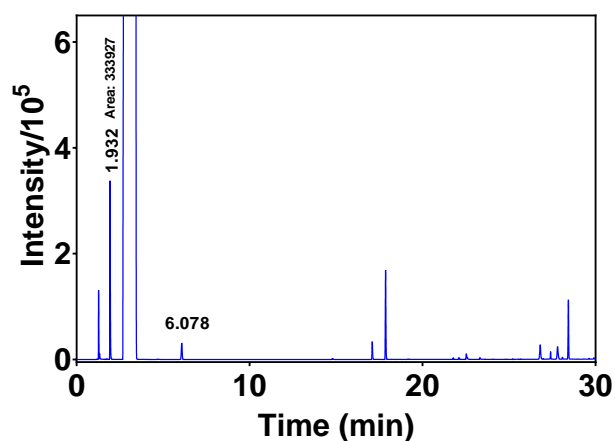


Fig. S43 GC chromatogram of the hydrodehalogenation reaction of 4-bromobenzotrifluoride in the presence of **2**, *N*-Boc proline, Cs_2CO_3 and 456-nm light irradiation for 24 h (entry 4, Table 3). The peak at 1.932 and 6.078 correspond to α,α,α -trifluorotoluene and 4-bromobenzotrifluoride, respectively.

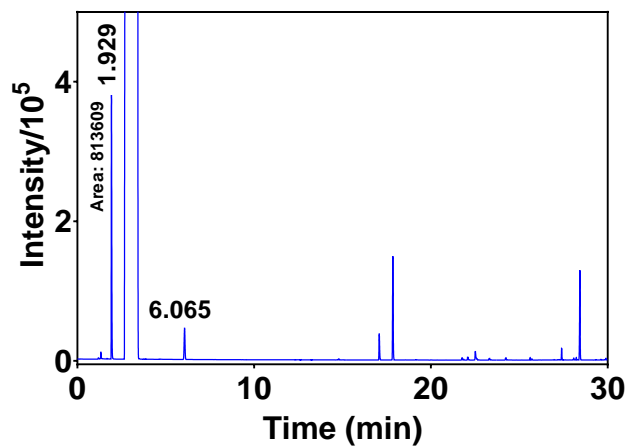


Fig. S44 GC chromatogram of the hydrodehalogenation reaction of 4-bromobenzotrifluoride in the presence of **Ir-mod** ($t_{\text{irra}} = 8$ h), *N*-Boc proline, Cs_2CO_3 and 456-nm light irradiation for 24 h (entry 5, Table 3). The peaks at 1.929 and 6.065 min correspond to α,α,α -trifluorotoluene and 4-bromobenzotrifluoride, respectively.

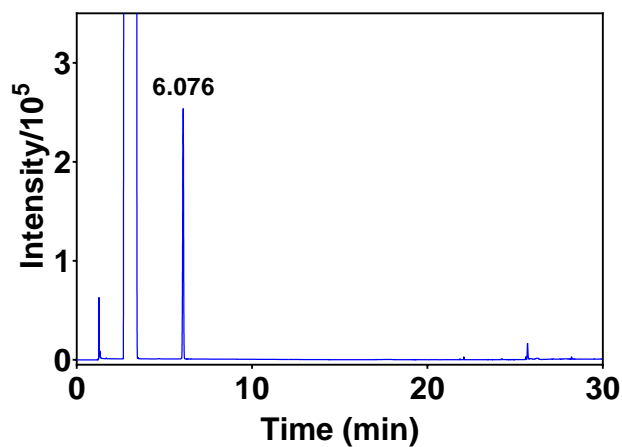


Fig. S45 GC chromatogram of the hydrodehalogenation reaction of 4-bromobenzotrifluoride in the presence of **Ir-mod** ($t_{\text{irra}} = 8$ h), *N*-Boc proline and Cs_2CO_3 in the dark (entry 6, Table 3). The peak at 6.078 min corresponds to 4-bromobenzotrifluoride.

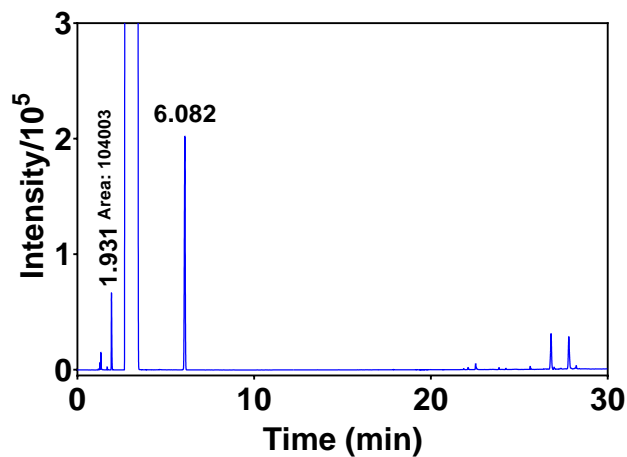


Fig. S46 GC chromatogram of the hydrodehalogenation reaction of 4-bromobenzotrifluoride in the presence of **Ir-mod** ($t_{\text{irra}} = 8$ h), Cs_2CO_3 and 456-nm light irradiation for 24 h, and absence of *N*-Boc proline (entry 7, Table 3). The peaks at 1.931, 6.082 min correspond to α,α,α -trifluorotoluene and 4-bromobenzotrifluoride.

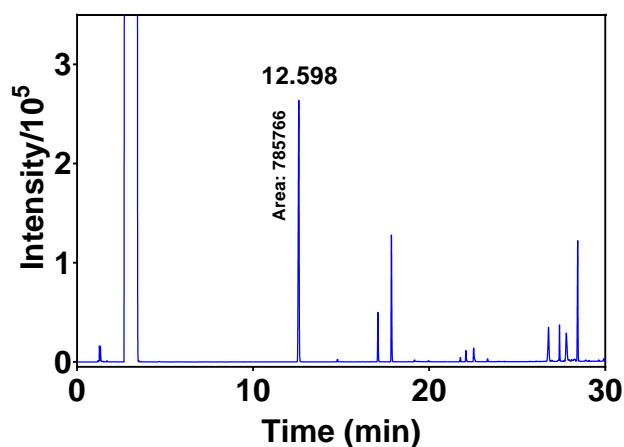


Fig. S47 GC chromatogram of the hydrodehalogenation reaction of 4-bromoacetophenone (Table 4) in the presence of **1**, *N*-Boc proline, Cs_2CO_3 and 456-nm light irradiation for 24 h. The peak at 12.598 min corresponds to acetophenone.

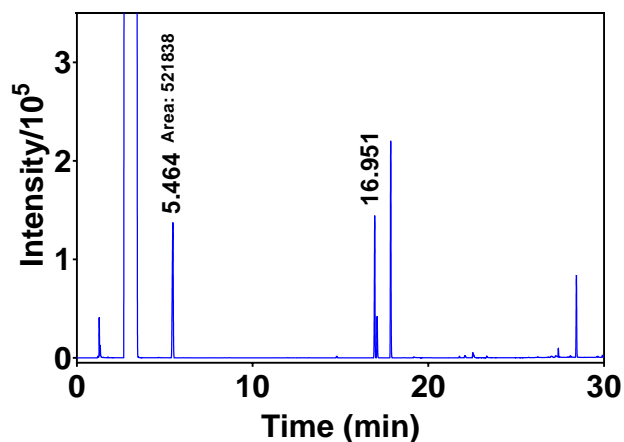


Fig. S48 GC chromatogram of the hydrodehalogenation reaction of 4-bromoanisole (Table 4) in the presence of **1**, *N*-Boc proline, Cs₂CO₃ and 456-nm light irradiation for 24 h. The peaks at 5.464 and 16.951 min correspond to anisole and 4-bromoanisole, respectively.

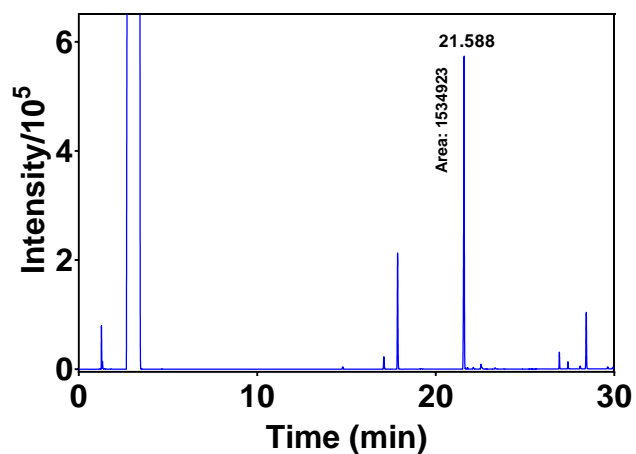


Fig. S49 GC chromatogram of the hydrodehalogenation reaction of 4-bromobiphenyl (Table 4) in the presence of **1**, *N*-Boc proline, Cs₂CO₃ and 456-nm light irradiation for 24 h. The peak at 21.588 min corresponds to biphenyl.

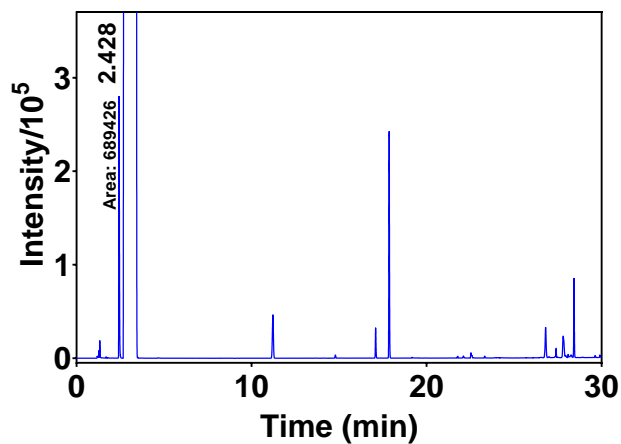


Fig. S50 GC chromatogram of the hydrodehalogenation reaction of 4-bromotoluene (Table 4) in the presence of **1**, *N*-Boc proline, Cs₂CO₃ and 456-nm light irradiation for 24 h. The peak at 2.428 min corresponds to toluene.

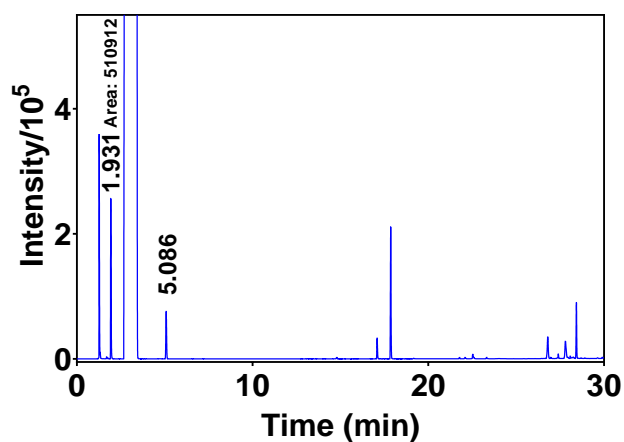


Fig. S51 GC chromatogram of the hydrodehalogenation reaction of 2-chlorobenzotrifluoride (Table 4) in the presence of **1**, *N*-Boc proline, Cs₂CO₃ and 456-nm light irradiation for 24 h. The peaks at 1.931 and 5.086 min corresponds to α,α,α -trifluorotoluene and 2-chlorobenzotrifluoride, respectively.

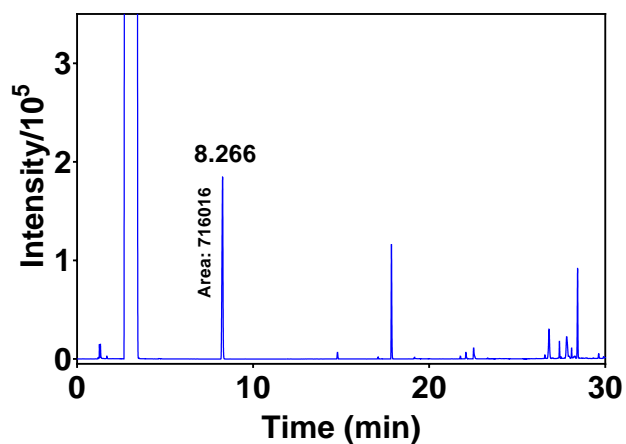


Fig. S52 GC chromatogram of the hydrodehalogenation reaction of 4-chlorobenzonitrile (Table 4) in the presence of **1**, *N*-Boc proline, Cs₂CO₃ and 456-nm light irradiation for 24 h. The peak at 8.266 corresponds to benzonitrile.

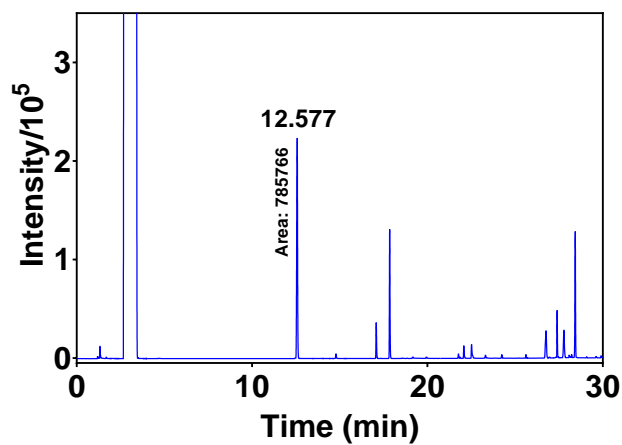


Fig. S53 GC chromatogram of the hydrodehalogenation reaction of 4-bromoacetophenone (Table 4) in the presence of **Ir-mod** ($t_{\text{irra}} = 8$ h), *N*-Boc proline, Cs₂CO₃ and 456-nm light irradiation for 24 h. The peak at 12.577 min correspond to acetophenone.

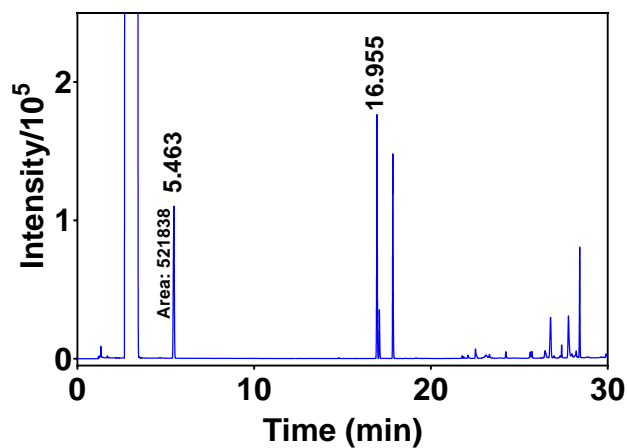


Fig. S54 GC chromatogram of the hydrodehalogenation reaction of 4-bromoanisole (Table 4) in the presence of **Ir-mod** ($t_{\text{irra}} = 8$ h), *N*-Boc proline, Cs_2CO_3 and 456-nm light irradiation for 24 h. The peaks at 5.463 and 16.955 correspond to anisole and 4-bromoanisole, respectively.

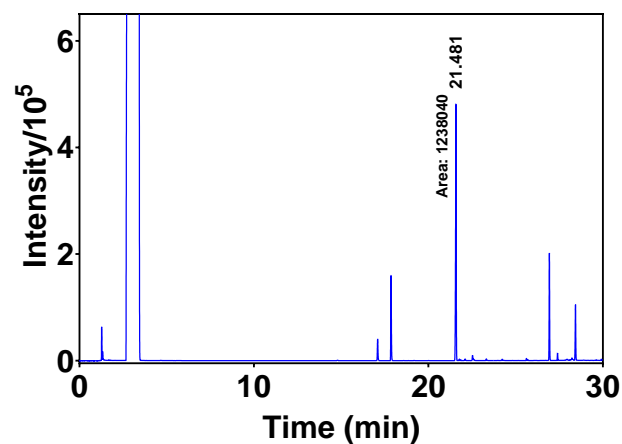


Fig. S55 GC chromatogram of the hydrodehalogenation reaction of 4-bromobiphenyl (Table 4) in the presence of **Ir-mod** ($t_{\text{irra}} = 8$ h), *N*-Boc proline, Cs_2CO_3 and 456-nm light irradiation for 24 h. The peak at 21.481 min corresponds to biphenyl.

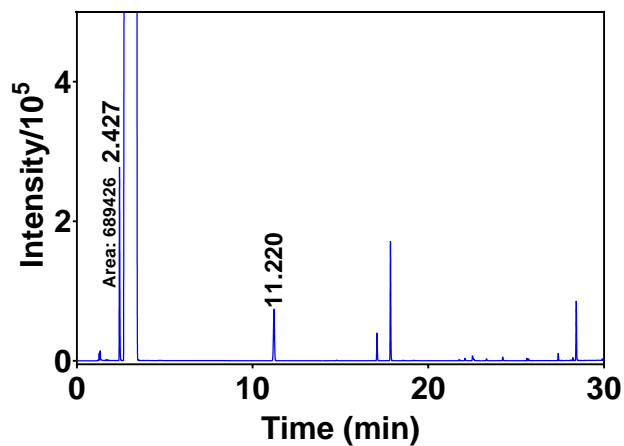


Fig. S56 GC chromatogram of the hydrodehalogenation reaction of 4-bromotoluene (Table 4) in the presence of **Ir-mod** ($t_{\text{irra}} = 8$ h), *N*-Boc proline, Cs₂CO₃ and 456-nm light irradiation for 24 h. The peaks at 2.428 and 11.220 min correspond to toluene and 4-bromotoluene, respectively.

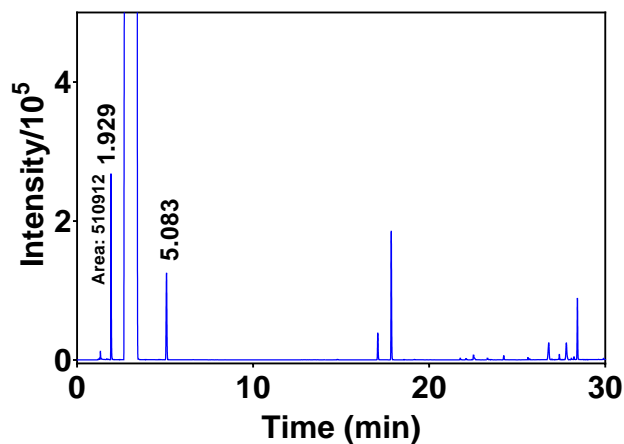


Fig. S57 GC chromatogram of the hydrodehalogenation reaction of 2-chlorobenzotrifluoride (Table 4) in the presence of **Ir-mod** ($t_{\text{irra}} = 8$ h), *N*-Boc proline, Cs₂CO₃ and 456-nm light irradiation for 24 h. The peaks at 1.929 and 5.083 min correspond to α, α, α -trifluorotoluene and 2-chlorobenzotrifluoride, respectively.

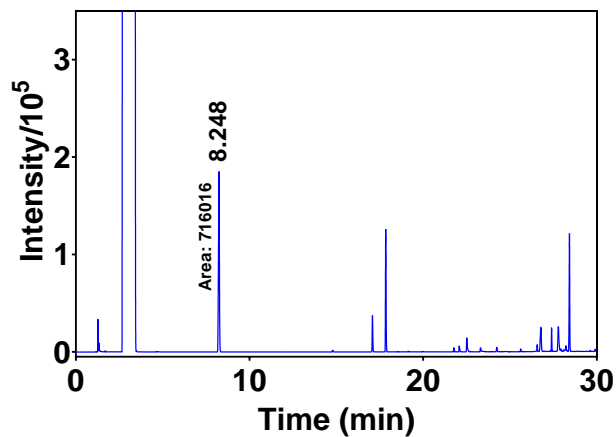


Fig. S58 GC chromatogram of the hydrodehalogenation reaction of 4-chlorobenzonitrile (Table 4) in the presence of **Ir-mod** ($t_{\text{irra}} = 8$ h), *N*-Boc proline, Cs_2CO_3 and 456-nm light irradiation for 24 h. The peak at 8.248 corresponds to benzonitrile.

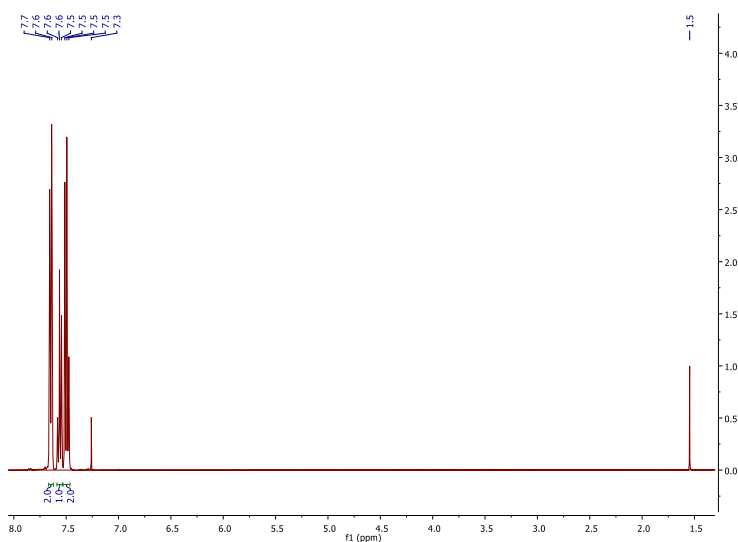


Fig. S59 ¹H NMR (400 MHz, CDCl_3) of a standard α,α,α -trifluorotoluene.

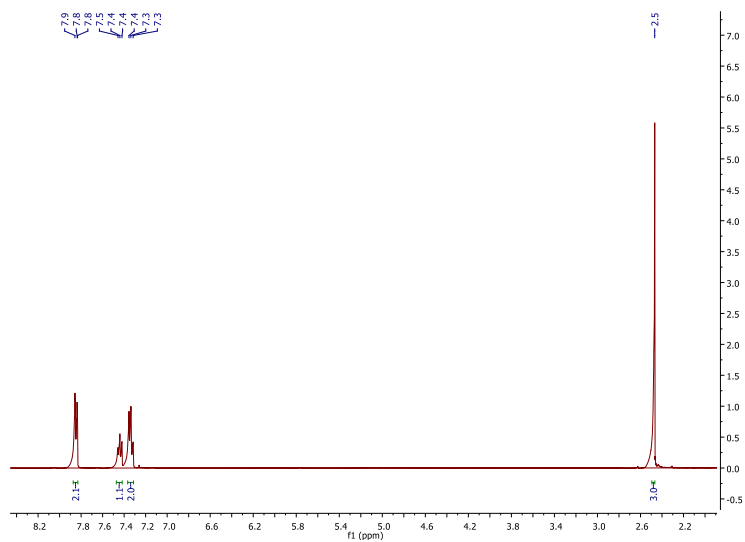


Fig. S60 ^1H NMR (400 MHz, CDCl_3) of a standard acetophenone.

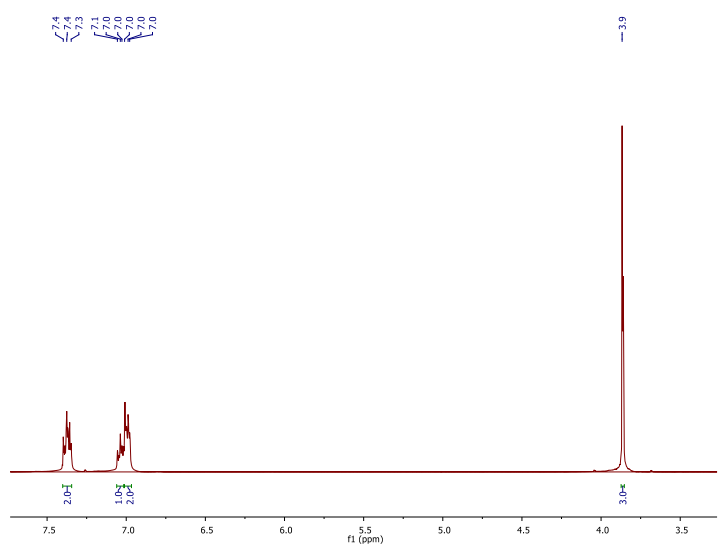


Fig. S61 ^1H NMR (400 MHz, CDCl_3) of a standard anisole.

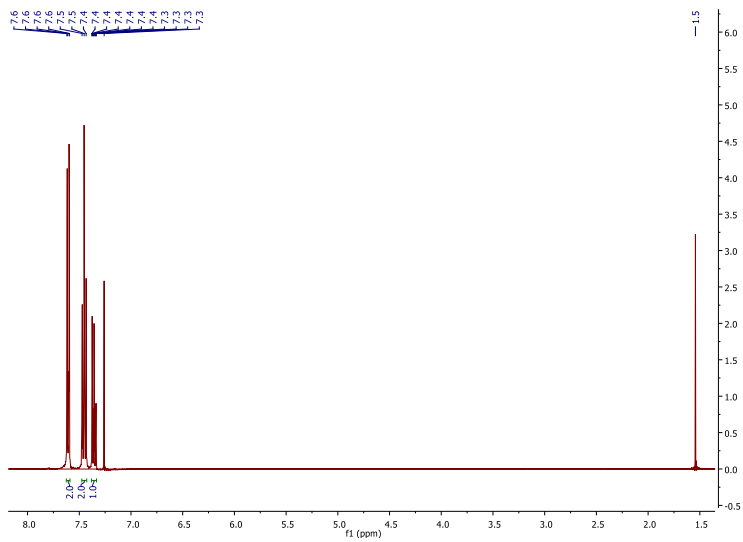


Fig. S62 ¹H NMR (400 MHz, CDCl₃) of a standard biphenyl.

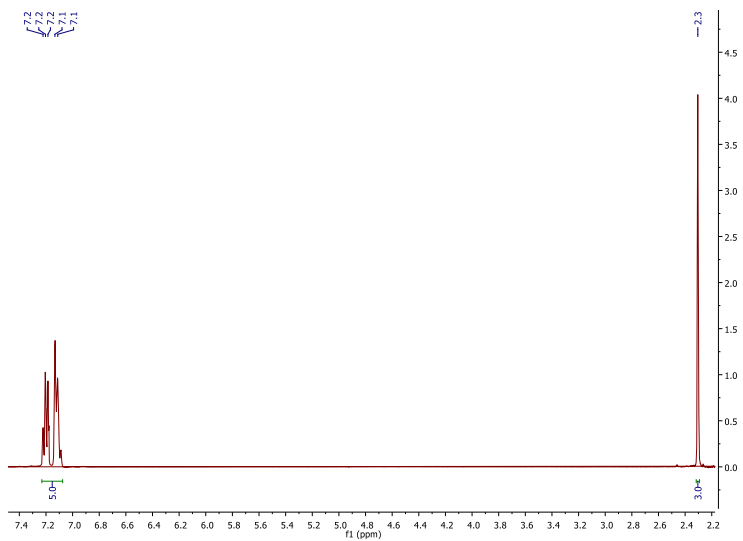


Fig. S63 ¹H NMR (400 MHz, CDCl₃) of a standard toluene.

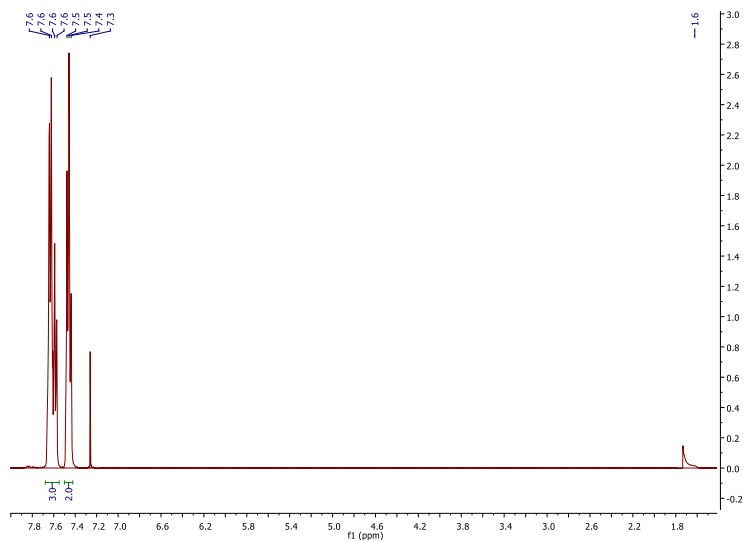


Fig. S64 ^1H NMR (400 MHz, CDCl_3) of a standard benzonitrile.

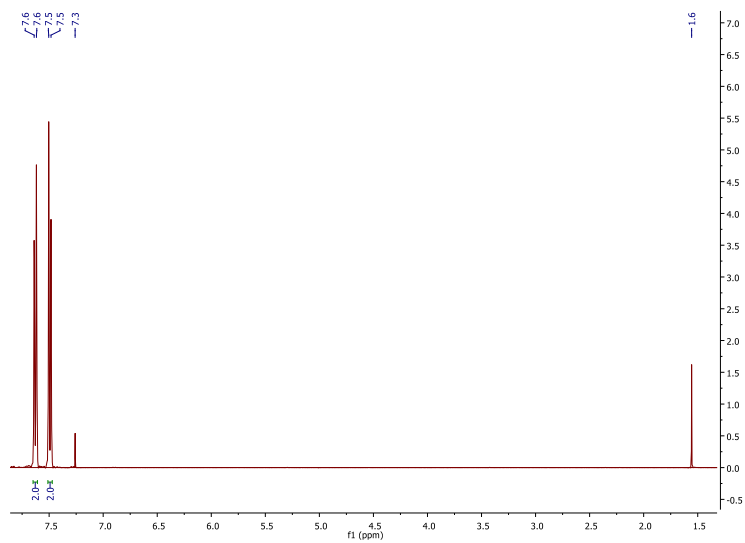


Fig. S65 ^1H NMR (400 MHz, CDCl_3) of a standard 4-bromobenzotrifluoride.

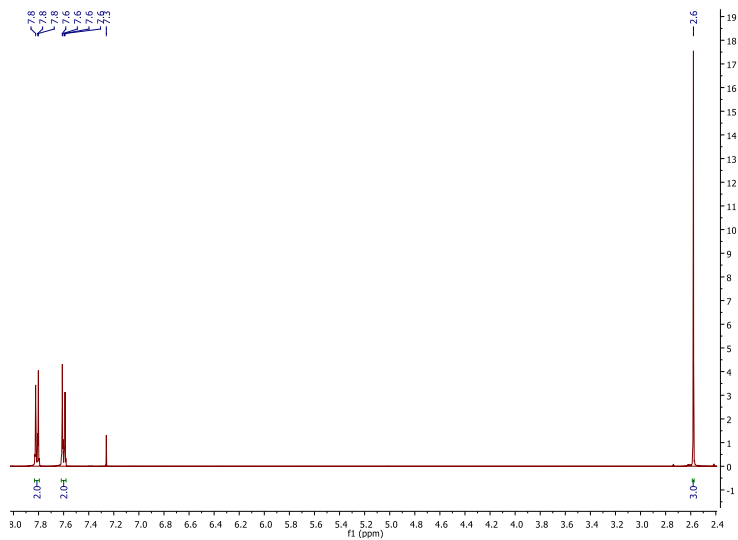


Fig. S66 ¹H NMR (400 MHz, CDCl₃) of a standard 4-bromoacetophenone

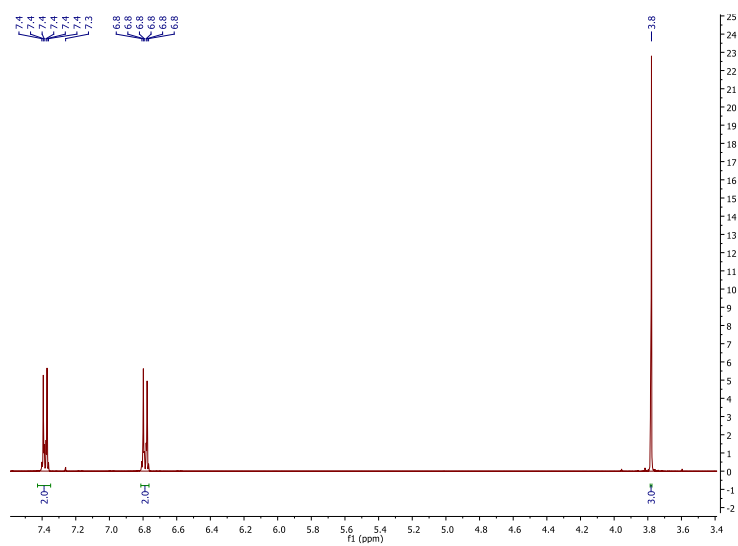


Fig. S67 ¹H NMR (400 MHz, CDCl₃) of a standard 4-bromoanisole.

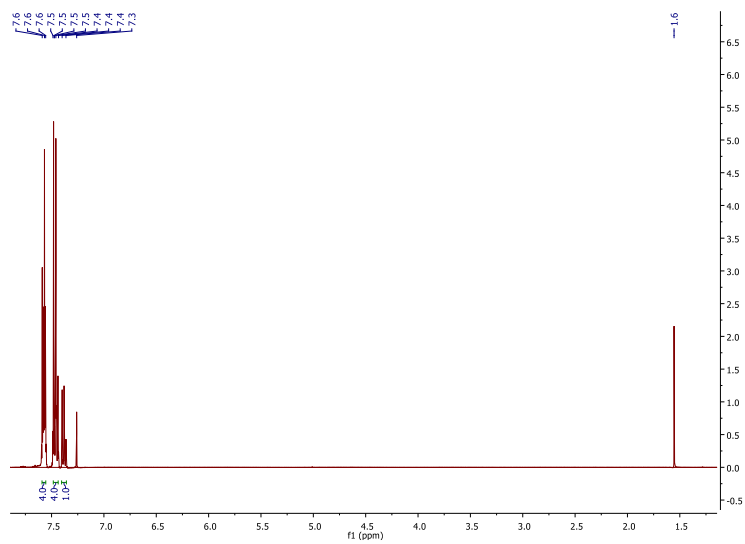


Fig. S68 ^1H NMR (400 MHz, CDCl_3) of a standard 4-bromobiphenyl.

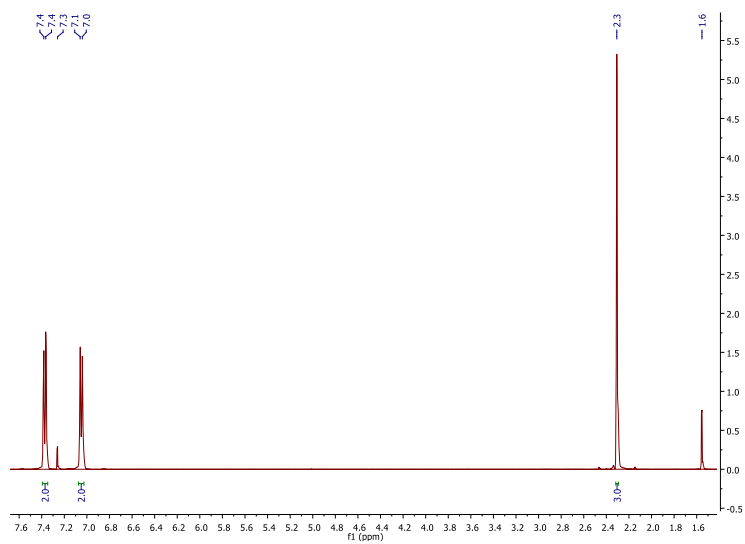


Fig. S69 ^1H NMR (400 MHz, CDCl_3) of a standard 4-bromotoluene.

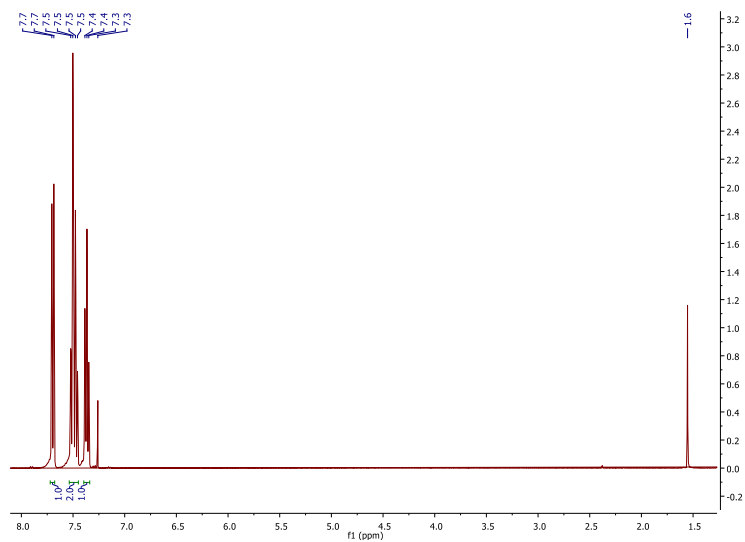


Fig. S70 ^1H NMR (400 MHz, CDCl_3) of a standard 2-chlorobenzotrifluoride.

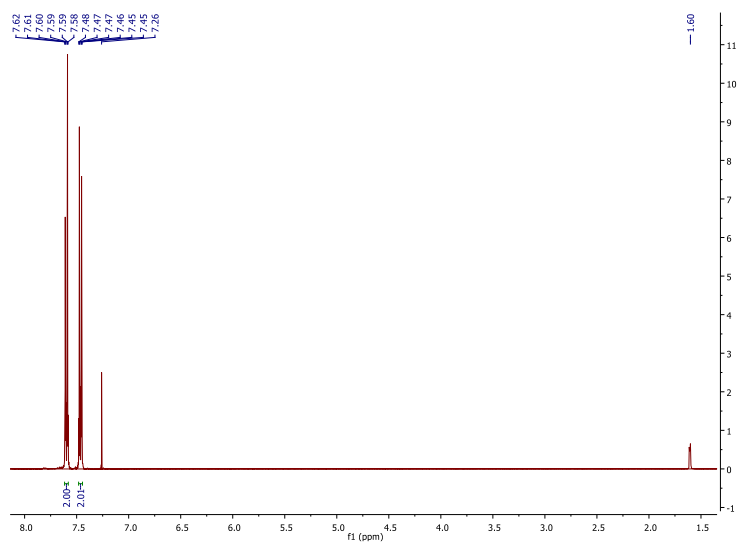


Fig. S71 ^1H NMR (400 MHz, CDCl_3) of a standard 4-chlorobenzonitrile.

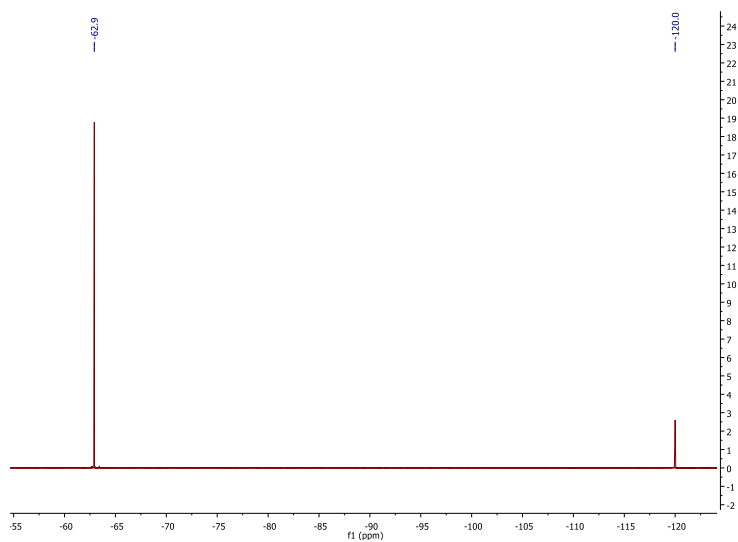


Fig. S72 ^{19}F NMR (400 MHz, DMF, 4-fluorotoluene as internal standard) of a standard 4-bromobenzotrifluoride.

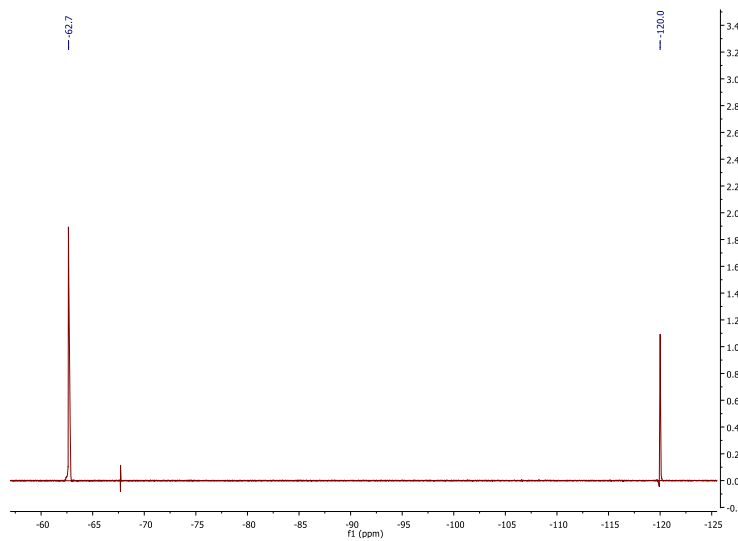


Fig. S73 ^{19}F NMR (400 MHz, DMF, 4-fluorotoluene as internal standard) of a standard 2-chlorobenzotrifluoride.

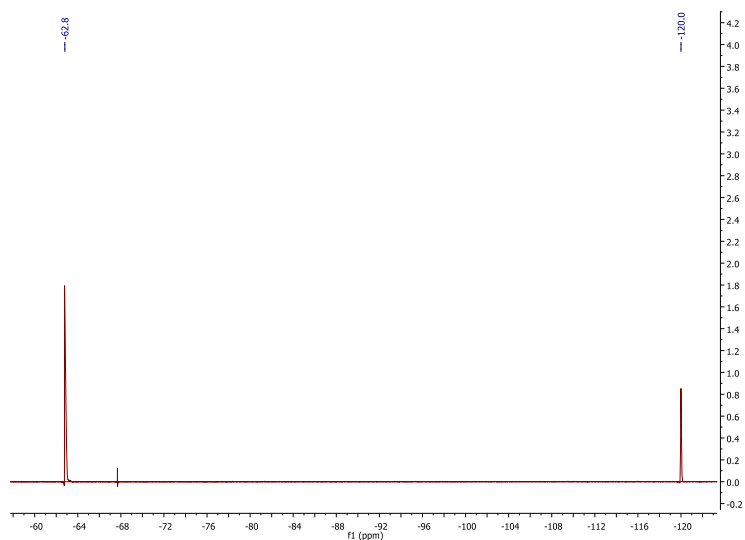


Fig. S74 ^{19}F NMR (400 MHz, DMF, 4-fluorotoluene as internal standard) of a standard α,α,α -trifluorotoluene.

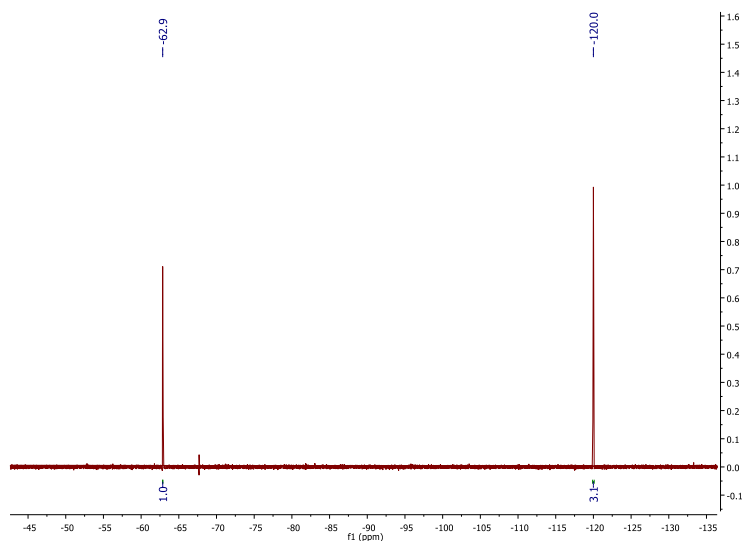


Fig. S75 ^{19}F NMR (400 MHz, DMF, 4-fluorotoluene as internal standard) of the hydrodehalogenation reaction of 4-bromobenzotrifluoride in the absence of iridium complex and *N*-Boc proline, and presence of Cs_2CO_3 and 456-nm light irradiation for 24 h (entry 1, Table 4). The peaks at -62.9 and -120.0 ppm correspond to 4-bromobenzotrifluoride and 4-fluorotoluene, respectively.

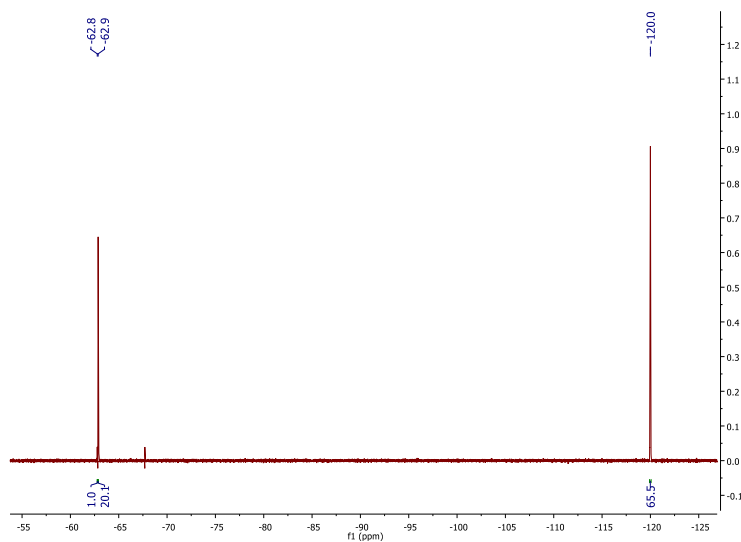


Fig. S76 ¹⁹F NMR (400 MHz, DMF, 4-fluorotoluene as internal standard) of the hydrodehalogenation reaction of 4-bromobenzotrifluoride in the presence of **1**, Cs₂CO₃ and 456-nm light irradiation for 24 h, and absence of *N*-Boc proline (entry 2, Table 4). The peaks at -62.8, -62.9 and -120.0 ppm correspond to α,α,α -trifluorotoluene, 4-bromobenzotrifluoride and 4-fluorotoluene, respectively.

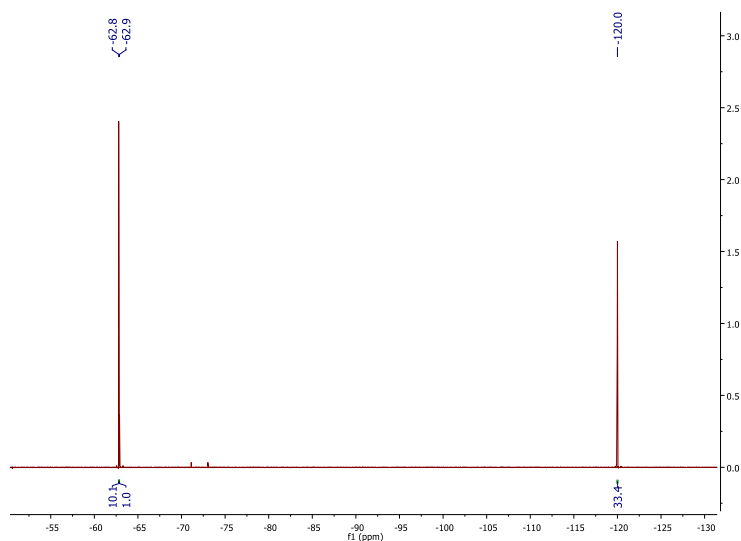


Fig. S77 ¹⁹F NMR (400 MHz, DMF, 4-fluorotoluene as internal standard) of the hydrodehalogenation reaction of 4-bromobenzotrifluoride of **1**, *N*-Boc proline, Cs₂CO₃ and 456-nm light irradiation for 24 h (entry 3, Table 5). The peak at -62.8, -62.9 and -120.0 correspond to α,α,α -trifluorotoluene, 4-bromobenzotrifluoride and 4-fluorotoluene, respectively

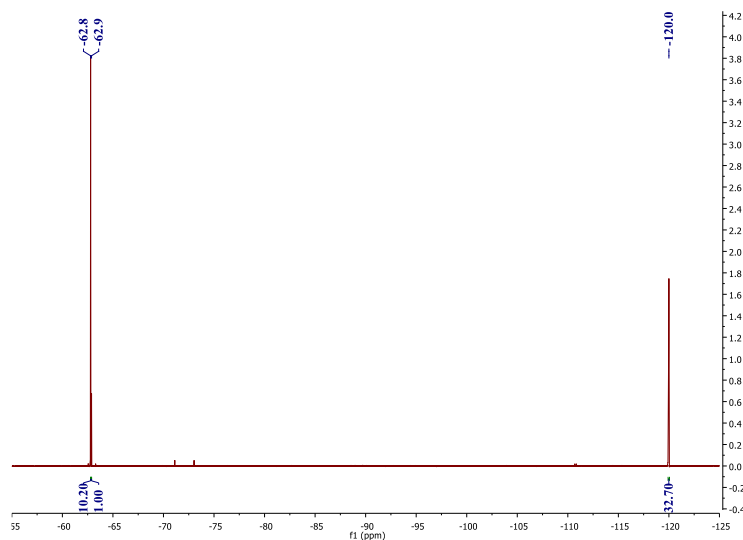


Fig. S78 ^{19}F NMR (400 MHz, DMF, 4-fluorotoluene as internal standard) of the hydrodehalogenation reaction of 4-bromobenzotrifluoride in the presence of **2**, *N*-Boc proline, Cs_2CO_3 and 456-nm light irradiation for 24 h (entry 4, Table 5). The peaks at -62.8, -62.9 and -120.0 ppm correspond to α,α,α -trifluorotoluene, 4-bromobenzotrifluoride and 4-fluorotoluene, respectively.

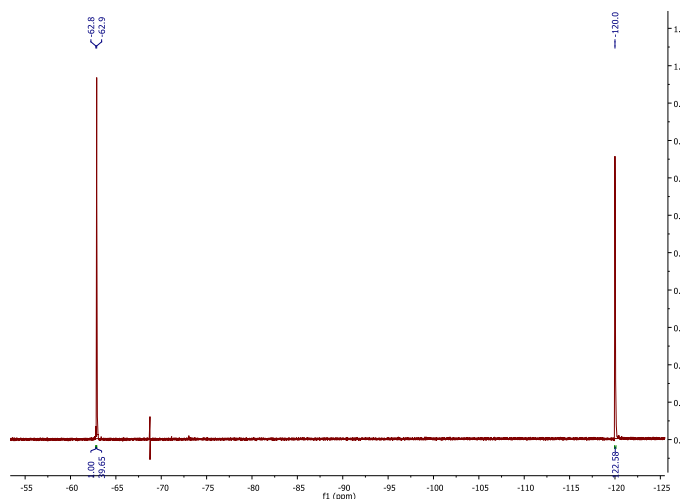


Fig. S79 ^{19}F NMR (400 MHz, DMF, 4-fluorotoluene as internal standard) of the hydrodehalogenation reaction of 4-bromobenzotrifluoride in the absence of *N*-Boc proline and Cs_2CO_3 , and presence of **2** and 456-nm light irradiation for 24 h. The peaks at -62.8, -62.9 and -120.0 ppm correspond to α,α,α -trifluorotoluene, 4-bromobenzotrifluoride and 4-fluorotoluene, respectively.

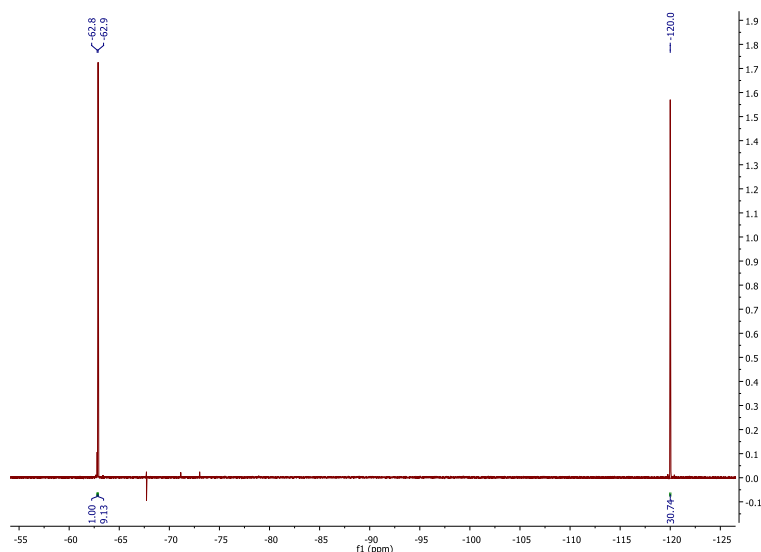


Fig. S80 ^{19}F NMR (400 MHz, DMF, 4-fluorotoluene as internal standard) of the hydrodehalogenation reaction of 4-bromobenzotrifluoride in the absence of *N*-Boc proline, and presence of **2** and Cs_2CO_3 and 456-nm light irradiation for 24 h. The peaks at -62.8, - 62.9 and - 120.0 ppm correspond to α,α,α -trifluorotoluene, 4-bromobenzotrifluoride and 4-fluorotoluene, respectively.

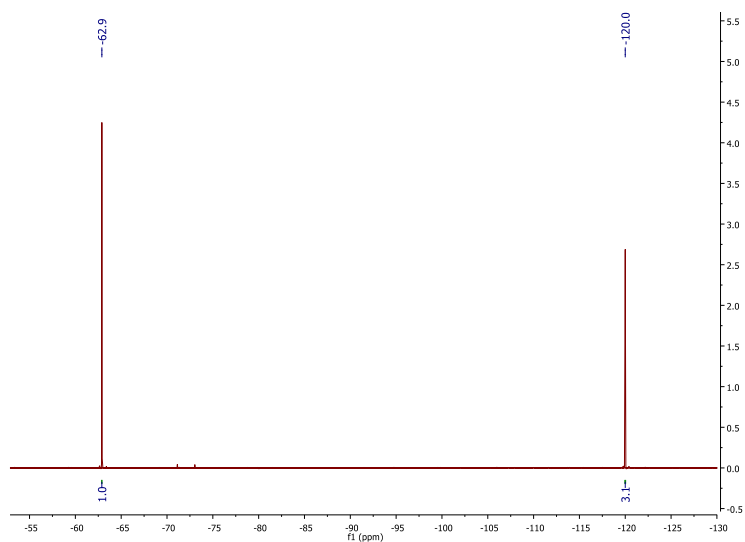


Fig. S81 ^{19}F NMR (400 MHz, DMF, 4-fluorotoluene as internal standard) of the hydrodehalogenation reaction of 4-bromobenzotrifluoride in the presence of **Ir-mod** ($t_{\text{irra}} = 8$ h), *N*-Boc proline and Cs_2CO_3 in the dark (entry 6, Table 4). The peaks at -62.90 and -120.00 ppm correspond to 4-bromobenzotrifluoride and 4-fluorotoluene, respectively.

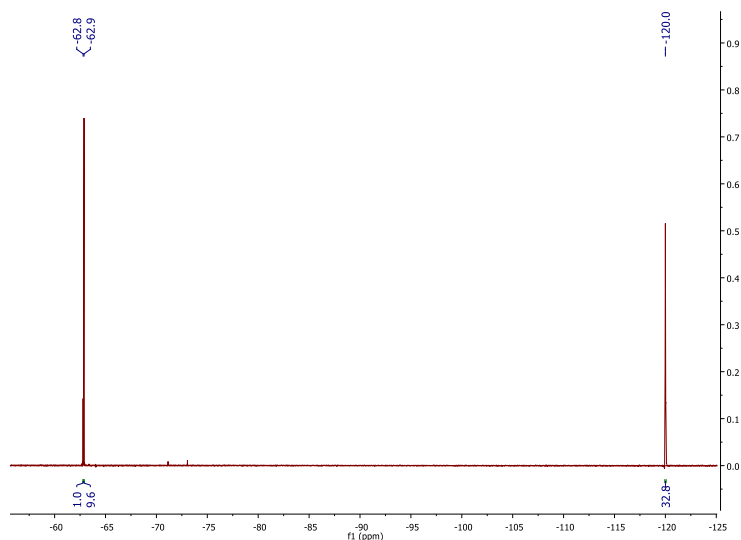


Fig. S82 ¹⁹F NMR (400 MHz, DMF, 4-fluorotoluene as internal standard) of the hydrodehalogenation reaction of 4-bromobenzotrifluoride in the presence of **Ir-mod** ($t_{\text{irra}} = 8$ h), Cs₂CO₃ and 456-nm light irradiation for 24 h, and absence of *N*-Boc proline (entry 7, Table 4). The peaks at -62.8, -62.9 and -120.0 ppm correspond to α,α,α -trifluorotoluene, 4-bromobenzotrifluoride and 4-fluorotoluene, respectively.

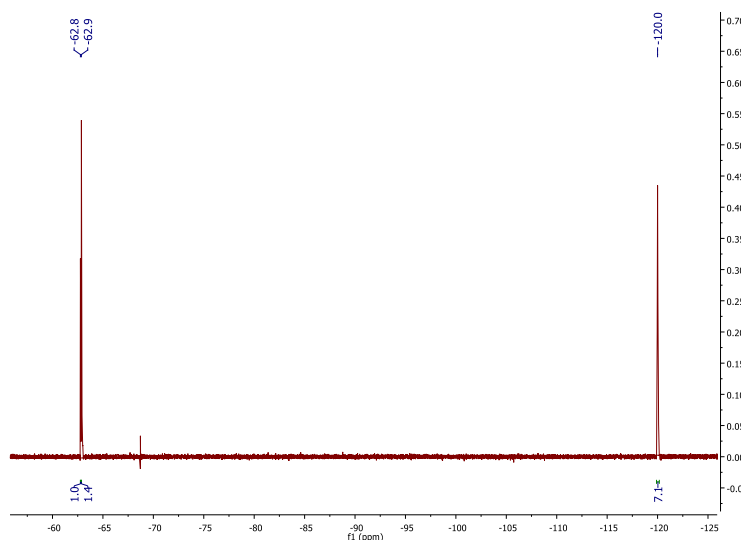


Fig. S83 ¹⁹F NMR (400 MHz, DMF, 4-fluorotoluene as internal standard) of the hydrodehalogenation reaction of 4-bromobenzotrifluoride in the presence of **Ir-mod** ($t_{\text{irra}} = 8$ h), DBU and 456-nm light irradiation for 24 h (entry 8, Table 4). The peaks at -62.8, -62.9 and -120.0 ppm correspond to α,α,α -trifluorotoluene, 4-bromobenzotrifluoride and 4-fluorotoluene, respectively.

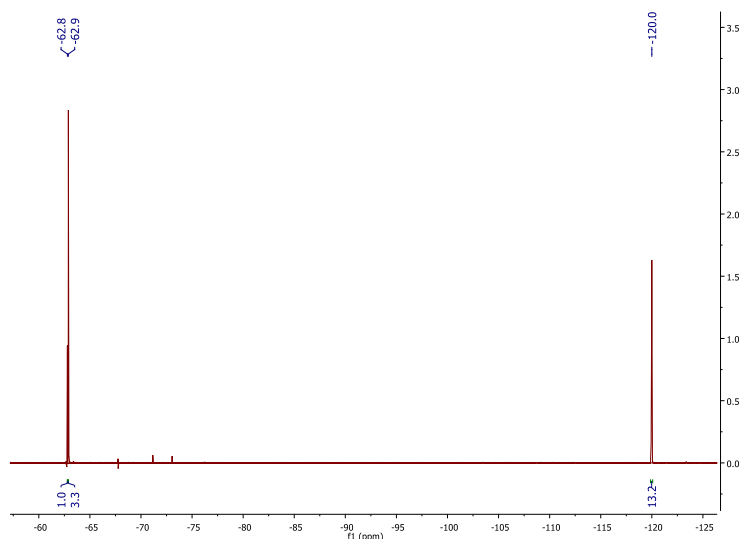


Fig. S84 ^{19}F NMR (400 MHz, DMF, 4-fluorotoluene as internal standard) of the hydrodehalogenation reaction of 4-bromobenzotrifluoride in the presence of **Ir-mod** ($t_{\text{irra}} = 8$ h), TMG and 456-nm light irradiation for 24 h (entry 9, Table 4). The peaks at -62.8, -62.9 and -120.0 ppm correspond to α,α,α -trifluorotoluene, 4-bromobenzotrifluoride and 4-fluorotoluene, respectively.

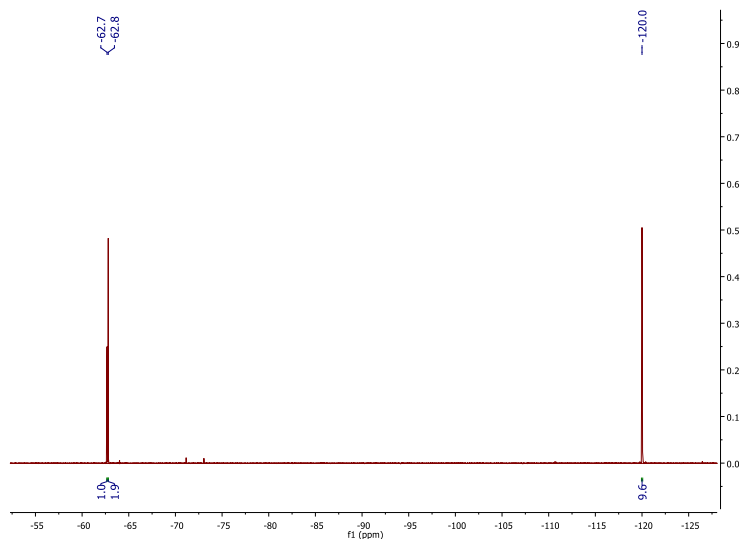


Fig. S85 ^{19}F NMR (400 MHz, DMF, 4-fluorotoluene as internal standard) of the hydrodehalogenation reaction of 2-chlorobenzotrifluoride (**6** in Table 5) in the presence of **1**, *N*-Boc proline, Cs_2CO_3 and 456-nm light irradiation for 24 h. The peaks at -62.7, -62.8 and -120.0 ppm correspond to 2-chlorobenzotrifluoride, α,α,α -trifluorotoluene and 4-fluorotoluene, respectively.

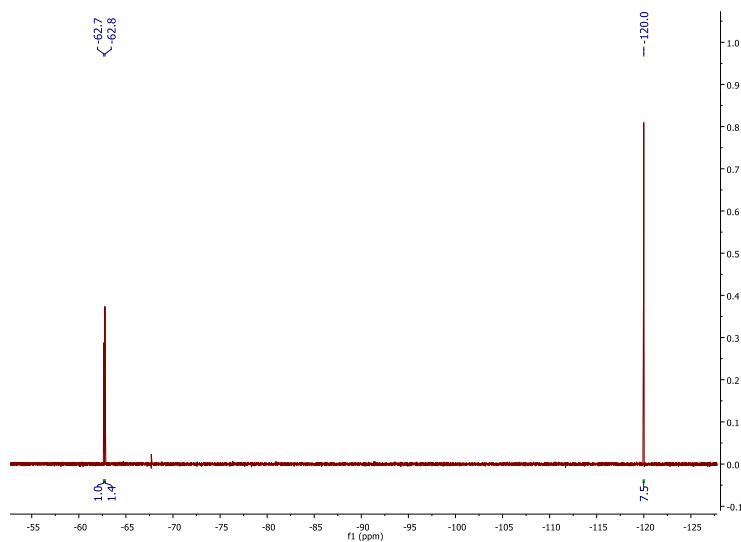


Fig. S86 ¹⁹F NMR (400 MHz, DMF, 4-fluorotoluene as internal standard) of the hydrodehalogenation reaction of 2-chlorobenzotrifluoride 2-chlorobenzotrifluoride (**6** in Table 5) in the presence of **Ir-mod** ($t_{\text{irra}} = 8$ h), *N*-Boc proline, Cs₂CO₃ and 456-nm light irradiation for 24 h. The peaks at -62.7, -62.8 and -120.0 correspond to α,α,α -trifluorotoluene, benzotrifluoride and 4-fluorotoluene, respectively.

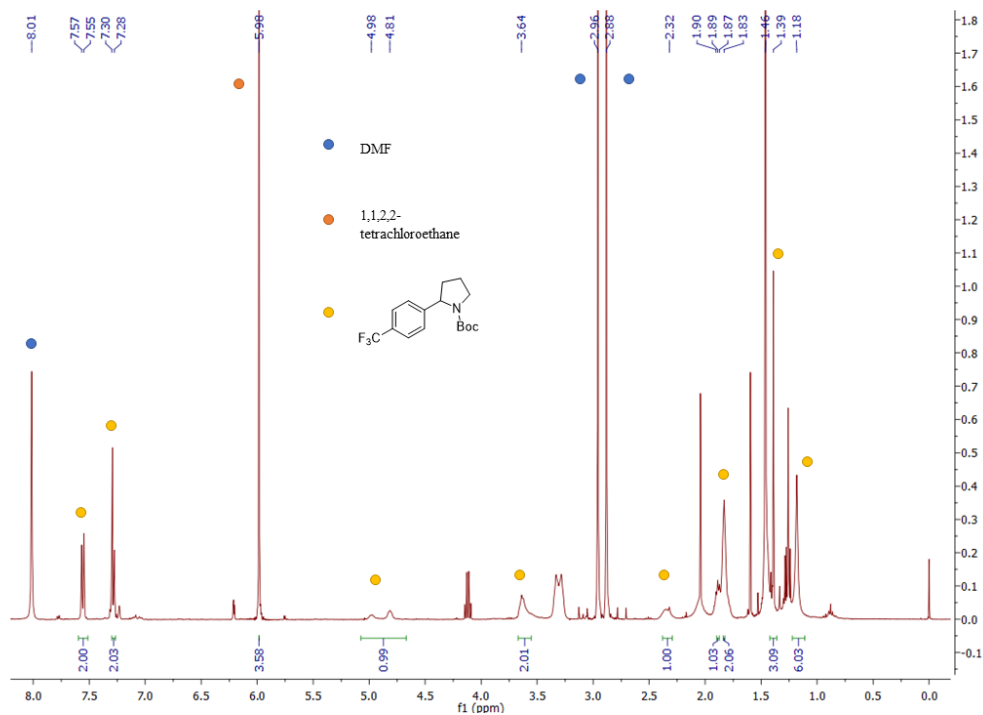
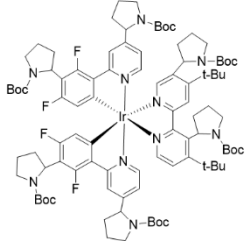
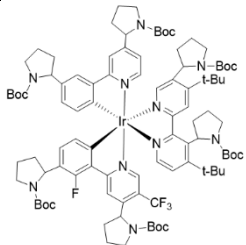
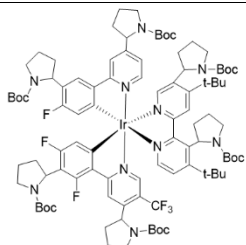
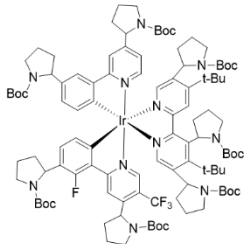
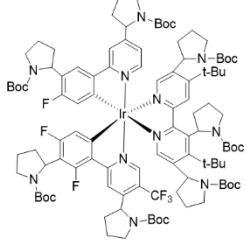
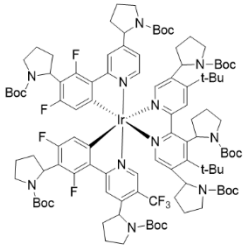
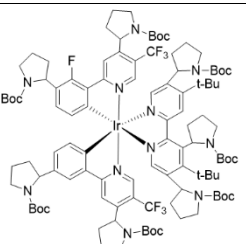
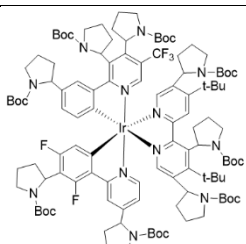
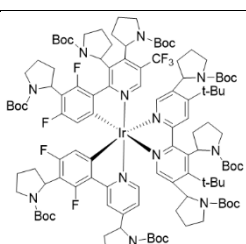


Fig. S87 ^1H NMR (400 MHz, CDCl_3 , 1,1,2,2-tetrachloroethane as internal standard) of the reaction **Ir-mod**/Ni dual-catalyzed decarboxylative cross-coupling of *N*-Boc proline and 4-bromobenzotrifluoride. Assignments are labelled.

S1. SUPPLEMENTARY TABLES

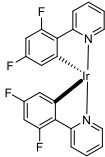
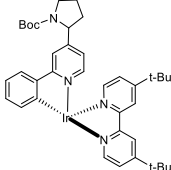
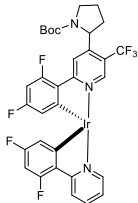
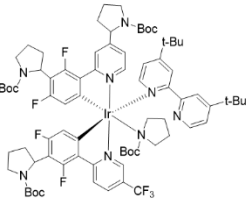
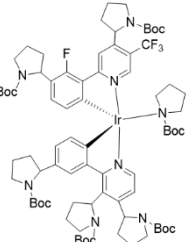
Table S1 Assignment of the experimental m/z peaks to possible intact Ir-complexes **Ir-int.**

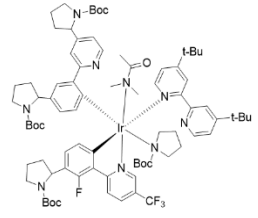
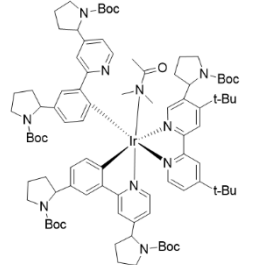
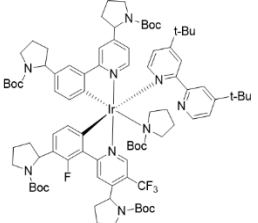
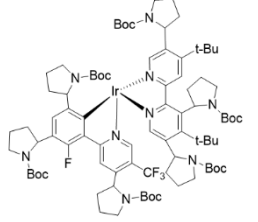
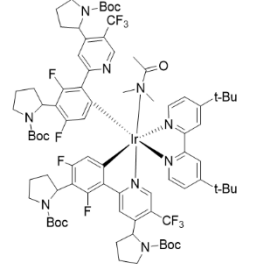
No	m/z	Loss of F	Loss of CF ₃	Substitution of NBP	Possible structure (Exact mass)
1	1855.5	0	2	6	 <p>(1855.9)</p>
2	1870.4	3	1	6	 <p>(1869.9)</p>
3	1907.3	1	1	6	 <p>(1905.9)</p>
4	2038.8	3	1	7	 <p>(2039.0)</p>

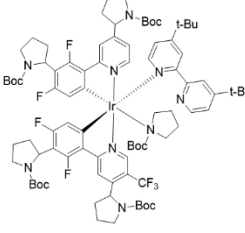
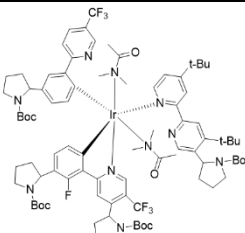
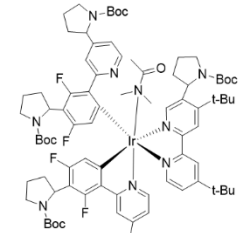
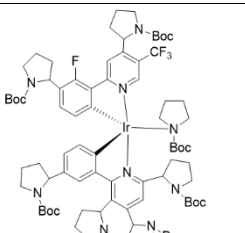
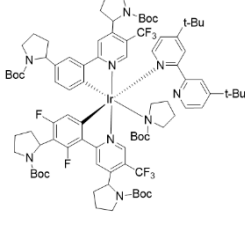
5	2075.6	1	1	7	 <p>(2075.0)</p>
6	2092.6	0	1	7	 <p>(2093.0)</p>
7	2108.5	3	0	7	 <p>(2107.0)</p>
8	2226.2	2	1	8	 <p>(2226.1)</p>
9	2263.2	0	1	8	 <p>(2262.1)</p>

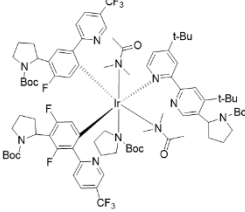
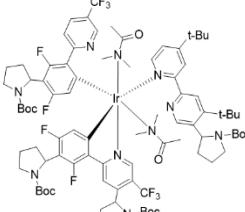
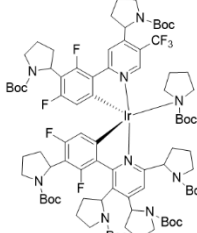
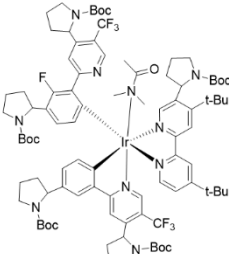
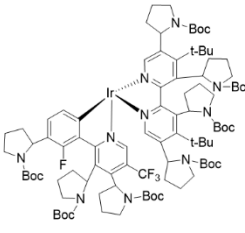
10	2277.0	3	0	8	<p>(2276.1)</p>
----	--------	---	---	---	-----------------

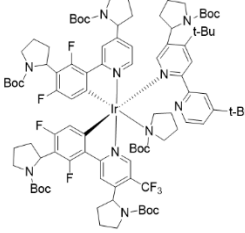
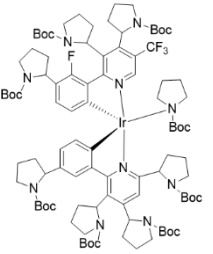
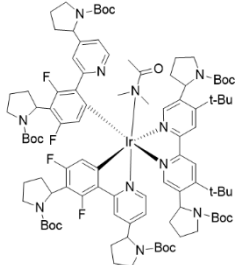
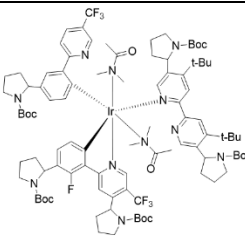
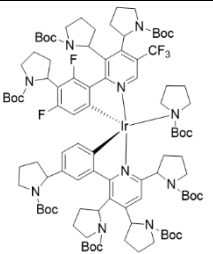
Table S2 Assignment of the experimental m/z peaks to possible degraded Ir-complexes **Ir-deg**.

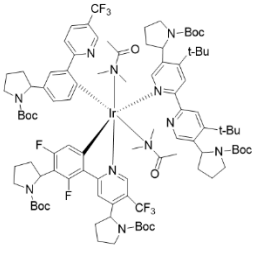
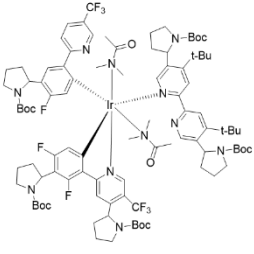
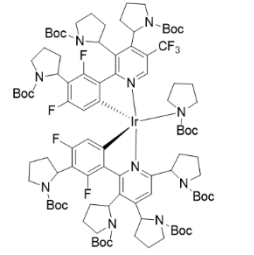
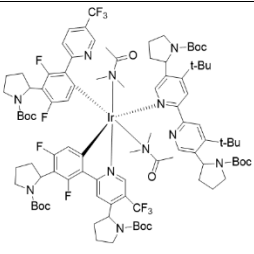
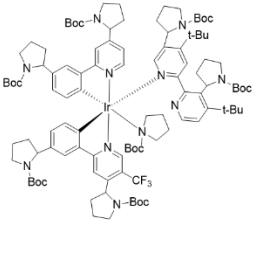
No	m/z	Loss of F	Loss of CF ₃	Substitution of NBP	Loss of ligand	N-Boc Proline coordination	DMF coordination	Proposed structure (Exact mass)
1	573.1	0	2	0	N^N	0	0	 (573.1)
2	783.6	2	1	1	C^N	0	0	 (784.3)
3	811.6	0	1	1	N^N	0	0	 (810.2)
4	1587.4	0	1	3	-	1	0	 (1587.7)
5	1605.1	3	1	5	N^N	1	0	 (1603.8)

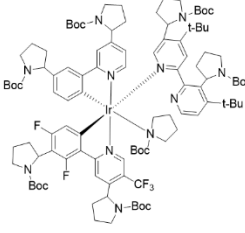
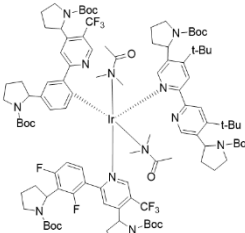
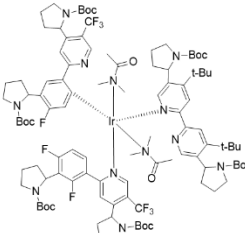
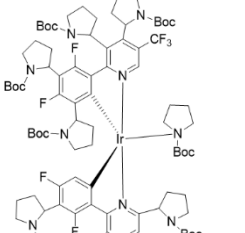
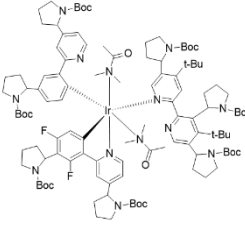
6	1621.2	3	1	3	-	1	1	 <p>(1620.8)</p>
7	1703.0	4	2	5	-	0	1	 <p>(1701.9)</p>
8	1703.0	3	1	4	-	1	0	 <p>(1702.8)</p>
9	1715.8	1	0	6	C^N	0	0	 <p>(1715.9)</p>
10	1740.8	0	0	4	-	0	1	 <p>(1740.7)</p>

11	1757.8	0	1	4	-	1	0	 <p>(1756.8)</p>
12	1773.7	3	0	4	-	0	2	 <p>(1773.8)</p>
13	1773.7	0	2	5	-	0	1	 <p>(1773.9)</p>
14	1773.7	3	1	5	N^N	1	0	 <p>(1772.9)</p>
15	1788.6	2	0	4	-	1	0	 <p>(1788.8)</p>

16	1812.5	1	0	3	-	1	2	 <p>(1811.8)</p>
17	1827.5	0	0	4	-	0	2	 <p>(1827.8)</p>
18	1827.5	0	1	6	N^N	1	0	 <p>(1826.8)</p>
19	1855.5	3	0	5	-	0	1	 <p>(1855.9)</p>
20	1885.3	1	0	7	C^N	0	0	 <p>(1885.0)</p>

21	1926.1	0	1	5	-	1	0	 <p>(1925.9)</p>
22	1942.0	3	1	7	-	1	0	 <p>(1942.0)</p>
23	1942.1	0	2	6	-	0	1	 <p>(1943.0)</p>
24	1942.1	3	0	5	-	0	2	 <p>(1942.9)</p>
25	1960.1	2	1	7	N^N	1	0	

								(1960.0)
26	1960.1	2	0	5	-	0	2	 (1960.9)
27	1980.1	1	0	5	-	0	2	 (1978.9)
28	1996.9	0	1	7	N^N	1	0	 (1995.9)
29	1996.9	0	0	5	-	0	2	 (1996.9)
30	2023.9	4	1	6	-	1	0	 (2023.0)

31	2059.7	2	1	6	-	1	0	 <p>(2059.0)</p>
32	2132.4	2	0	6	-	0	2	 <p>(2131.0)</p>
33	2150.3	1	0	6	-	0	2	 <p>(2149.0)</p>
34	2165.3	0	1	8	N^N	1	0	 <p>(2165.0)</p>
35	2165.3	2	1	7	-	1	0	 <p>(2165.0)</p>

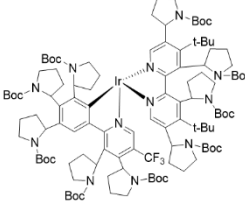
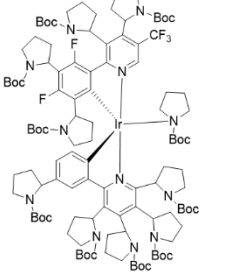
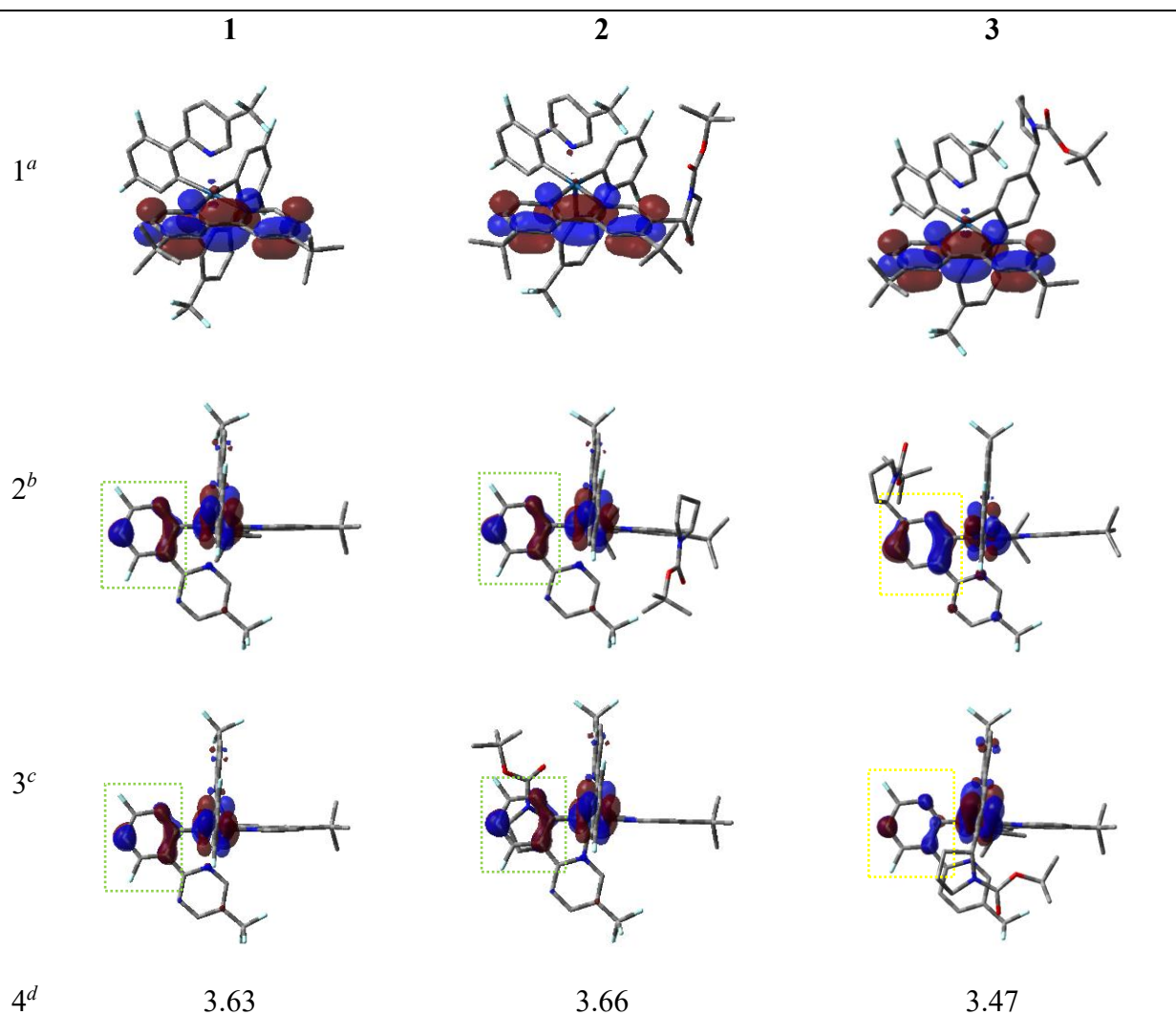
36	2206.2	2	0	9	C^N	0	0	 <p>(2205.2)</p>
37	2298.9	2	1	9	N^N	1	0	 <p>(2298.2)</p>

Table S3 Isodensity surface plots of the LUMO (row 1) and HOMO (row 2 and 3), and HOMO-LUMO gap (row 4) for **1**, **2** and **3**.



a isodensity surface plot of the LUMO; b isodensity surface plot of the HOMO with a planar view of the phenyl ring of the modified C[^]N ligand in **3** (in yellow box), and corresponding phenyl ring in **1** and **2** (in green box); c isodensity surface plot of the HOMO with a planar view of the phenyl ring of the unmodified C[^]N ligand in **3** (in yellow box), and corresponding phenyl ring in **1** and **2** (in green box); d HOMO-LUMO gap (eV).

Density Functional Theory (DFT) calculations are performed on **1** and **2**. In addition, an Ir complex with a NBP attached onto one of the C[^]N ligands with both F atoms removed is also examined (**3** in Fig. 1). Compound **3** is chosen as a model compound to demonstrate, *via* computational

chemistry calculation, the effect of NBP unit substituted on the cyclometallating (C[^]N) ligand. **3** was not isolated experimentally but is instead used solely to understand through computational chemistry calculations the destabilisation of the HOMO upon addition of an electron-donating NBP and removal of electron-withdrawing fluorine atoms from the C[^]N ligand. In all the complexes studied, the LUMO is exclusively localized on the dtbbpy ligand (row 1, Table S3). On the other hand, for **1**, the HOMO is located on the metal center and phenyl rings of both dF(CF₃)ppy ligands (row 2 and row 3, Table S3). The NBP on dtbbpy in **2** does not affect the arrangement of either the LUMO or HOMO.

The removal of fluorine atoms from and attachment of NBP substituents to the phenyl ring of a C[^]N ligand in **3** result in a positive inductive effect that causes the HOMO to be more spread out over the carbon atoms of the aromatic ring (row 2, Table S3). In particular, the lobe size around the carbon substituted with the NBP is significantly increased. Furthermore, the contribution of the unmodified dF(CF₃)ppy ligand to the HOMO is decreased in **3** (row 3, Table S3). This is seen from the reduction in lobe size on the phenyl ring. Since the HOMO is dominated primarily by the transformed rather than intact C[^]N ligand, destabilization *via* NBP substitution and F atom elimination leads to a substantial rise in the HOMO energy relative to the energetically invariant LUMO in **3** (Fig. S9[†]), and the HOMO-LUMO energy gap decreases (row 4, Table S3).

Table S4 Crystallographic data collection details for **2**.

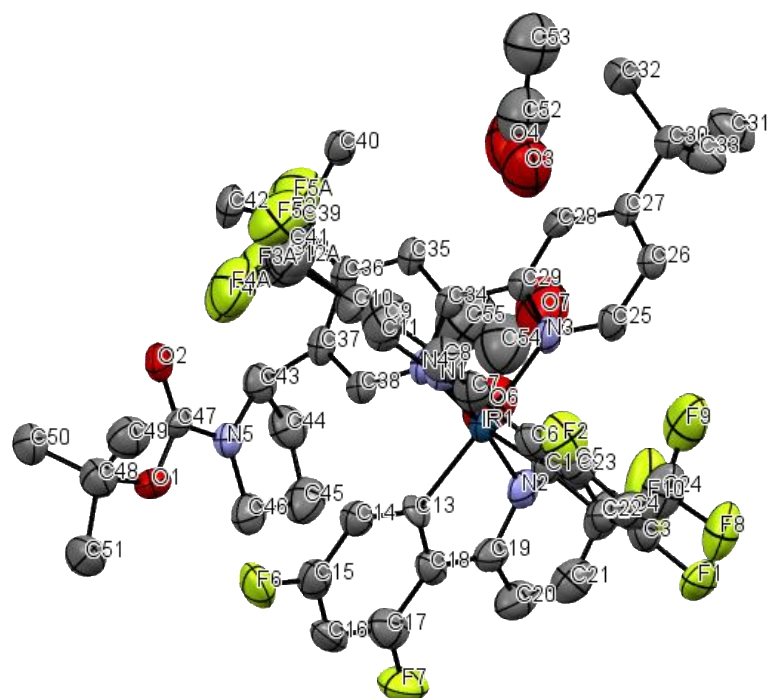
Axis	dx (mm)	2 θ ($^{\circ}$)	ω ($^{\circ}$)	φ ($^{\circ}$)	χ ($^{\circ}$)	Width ($^{\circ}$)	Frames	λ (\AA)	Voltage (kV)	Current (mA)
Omega	60.117	24.08	9.34	168.42	- 44.66	1.10	124	0.71073	50	1.4
Phi	60.117	24.05	-77.10	29.00	24.00	1.10	144	0.71073	50	1.4
Omega	60.117	- 24.08	- 124.04	- 123.39	23.00	1.10	115	0.71073	50	1.4

Table S5 Sample and Crystal Data for **2**.

Chemical Formula	$C_{53}H_{52}F_{10}IrN_5O_4$	
Formula Weight	1205.19 g/mol	
Temperature (K)	100(2)	
Wavelength (Å)	0.71073 Å	
Crystal Size (mm)	0.02 x 0.200 x 0.220	
Crystal Habit	Orange plate	
Crystal System	Orthorhombic	
Space Group	P b c n	
Unit Cell Dimensions	$a = 25.7591(5) \text{ \AA}$	$\alpha = 90^\circ$
	$b = 19.7247(4) \text{ \AA}$	$\beta = 90^\circ$
	$c = 22.7912(4) \text{ \AA}$	$\gamma = 90^\circ$
Volume (Å³)	11580.0(4)	
Z	8	
Density (calculated) (g/cm³)	1.383	
Absorption Coefficient (mm⁻¹)	2.382	
F(000)	4832	

Table S6 Data Collection and Structure Refinement for **2**.

Theta range for data collection	2.09 to 25.00°	
Index ranges	-28<=h<=30, -23<=k<=23, -22<=l<=27	
Reflections collected	89115	
Independent reflections	10205 [R(int) = 0.0761]	
Coverage of independent reflections	99.8%	
Absorption correction	Multi-Scan	
Max. and min. transmission	0.9540 and 0.6220	
Structure solution technique	Direct methods	
Structure solution program	XT, VERSION 2018/2	
Refinement method	Full-matrix least-squares on F2	
Refinement program	SHELXL-2018/3 (Sheldrick, 2018)	
Function minimized	$\Sigma w(F_o^2 - F_c^2)^2$	
Data / restraints / parameters	10180 / 332 / 728	
Goodness-of-fit on F²	1.115	
Δ/σ_{\max}	0.001	
Final R indices	7312 data; I>2 σ (I)	R1 = 0.0851, wR2 = 0.2300
	All data	R1 = 0.1087, wR2 = 0.2591
Weighting scheme	w=1/[$\sigma^2(F_o^2)+(0.1164P)^2+66.0654P$] where P=(F _o ² +2F _c ²)/3	
Largest diff. peak and hole	2.170 and -2.132 eÅ ⁻³	
R.M.S. deviation from mean	0.163 eÅ ⁻³	



The full structure and numbering scheme of **2**. Acetate counter anions are shown whereas hydrogen atoms are removed for clarity.

Table S7 Atomic coordinates and equivalent isotropic atomic displacement parameters (\AA^2) for **2**.

	x/a	y/b	z/c	U(eq)
Ir1	0.73427(2)	0.56287(2)	0.32951(2)	0.0732(2)
C1	0.7765(5)	0.5771(6)	0.4031(5)	0.078(3)
C2	0.7630(5)	0.6168(6)	0.4513(5)	0.081(3)
C3	0.7957(6)	0.6179(7)	0.4990(5)	0.090(3)
C4	0.8416(6)	0.5822(8)	0.5015(6)	0.099(4)
C5	0.8543(5)	0.5442(7)	0.4540(6)	0.094(4)
C6	0.8239(5)	0.5406(7)	0.4040(5)	0.087(3)
C7	0.8352(5)	0.5004(7)	0.3522(6)	0.089(3)
C8	0.8785(6)	0.4614(9)	0.3388(8)	0.110(4)
C9	0.8850(7)	0.4304(8)	0.2873(8)	0.113(5)
C10	0.8457(6)	0.4357(7)	0.2461(7)	0.101(4)
C11	0.8034(5)	0.4725(6)	0.2583(5)	0.084(3)
C12	0.8535(13)	0.4031(16)	0.1870(11)	0.147(4)
F3	0.8065(7)	0.3872(12)	0.1651(8)	0.152(5)
F4	0.8756(8)	0.4415(9)	0.1487(8)	0.146(4)
F5	0.8764(8)	0.3442(9)	0.1903(8)	0.159(5)
C12A	0.8456(16)	0.4037(18)	0.1843(12)	0.148(5)
F3A	0.8214(14)	0.4425(16)	0.1435(14)	0.146(5)
F4A	0.8918(11)	0.394(2)	0.1636(15)	0.157(6)
F5A	0.8185(15)	0.3476(15)	0.1793(14)	0.151(6)
C13	0.7646(4)	0.6469(6)	0.2925(5)	0.074(3)
C14	0.8104(5)	0.6503(7)	0.2582(5)	0.085(3)
C15	0.8248(6)	0.7114(9)	0.2340(6)	0.100(4)
C16	0.7973(6)	0.7702(7)	0.2429(6)	0.096(4)

C17	0.7535(7)	0.7668(8)	0.2768(7)	0.103(4)
C18	0.7348(5)	0.7056(6)	0.3010(5)	0.077(3)
C19	0.6872(5)	0.6978(6)	0.3337(5)	0.080(3)
C20	0.6518(6)	0.7474(8)	0.3473(6)	0.100(4)
C21	0.6074(6)	0.7322(9)	0.3768(6)	0.107(4)
C22	0.5978(5)	0.6658(9)	0.3944(6)	0.099(4)
C23	0.6345(5)	0.6168(8)	0.3797(5)	0.089(3)
C24	0.5509(6)	0.6474(10)	0.4261(7)	0.111(5)
C25	0.6989(5)	0.4521(6)	0.4162(5)	0.082(3)
C26	0.6729(5)	0.3935(6)	0.4345(5)	0.082(3)
C27	0.6410(5)	0.3590(6)	0.3959(5)	0.080(3)
C28	0.6375(5)	0.3840(6)	0.3390(5)	0.079(3)
C29	0.6639(5)	0.4420(6)	0.3234(5)	0.075(3)
C30	0.6103(5)	0.2957(6)	0.4146(5)	0.085(3)
C31	0.6298(7)	0.2666(9)	0.4724(7)	0.126(6)
C32	0.6181(7)	0.2388(7)	0.3707(6)	0.114(5)
C33	0.5547(6)	0.3180(8)	0.4235(8)	0.121(5)
C34	0.6621(4)	0.4724(6)	0.2634(5)	0.076(3)
C35	0.6359(4)	0.4436(6)	0.2167(5)	0.076(3)
C36	0.6342(4)	0.4760(6)	0.1614(4)	0.075(3)
C37	0.6577(4)	0.5392(7)	0.1576(5)	0.079(3)
C38	0.6862(5)	0.5624(6)	0.2053(5)	0.078(3)
C39	0.6071(5)	0.4387(6)	0.1096(5)	0.080(3)
C40	0.5853(5)	0.3690(6)	0.1278(5)	0.088(3)
C41	0.5607(5)	0.4794(7)	0.0859(5)	0.093(4)
C42	0.6499(5)	0.4241(8)	0.0630(5)	0.093(4)

C43	0.6507(5)	0.5874(7)	0.1071(5)	0.085(3)
C44	0.6049(5)	0.6386(7)	0.1195(6)	0.099(4)
C45	0.6311(6)	0.6978(8)	0.1509(7)	0.112(4)
C46	0.6856(6)	0.7048(7)	0.1228(6)	0.099(4)
C47	0.7379(5)	0.6151(6)	0.0719(5)	0.075(3)
C48	0.8230(6)	0.6546(7)	0.0395(6)	0.098(4)
C49	0.8550(6)	0.6006(8)	0.0716(7)	0.112(4)
C50	0.8152(6)	0.6371(7)	0.9756(6)	0.101(4)
C51	0.8481(6)	0.7252(7)	0.0460(7)	0.111(4)
F1	0.7820(4)	0.6548(4)	0.5459(3)	0.112(2)
F2	0.8989(3)	0.5076(5)	0.4572(4)	0.119(3)
F6	0.8684(3)	0.7140(4)	0.2011(3)	0.112(2)
F7	0.7279(3)	0.8248(4)	0.2864(4)	0.116(3)
F8	0.5479(3)	0.6751(5)	0.4789(4)	0.126(3)
F9	0.5455(4)	0.5802(7)	0.4367(5)	0.146(4)
F10	0.5080(4)	0.6651(8)	0.3982(4)	0.188(6)
N1	0.7969(4)	0.5027(5)	0.3099(4)	0.083(3)
N2	0.6782(4)	0.6321(5)	0.3511(4)	0.083(3)
N3	0.6958(4)	0.4748(5)	0.3621(4)	0.081(2)
N4	0.6893(4)	0.5302(5)	0.2573(4)	0.079(2)
N5	0.6949(4)	0.6352(5)	0.1012(4)	0.082(2)
O1	0.7721(3)	0.6658(4)	0.0685(4)	0.091(2)
O2	0.7432(4)	0.5581(5)	0.0519(4)	0.088(2)
O3	0.535625	0.367126	0.269691	0.175(8)
O4	0.464362	0.367126	0.230309	0.175(8)
C52	0.500000	0.331349	0.250000	0.153(6)

C53	0.500000	0.260762	0.250000	0.165(8)
O6	0.5564(10)	0.5926(11)	0.2721(10)	0.153(7)
O7	0.5525(10)	0.4982(12)	0.3099(11)	0.160(8)
C54	0.5321(13)	0.5382(13)	0.2747(17)	0.156(8)
C55	0.4939(16)	0.5172(16)	0.2351(19)	0.155(9)

Table S8 Bond lengths (Å) for **2**.

Bond	Length (Å)	Bond	Length (Å)
Ir1-C13	2.017(11)	Ir1-C1	2.020(10)
Ir1-N2	2.046(10)	Ir1-N1	2.052(10)
Ir1-N4	2.112(9)	Ir1-N3	2.134(9)
C1-C2	1.393(16)	C1-C6	1.417(18)
C2-C3	1.376(17)	C3-F1	1.341(15)
C3-C4	1.38(2)	C4-C5	1.36(2)
C5-F2	1.357(16)	C5-C6	1.384(17)
C6-C7	1.453(18)	C7-N1	1.380(16)
C7-C8	1.39(2)	C8-C9	1.33(2)
C9-C10	1.39(2)	C10-C11	1.337(18)
C10-C12	1.51(3)	C10-C12A	1.54(3)
C11-N1	1.329(14)	C12-F4	1.29(3)
C12-F5	1.30(3)	C12-F3	1.35(3)
C12A-F4A	1.29(3)	C12A-F5A	1.31(3)
C12A-F3A	1.36(3)	C13-C18	1.402(17)
C13-C14	1.416(16)	C14-C15	1.375(18)
C15-F6	1.350(15)	C15-C16	1.38(2)
C16-C17	1.37(2)	C17-F7	1.339(18)
C17-C18	1.412(19)	C18-C19	1.443(17)
C19-C20	1.371(18)	C19-N2	1.376(15)
C20-C21	1.36(2)	C21-C22	1.39(2)
C22-C23	1.392(19)	C22-C24	1.45(2)
C23-N2	1.335(15)	C24-F10	1.322(17)
C24-F8	1.322(17)	C24-F9	1.35(2)

C25-N3	1.313(14)	C25-C26	1.399(16)
C26-C27	1.382(16)	C27-C28	1.391(15)
C27-C30	1.538(16)	C28-C29	1.377(16)
C29-N3	1.367(14)	C29-C34	1.494(15)
C30-C33	1.511(19)	C30-C32	1.519(17)
C30-C31	1.523(18)	C34-N4	1.347(14)
C34-C35	1.382(15)	C35-C36	1.414(15)
C36-C37	1.388(17)	C36-C39	1.557(15)
C37-C38	1.390(16)	C37-C43	1.504(16)
C38-N4	1.347(14)	C39-C41	1.539(16)
C39-C40	1.542(16)	C39-C42	1.558(17)
C43-N5	1.484(15)	C43-C44	1.579(18)
C44-C45	1.53(2)	C45-C46	1.55(2)
C46-N5	1.477(16)	C47-O2	1.219(13)
C47-O1	1.336(14)	C47-N5	1.354(15)
C48-O1	1.485(16)	C48-C50	1.510(18)
C48-C49	1.53(2)	C48-C51	1.543(19)
O3-C52	1.241359(15)	O4-C52	1.241619(15)
C52-C53	1.39201(2)	O6-C54	1.244(10)
O7-C54	1.242(10)	C54-C55	1.397(10)

Table S9 Bond angles (°) for **2**.

Atoms	Angle (°)	Atoms	Angle (°)
C13-Ir1-C1	91.4(4)	C13-Ir1-N2	80.0(5)
C1-Ir1-N2	95.0(5)	C13-Ir1-N1	94.5(4)
C1-Ir1-N1	80.7(5)	N2-Ir1-N1	173.0(4)
C13-Ir1-N4	97.9(4)	C1-Ir1-N4	170.0(4)
N2-Ir1-N4	90.3(4)	N1-Ir1-N4	94.9(4)
C13-Ir1-N3	174.0(4)	C1-Ir1-N3	94.3(4)
N2-Ir1-N3	97.6(4)	N1-Ir1-N3	88.3(4)
N4-Ir1-N3	76.6(3)	C2-C1-C6	119.3(10)
C2-C1-Ir1	126.7(10)	C6-C1-Ir1	113.9(9)
C3-C2-C1	118.5(12)	F1-C3-C2	118.5(13)
F1-C3-C4	118.1(12)	C2-C3-C4	123.5(13)
C5-C4-C3	117.2(12)	C4-C5-F2	117.1(12)
C4-C5-C6	123.2(14)	F2-C5-C6	119.7(14)
C5-C6-C1	118.3(13)	C5-C6-C7	125.8(13)
C1-C6-C7	115.9(11)	N1-C7-C8	116.1(13)
N1-C7-C6	114.0(11)	C8-C7-C6	129.8(13)
C9-C8-C7	123.1(15)	C8-C9-C10	118.1(15)
C11-C10-C9	119.6(14)	C11-C10-C12	121.8(19)
C9-C10-C12	118.4(18)	C11-C10-C12A	114.(2)
C9-C10-C12A	126.(2)	N1-C11-C10	122.0(13)
F4-C12-F5	111.(2)	F4-C12-F3	106.(3)
F5-C12-F3	103.(3)	F4-C12-C10	114.(2)
F5-C12-C10	113.(2)	F3-C12-C10	108.(2)
F4A-C12A-F5A	109.(3)	F4A-C12A-F3A	105.(3)

F5A-C12A-F3A	100.(3)	F4A-C12A-C10	113.(3)
F5A-C12A-C10	115.(3)	F3A-C12A-C10	113.(3)
C18-C13-C14	119.5(10)	C18-C13-Ir1	114.1(8)
C14-C13-Ir1	126.4(9)	C15-C14-C13	119.3(13)
F6-C15-C16	118.5(14)	F6-C15-C14	118.8(14)
C16-C15-C14	122.6(13)	C17-C16-C15	117.8(13)
F7-C17-C16	117.1(14)	F7-C17-C18	120.0(14)
C16-C17-C18	122.9(15)	C13-C18-C17	117.7(12)
C13-C18-C19	116.7(10)	C17-C18-C19	125.5(13)
C20-C19-N2	119.6(12)	C20-C19-C18	127.4(12)
N2-C19-C18	113.0(10)	C21-C20-C19	121.0(15)
C20-C21-C22	119.9(15)	C21-C22-C23	117.6(13)
C21-C22-C24	121.7(16)	C23-C22-C24	120.7(16)
N2-C23-C22	122.3(14)	F10-C24-F8	106.2(14)
F10-C24-F9	104.9(15)	F8-C24-F9	103.7(14)
F10-C24-C22	113.0(15)	F8-C24-C22	113.5(13)
F9-C24-C22	114.7(15)	N3-C25-C26	122.2(11)
C27-C26-C25	120.1(10)	C26-C27-C28	117.2(11)
C26-C27-C30	122.0(10)	C28-C27-C30	120.9(11)
C29-C28-C27	120.2(11)	N3-C29-C28	121.6(10)
N3-C29-C34	114.8(10)	C28-C29-C34	123.6(10)
C33-C30-C32	115.4(13)	C33-C30-C31	107.9(12)
C32-C30-C31	104.4(12)	C33-C30-C27	106.8(11)
C32-C30-C27	110.4(10)	C31-C30-C27	112.0(11)
N4-C34-C35	121.5(10)	N4-C34-C29	114.7(9)
C35-C34-C29	123.8(11)	C34-C35-C36	121.0(11)

C37-C36-C35	116.7(10)	C37-C36-C39	124.9(10)
C35-C36-C39	118.4(11)	C36-C37-C38	118.4(11)
C36-C37-C43	124.3(10)	C38-C37-C43	117.1(11)
N4-C38-C37	124.4(11)	C41-C39-C40	106.1(10)
C41-C39-C36	111.6(10)	C40-C39-C36	112.4(9)
C41-C39-C42	113.9(10)	C40-C39-C42	106.0(10)
C36-C39-C42	106.8(9)	N5-C43-C37	112.2(9)
N5-C43-C44	100.5(10)	C37-C43-C44	111.0(10)
C45-C44-C43	104.0(11)	C44-C45-C46	106.1(12)
N5-C46-C45	101.7(11)	O2-C47-O1	126.5(12)
O2-C47-N5	123.2(11)	O1-C47-N5	110.4(10)
O1-C48-C50	110.3(11)	O1-C48-C49	111.4(11)
C50-C48-C49	111.9(12)	O1-C48-C51	101.1(11)
C50-C48-C51	110.8(12)	C49-C48-C51	110.8(12)
C11-N1-C7	120.8(12)	C11-N1-Ir1	123.5(9)
C7-N1-Ir1	115.4(8)	C23-N2-C19	119.6(11)
C23-N2-Ir1	124.2(10)	C19-N2-Ir1	116.2(8)
C25-N3-C29	118.7(10)	C25-N3-Ir1	125.2(8)
C29-N3-Ir1	116.1(7)	C38-N4-C34	117.3(10)
C38-N4-Ir1	125.1(8)	C34-N4-Ir1	117.6(7)
C47-N5-C46	124.7(11)	C47-N5-C43	119.1(10)
C46-N5-C43	115.8(10)	C47-O1-C48	119.7(10)
O3-C52-O4	110.736(2)	O3-C52-C53	124.6360(10)
O4-C52-C53	124.6280(10)	O7-C54-O6	111.3(15)
O7-C54-C55	121.9(16)	O6-C54-C55	125.4(16)

Table S10 Anisotropic displacement parameters (\AA^2) for **2**.

Atom	U ₁₁	U ₂₂	U ₃₃	U ₂₃	U ₁₃	U ₁₂
Ir1	0.0880(4)	0.0738(3)	0.0576(3)	0.00147(18)	-0.00200(19)	-0.0061(2)
C1	0.102(8)	0.084(7)	0.047(5)	0.001(5)	-0.015(5)	-0.020(6)
C2	0.106(9)	0.074(7)	0.064(6)	0.001(5)	-0.005(6)	-0.006(6)
C3	0.111(10)	0.091(8)	0.069(7)	0.008(6)	-0.008(7)	-0.025(8)
C4	0.116(11)	0.106(10)	0.076(8)	0.011(7)	-0.032(7)	-0.030(8)
C5	0.094(9)	0.095(9)	0.092(9)	0.016(7)	-0.020(7)	-0.017(7)
C6	0.094(8)	0.089(8)	0.077(7)	0.013(6)	-0.008(6)	-0.010(7)
C7	0.082(7)	0.101(9)	0.083(7)	0.003(7)	-0.005(6)	-0.012(7)
C8	0.093(9)	0.118(11)	0.120(12)	0.006(10)	-0.002(8)	0.009(9)
C9	0.109(11)	0.120(12)	0.110(12)	-0.010(9)	0.013(10)	0.010(9)
C10	0.114(11)	0.094(9)	0.095(10)	-0.013(7)	0.027(9)	-0.003(8)
C11	0.096(8)	0.081(7)	0.076(7)	-0.005(6)	0.009(6)	-0.008(6)
C12	0.160(7)	0.144(7)	0.135(7)	-0.014(6)	0.014(6)	0.009(6)
F3	0.171(8)	0.164(9)	0.121(8)	-0.033(8)	0.006(7)	0.006(8)
F4	0.179(9)	0.140(8)	0.118(7)	-0.014(7)	0.032(7)	0.008(7)
F5	0.187(9)	0.142(8)	0.149(8)	-0.026(7)	0.013(8)	0.027(8)
C12A	0.162(7)	0.146(7)	0.136(7)	-0.014(6)	0.013(6)	0.008(6)
F3A	0.175(10)	0.142(9)	0.121(9)	-0.020(8)	0.013(9)	0.014(9)
F4A	0.170(9)	0.159(10)	0.141(10)	-0.017(9)	0.027(9)	0.013(8)
F5A	0.176(10)	0.145(9)	0.130(9)	-0.017(9)	0.011(9)	0.006(9)
C13	0.092(8)	0.071(7)	0.058(6)	0.018(5)	-0.013(5)	-0.008(6)
C14	0.099(8)	0.092(8)	0.065(6)	0.002(6)	0.001(6)	-0.011(7)
C15	0.102(9)	0.122(12)	0.075(8)	-0.013(8)	0.003(7)	-0.027(9)
C16	0.123(11)	0.087(9)	0.077(8)	0.010(7)	-0.013(8)	-0.027(8)

C17	0.119(10)	0.100(11)	0.089(9)	0.000(8)	-0.021(8)	-0.002(9)
C18	0.094(8)	0.071(7)	0.065(6)	0.006(5)	-0.013(5)	-0.010(6)
C19	0.095(8)	0.076(7)	0.070(7)	0.001(6)	-0.009(6)	0.005(6)
C20	0.109(10)	0.094(9)	0.096(9)	-0.008(7)	-0.005(8)	0.008(8)
C21	0.108(11)	0.117(12)	0.095(9)	-0.021(9)	-0.018(8)	0.014(9)
C22	0.073(7)	0.136(13)	0.086(8)	-0.020(8)	-0.010(6)	-0.001(8)
C23	0.086(8)	0.112(10)	0.069(7)	0.000(7)	-0.011(6)	-0.015(7)
C24	0.081(9)	0.150(15)	0.102(11)	-0.015(10)	-0.016(8)	0.000(9)
C25	0.097(8)	0.087(8)	0.061(6)	0.003(5)	-0.007(6)	-0.013(6)
C26	0.100(8)	0.080(7)	0.066(6)	0.003(5)	-0.004(6)	0.003(6)
C27	0.097(8)	0.083(7)	0.060(6)	-0.001(5)	0.019(6)	-0.002(6)
C28	0.094(8)	0.072(7)	0.070(6)	-0.013(5)	0.006(5)	-0.007(6)
C29	0.083(7)	0.076(7)	0.066(6)	-0.005(5)	0.008(5)	-0.004(5)
C30	0.102(8)	0.082(7)	0.070(7)	-0.004(6)	0.011(6)	-0.005(6)
C31	0.153(14)	0.117(12)	0.108(11)	0.034(9)	-0.021(10)	-0.028(11)
C32	0.146(13)	0.095(10)	0.100(10)	-0.010(8)	0.030(9)	-0.026(9)
C33	0.103(10)	0.101(10)	0.157(15)	0.021(10)	0.024(10)	-0.010(9)
C34	0.080(7)	0.088(8)	0.061(6)	-0.004(5)	0.000(5)	-0.005(6)
C35	0.079(7)	0.085(8)	0.064(6)	0.000(5)	0.000(5)	0.001(5)
C36	0.076(6)	0.093(8)	0.057(6)	-0.004(5)	-0.001(5)	-0.001(6)
C37	0.076(7)	0.097(8)	0.063(6)	0.000(6)	0.002(5)	0.002(6)
C38	0.092(8)	0.078(7)	0.063(6)	0.000(5)	0.003(6)	-0.001(6)
C39	0.078(7)	0.106(9)	0.057(6)	0.000(5)	-0.008(5)	-0.001(6)
C40	0.102(8)	0.095(8)	0.066(6)	-0.003(6)	-0.005(6)	-0.026(7)
C41	0.086(8)	0.113(10)	0.079(7)	0.003(7)	-0.008(6)	0.003(7)
C42	0.087(8)	0.134(11)	0.059(6)	-0.010(6)	0.003(6)	-0.011(7)

C43	0.083(7)	0.100(8)	0.072(7)	0.006(6)	-0.009(6)	-0.005(7)
C44	0.102(9)	0.110(10)	0.086(8)	0.008(7)	-0.003(7)	0.002(8)
C45	0.119(11)	0.117(12)	0.100(10)	-0.002(9)	0.008(8)	0.021(9)
C46	0.129(11)	0.096(9)	0.071(7)	0.008(7)	-0.006(7)	0.011(8)
C47	0.106(9)	0.064(7)	0.056(6)	-0.003(5)	-0.007(6)	-0.002(6)
C48	0.108(10)	0.097(9)	0.090(8)	0.003(7)	0.004(7)	-0.011(8)
C49	0.113(10)	0.117(12)	0.107(10)	-0.012(9)	0.003(8)	-0.011(9)
C50	0.118(10)	0.101(9)	0.083(8)	-0.003(7)	0.011(7)	-0.012(8)
C51	0.120(11)	0.100(10)	0.113(11)	-0.004(8)	0.026(9)	-0.020(9)
F1	0.153(7)	0.112(6)	0.070(4)	-0.010(4)	-0.016(4)	-0.012(5)
F2	0.106(5)	0.139(7)	0.113(6)	0.016(5)	-0.024(5)	0.003(5)
F6	0.126(6)	0.118(6)	0.091(5)	0.013(4)	0.011(5)	-0.031(5)
F7	0.145(7)	0.077(5)	0.124(7)	0.011(4)	-0.006(5)	0.007(5)
F8	0.117(6)	0.175(8)	0.085(5)	-0.013(5)	0.009(4)	0.011(6)
F9	0.118(7)	0.193(11)	0.128(8)	-0.037(7)	0.033(6)	-0.043(7)
F10	0.090(6)	0.357(19)	0.117(7)	0.024(9)	-0.015(5)	0.002(8)
N1	0.110(7)	0.063(5)	0.078(6)	-0.002(4)	0.010(5)	-0.005(5)
N2	0.088(6)	0.100(7)	0.062(5)	0.001(5)	-0.009(5)	-0.001(5)
N3	0.098(6)	0.090(7)	0.055(5)	-0.002(4)	0.001(4)	-0.016(5)
N4	0.098(7)	0.083(6)	0.057(5)	0.001(4)	-0.004(4)	-0.008(5)
N5	0.093(6)	0.085(6)	0.067(5)	0.001(5)	0.000(5)	-0.004(5)
O1	0.108(6)	0.079(5)	0.086(6)	-0.005(4)	0.004(4)	-0.008(5)
O2	0.096(6)	0.098(7)	0.070(5)	0.004(4)	0.003(4)	0.004(4)
O3	0.186(12)	0.193(14)	0.146(14)	-0.002(13)	0.020(11)	-0.042(12)
O4	0.183(12)	0.193(14)	0.147(14)	0.002(13)	0.023(11)	0.043(12)
C52	0.153(9)	0.164(9)	0.143(9)	0.000(9)	0.009(8)	0.000(9)

C53	0.154(13)	0.180(11)	0.161(14)	0.000(15)	-0.004(12)	0.000(13)
O6	0.170(13)	0.156(12)	0.133(12)	-0.027(10)	-0.004(11)	0.001(11)
O7	0.158(13)	0.176(13)	0.148(12)	-0.002(11)	0.017(10)	0.019(12)
C54	0.157(11)	0.162(11)	0.150(10)	-0.005(8)	0.006(8)	0.003(8)
C55	0.147(14)	0.172(15)	0.148(16)	-0.012(13)	0.015(11)	-0.005(13)

Table S11 Hydrogen atomic coordinates and isotropic atomic displacement parameters (\AA^2) for **2**.

H-Atom	x/a	y/b	z/c	U(eq)
H2	0.7317	0.6424	0.4513	0.098000
H4	0.8635	0.5842	0.5350	0.119000
H8	0.9048	0.4566	0.3678	0.132000
H9	0.9157	0.4054	0.2792	0.136000
H11	0.7773	0.4772	0.2292	0.101000
H14	0.8308	0.6109	0.2519	0.102000
H16	0.8083	0.8119	0.2261	0.115000
H20	0.6585	0.7929	0.3361	0.120000
H21	0.5830	0.7669	0.3854	0.128000
H23	0.6283	0.5710	0.3904	0.107000
H25	0.7196	0.4762	0.4437	0.098000
H26	0.6771	0.3775	0.4735	0.098000
H28	0.6169	0.3610	0.3108	0.095000
H31A	0.6130	0.2229	0.4798	0.189000
H31B	0.6216	0.2980	0.5044	0.189000
H31C	0.6675	0.2602	0.4703	0.189000
H32A	0.6554	0.2311	0.3649	0.171000
H32B	0.6021	0.2512	0.3332	0.171000
H32C	0.6020	0.1972	0.3856	0.171000
H33A	0.5342	0.2799	0.4386	0.181000
H33B	0.5401	0.3329	0.3859	0.181000
H33C	0.5536	0.3555	0.4516	0.181000
H35	0.6188	0.4013	0.2218	0.091000
H38	0.7047	0.6038	0.2010	0.093000

H40A	0.5673	0.3484	0.0943	0.131000
H40B	0.5610	0.3747	0.1604	0.131000
H40C	0.6139	0.3394	0.1400	0.131000
H41A	0.5445	0.4545	0.0535	0.139000
H41B	0.5728	0.5236	0.0716	0.139000
H41C	0.5353	0.4862	0.1173	0.139000
H42A	0.6761	0.3937	0.0797	0.140000
H42B	0.6664	0.4668	0.0513	0.140000
H42C	0.6341	0.4027	0.0285	0.140000
H43	0.6447	0.5622	0.0696	0.102000
H44A	0.5885	0.6538	0.0825	0.119000
H44B	0.5781	0.6176	0.1448	0.119000
H45A	0.6341	0.6884	0.1934	0.134000
H45B	0.6109	0.7400	0.1454	0.134000
H46A	0.6855	0.7380	0.0903	0.119000
H46B	0.7119	0.7183	0.1523	0.119000
H49A	0.8349	0.5586	0.0744	0.168000
H49B	0.8636	0.6168	0.1111	0.168000
H49C	0.8872	0.5920	0.0498	0.168000
H50A	0.8019	0.5907	-0.0277	0.151000
H50B	0.8484	0.6406	-0.0452	0.151000
H50C	0.7902	0.6687	-0.0419	0.151000
H51A	0.8832	0.7244	0.0293	0.167000
H51B	0.8500	0.7372	0.0877	0.167000
H51C	0.8270	0.7589	0.0252	0.167000
H53A	0.4678	0.2442	0.2322	0.248000

H53B	0.5298	0.2442	0.2274	0.248000
H53C	0.5025	0.2442	0.2904	0.248000
H55A	0.4827	0.5559	0.2113	0.233000
H55B	0.5080	0.4819	0.2095	0.233000
H55C	0.4641	0.4991	0.2568	0.233000

Table S12 Crystallographic data collection details for **1**.

Axis	dx (mm)	2θ (°)	ω (°)	φ (°)	χ (°)	Width (°)	Frames	λ (Å)	Voltage (kV)	Current (mA)
Omega	45.038	0.00	0.00	0.00	54.74	1.00	180	0.71073	50	1.4
Phi	45.038	15.56	-85.59	-187.00	24.00	1.00	158	0.71073	50	1.4
Omega	45.038	15.61	-56.78	-113.58	57.67	1.00	82	0.71073	50	1.4

Table S13 Sample and crystal data for **1**.

Chemical Formula	$C_{47.25}H_{43.50}F_{2.50}IrN_4O_4$	
Formula Weight	1202.18 g/mol	
Temperature (K)	100(2)	
Wavelength (Å)	0.71073 Å	
Crystal Size (mm)	0.005 x 0.010 x 0.100	
Crystal Habit	Orange needle	
Crystal System	Orthorhombic	
Space Group	P c c n	
Unit Cell Dimensions	a = 17.9150(8) Å	$\alpha = 90^\circ$
	b = 22.4618(9) Å	$\beta = 90^\circ$
	c = 25.0531(8) Å	$\gamma = 90^\circ$
Volume (Å³)	10081.4(7)	
Z	8	
Density (calculated) (g/cm³)	1.584	
Absorption Coefficient (mm⁻¹)	2.864	
F(000)	4772	

Table S14 Data collection and structure refinement for **1**.

Theta range for data collection	2.18 to 27.00°	
Index ranges	-22<=h<=22, -28<=k<=28, -32<=l<=31	
Reflections collected	141121	
Independent reflections	10989 [R(int) = 0.1430]	
Coverage of independent reflections	99.9%	
Absorption correction	Multi-Scan	
Max. and min. transmission	0.9860 and 0.7630	
Structure solution technique	Direct methods	
Structure solution program	XT, VERSION 2018/2	
Refinement method	Full-matrix least-squares on F2	
Refinement program	SHELXL-2018/3 (Sheldrick, 2018)	
Function minimized	$\Sigma w(F_o^2 - F_c^2)^2$	
Data / restraints / parameters	10989 / 584 / 795	
Goodness-of-fit on F²	1.066	
Δ/σ_{\max}	0.002	
Final R indices	7185 data; I>2 σ (I)	R1 = 0.0477, wR2 = 0.1185
	All data	R1 = 0.0918, wR2 = 0.1493
Weighting scheme	$w=1/[\sigma^2(F_o^2)+(0.0587P)^2+58.9019P]$ where $P=(F_o^2+2F_c^2)/3$	
Largest diff. peak and hole	1.828 and -0.894 eÅ ⁻³	
R.M.S. deviation from mean	0.159 eÅ ⁻³	

Table S15 Atomic coordinates and equivalent isotropic atomic displacement parameters (\AA^2) for 1.

	x/a	y/b	z/c	U(eq)
C1	0.5486(4)	0.4667(3)	0.2850(3)	0.0313(16)
C2	0.5519(4)	0.4063(3)	0.2922(3)	0.0360(17)
C3	0.6015(4)	0.3813(4)	0.3293(3)	0.0371(18)
C4	0.6491(4)	0.4214(3)	0.3560(3)	0.0349(17)
C5	0.6447(4)	0.4822(3)	0.3464(3)	0.0288(15)
C6	0.6929(4)	0.5274(3)	0.3719(3)	0.0288(15)
C7	0.7533(4)	0.5137(4)	0.4052(3)	0.0345(17)
C8	0.7979(4)	0.5584(4)	0.4259(3)	0.0383(19)
C9	0.7788(4)	0.6166(4)	0.4133(3)	0.0410(19)
C10	0.7186(4)	0.6277(4)	0.3801(3)	0.0345(17)
C11	0.8640(4)	0.5436(4)	0.4617(3)	0.042(2)
C12	0.9080(5)	0.5997(5)	0.4779(4)	0.062(3)
C13	0.9161(5)	0.5031(6)	0.4316(4)	0.068(3)
C14	0.8372(5)	0.5132(5)	0.5122(3)	0.058(3)
C15	0.598(2)	0.3145(5)	0.3373(13)	0.047(3)
C16	0.558(3)	0.3079(18)	0.3915(14)	0.050(4)
C17	0.555(2)	0.280(2)	0.2939(16)	0.047(4)
C18	0.6778(19)	0.289(2)	0.341(2)	0.048(4)
C15A	0.6023(11)	0.3146(4)	0.3388(8)	0.046(3)
C16A	0.6801(12)	0.2904(13)	0.3229(12)	0.049(4)
C17A	0.5896(17)	0.3038(11)	0.3991(9)	0.053(4)
C18A	0.5415(14)	0.2805(12)	0.3072(10)	0.047(4)
C15B	0.6057(9)	0.3151(5)	0.3407(7)	0.046(3)

C16B	0.6557(12)	0.2963(10)	0.3880(8)	0.051(4)
C17B	0.6363(13)	0.2870(9)	0.2887(8)	0.046(4)
C18B	0.5257(10)	0.2911(10)	0.3494(10)	0.054(4)
C19	0.5068(4)	0.6054(3)	0.2495(3)	0.0308(15)
C20	0.4292(4)	0.6088(3)	0.2583(3)	0.0351(18)
C21	0.3831(4)	0.6152(3)	0.2148(4)	0.0403(19)
C22	0.4075(5)	0.6186(4)	0.1627(3)	0.043(2)
C23	0.4827(5)	0.6152(4)	0.1557(3)	0.0402(19)
C24	0.5337(4)	0.6086(3)	0.1969(3)	0.0320(16)
C25	0.6138(4)	0.6010(3)	0.1913(3)	0.0342(16)
C26	0.6548(5)	0.6005(4)	0.1434(3)	0.049(2)
C27	0.7303(5)	0.5886(4)	0.1434(3)	0.049(2)
C28	0.7648(4)	0.5772(3)	0.1916(3)	0.0361(17)
C29	0.7239(4)	0.5801(3)	0.2383(3)	0.0281(15)
C30	0.8467(4)	0.5629(4)	0.1934(3)	0.0410(19)
C31	0.5863(4)	0.6883(3)	0.3081(3)	0.0287(14)
C32	0.6337(4)	0.7265(3)	0.2808(3)	0.0368(18)
C33	0.6284(5)	0.7862(4)	0.2900(3)	0.045(2)
C34	0.5775(5)	0.8124(4)	0.3233(4)	0.046(2)
C35	0.5304(5)	0.7738(4)	0.3503(3)	0.046(2)
C36	0.5344(4)	0.7126(3)	0.3446(3)	0.0370(18)
C37	0.4923(4)	0.6682(3)	0.3758(3)	0.0341(17)
C38	0.4346(5)	0.6801(4)	0.4129(3)	0.048(2)
C39	0.4047(5)	0.6342(4)	0.4420(4)	0.053(2)
C40	0.4307(5)	0.5775(4)	0.4340(3)	0.048(2)
C41	0.4846(4)	0.5667(4)	0.3963(3)	0.0372(18)

C42	0.3983(6)	0.5261(5)	0.4650(4)	0.066(3)
C43	0.1170(5)	0.6699(6)	0.5044(4)	0.080(4)
C44	0.1954(5)	0.6565(4)	0.5225(3)	0.047(2)
O1	0.2478(4)	0.6761(4)	0.4921(2)	0.070(2)
O2	0.2098(4)	0.6293(3)	0.5638(2)	0.0623(19)
C45	0.2267(11)	0.7541(14)	0.3213(5)	0.065(6)
C46	0.247(3)	0.752(2)	0.3792(4)	0.055(4)
O3	0.199(2)	0.7200(17)	0.4022(10)	0.040(4)
O4	0.289(2)	0.789(2)	0.4043(12)	0.064(8)
C49	0.1622(9)	0.5809(9)	0.3634(5)	0.064(3)
Cl1	0.0720(6)	0.5525(8)	0.3555(7)	0.054(2)
Cl2	0.2095(3)	0.5801(2)	0.30222(18)	0.0666(15)
C49A	0.1588(9)	0.6063(9)	0.3383(10)	0.061(4)
Cl1A	0.0831(8)	0.5611(12)	0.3559(12)	0.073(4)
Cl2A	0.2411(3)	0.5770(3)	0.3655(3)	0.070(2)
C50	0.7216(9)	0.7487(17)	0.1083(8)	0.054(6)
Cl3	0.6301(5)	0.7499(4)	0.1314(4)	0.064(3)
Cl4	0.7831(5)	0.7346(3)	0.1604(3)	0.052(2)
C47	0.6003(8)	0.8450(8)	0.0033(7)	0.052(4)
C48	0.6728(8)	0.8124(7)	0.0029(6)	0.049(3)
O5	0.7166(6)	0.8475(5)	0.0274(4)	0.048(3)
O6	0.6888(6)	0.7659(4)	0.9735(4)	0.045(3)
F1	0.3079(3)	0.6172(2)	0.2234(2)	0.0592(14)
F2	0.5070(3)	0.6190(3)	0.10412(19)	0.0621(15)
F3	0.8722(3)	0.5541(2)	0.24249(19)	0.0498(12)
F4	0.8876(3)	0.6064(3)	0.1720(2)	0.0638(15)

F5	0.8633(3)	0.5137(3)	0.1655(2)	0.0677(16)
F6	0.6760(3)	0.8242(2)	0.2650(2)	0.0607(14)
F7	0.4801(3)	0.7984(2)	0.3853(2)	0.0630(15)
F8	0.4343(4)	0.4759(3)	0.4575(3)	0.096(2)
F9	0.3986(4)	0.5374(3)	0.5175(3)	0.098(2)
F10	0.3275(4)	0.5159(3)	0.4517(3)	0.094(2)
Ir1	0.58699(2)	0.59857(2)	0.30549(2)	0.02513(9)
N1	0.5921(3)	0.5044(2)	0.3119(2)	0.0262(12)
N2	0.6766(3)	0.5845(3)	0.3598(2)	0.0296(13)
N3	0.6506(3)	0.5926(3)	0.2381(2)	0.0273(12)
N4	0.5144(3)	0.6114(3)	0.3673(2)	0.0280(13)

U(eq) is defined as one third of the trace of the orthogonalized U_{ij} tensor.

Table S16 Bond lengths (Å) for **1**. Refer to Fig S4†.

Bond	Length (Å)	Bond	Length (Å)
C1-N1	1.333(9)	C1-C2	1.370(10)
C2-C3	1.403(11)	C3-C4	1.408(11)
C3-C15	1.515(13)	C3-C15B	1.516(12)
C3-C15A	1.517(12)	C4-C5	1.389(10)
C5-N1	1.374(9)	C5-C6	1.478(10)
C6-N2	1.350(9)	C6-C7	1.401(10)
C7-C8	1.384(11)	C8-C9	1.387(12)
C8-C11	1.524(10)	C9-C10	1.384(10)
C10-N2	1.329(9)	C11-C13	1.505(12)
C11-C14	1.515(11)	C11-C12	1.541(12)
C15-C18	1.545(10)	C15-C16	1.545(10)
C15-C17	1.547(10)	C15A-C17A	1.546(10)
C15A-C16A	1.547(10)	C15A-C18A	1.549(10)
C15B-C16B	1.546(10)	C15B-C18B	1.546(10)
C15B-C17B	1.547(10)	C19-C24	1.404(10)
C19-C20	1.410(10)	C19-Ir1	2.014(7)
C20-C21	1.374(11)	C21-F1	1.365(9)
C21-C22	1.379(12)	C22-C23	1.361(11)
C23-F2	1.365(9)	C23-C24	1.387(10)
C24-C25	1.452(11)	C25-N3	1.358(9)
C25-C26	1.406(11)	C26-C27	1.380(12)
C27-C28	1.379(11)	C28-C29	1.382(10)
C28-C30	1.502(11)	C29-N3	1.342(9)
C30-F3	1.328(9)	C30-F4	1.333(10)

C30-F5	1.340(9)	C31-C32	1.388(10)
C31-C36	1.414(10)	C31-Ir1	2.016(7)
C32-C33	1.365(11)	C33-F6	1.359(9)
C33-C34	1.369(13)	C34-C35	1.386(12)
C35-F7	1.374(10)	C35-C36	1.384(11)
C36-C37	1.475(11)	C37-N4	1.353(9)
C37-C38	1.415(11)	C38-C39	1.371(13)
C39-C40	1.371(13)	C40-C41	1.373(11)
C40-C42	1.506(13)	C41-N4	1.350(9)
C42-F8	1.313(12)	C42-F10	1.332(12)
C42-F9	1.340(12)	C43-C44	1.506(12)
C44-O2	1.229(9)	C44-O1	1.287(9)
C45-C46	1.498(15)	C46-O3	1.266(14)
C46-O4	1.288(14)	C49-C11	1.749(14)
C49-C12	1.751(13)	C49A-C11A	1.750(15)
C49A-C12A	1.752(14)	C50-C14	1.738(14)
C50-C13	1.739(15)	C47-C48	1.491(15)
C48-O5	1.270(14)	C48-O6	1.310(14)
Ir1-N4	2.041(6)	Ir1-N3	2.043(6)
Ir1-N1	2.123(6)	Ir1-N2	2.129(5)

Table S17 Bond angles (°) for **1**. Refer to Fig S4†.

Atoms	Angle (°)	Atoms	Angle (°)
N1-C1-C2	122.5(7)	C1-C2-C3	120.7(7)
C2-C3-C4	116.3(7)	C2-C3-C15	117.2(15)
C4-C3-C15	126.5(15)	C2-C3-C15B	123.2(9)
C4-C3-C15B	120.5(9)	C2-C3-C15A	120.3(10)
C4-C3-C15A	123.4(10)	C5-C4-C3	120.8(7)
N1-C5-C4	120.3(7)	N1-C5-C6	115.0(6)
C4-C5-C6	124.6(7)	N2-C6-C7	120.6(7)
N2-C6-C5	115.5(6)	C7-C6-C5	123.9(7)
C8-C7-C6	120.6(7)	C7-C8-C9	117.2(7)
C7-C8-C11	120.6(8)	C9-C8-C11	122.1(7)
C10-C9-C8	119.8(7)	N2-C10-C9	122.7(8)
C13-C11-C14	110.1(8)	C13-C11-C8	108.6(7)
C14-C11-C8	110.2(7)	C13-C11-C12	107.9(8)
C14-C11-C12	108.1(7)	C8-C11-C12	111.9(7)
C3-C15-C18	110.(3)	C3-C15-C16	103.(2)
C18-C15-C16	110.3(16)	C3-C15-C17	115.(3)
C18-C15-C17	108.3(15)	C16-C15-C17	109.5(16)
C3-C15A-C17A	107.9(15)	C3-C15A-C16A	108.4(16)
C17A-C15A-C16A	109.1(13)	C3-C15A-C18A	113.7(16)
C17A-C15A-C18A	108.5(13)	C16A-C15A-C18A	109.1(13)
C3-C15B-C16B	116.2(13)	C3-C15B-C18B	108.9(12)
C16B-C15B-C18B	109.5(13)	C3-C15B-C17B	105.1(11)
C16B-C15B-C17B	109.1(13)	C18B-C15B-C17B	107.8(13)
C24-C19-C20	118.9(7)	C24-C19-Ir1	114.4(5)

C20-C19-Ir1	126.7(6)	C21-C20-C19	118.3(8)
F1-C21-C20	118.2(8)	F1-C21-C22	117.4(7)
C20-C21-C22	124.4(8)	C23-C22-C21	115.7(7)
C22-C23-F2	115.7(7)	C22-C23-C24	124.2(8)
F2-C23-C24	120.1(7)	C23-C24-C19	118.5(7)
C23-C24-C25	126.2(7)	C19-C24-C25	115.1(6)
N3-C25-C26	118.7(7)	N3-C25-C24	114.4(6)
C26-C25-C24	126.9(7)	C27-C26-C25	120.9(8)
C28-C27-C26	118.4(7)	C27-C28-C29	119.6(7)
C27-C28-C30	120.2(7)	C29-C28-C30	120.2(7)
N3-C29-C28	121.7(7)	F3-C30-F4	107.0(7)
F3-C30-F5	106.4(7)	F4-C30-F5	105.8(7)
F3-C30-C28	113.3(6)	F4-C30-C28	111.7(7)
F5-C30-C28	112.2(7)	C32-C31-C36	118.8(7)
C32-C31-Ir1	126.8(6)	C36-C31-Ir1	114.3(5)
C33-C32-C31	118.8(8)	F6-C33-C32	119.7(8)
F6-C33-C34	115.4(7)	C32-C33-C34	124.9(8)
C33-C34-C35	115.7(8)	F7-C35-C36	120.0(8)
F7-C35-C34	117.3(7)	C36-C35-C34	122.7(8)
C35-C36-C31	119.0(8)	C35-C36-C37	126.2(7)
C31-C36-C37	114.8(6)	N4-C37-C38	119.8(7)
N4-C37-C36	113.7(6)	C38-C37-C36	126.5(7)
C39-C38-C37	119.4(8)	C40-C39-C38	119.3(8)
C39-C40-C41	120.2(8)	C39-C40-C42	120.3(8)
C41-C40-C42	119.4(9)	N4-C41-C40	121.2(8)
F8-C42-F10	106.5(10)	F8-C42-F9	107.5(10)

F10-C42-F9	106.4(8)	F8-C42-C40	113.2(8)
F10-C42-C40	111.7(10)	F9-C42-C40	111.1(9)
O2-C44-O1	121.0(8)	O2-C44-C43	123.3(8)
O1-C44-C43	115.7(7)	O3-C46-O4	123.1(11)
O3-C46-C45	106.7(16)	O4-C46-C45	127.(2)
C11-C49-C12	110.2(10)	C11A-C49A-C12A	109.7(11)
C14-C50-C13	110.5(11)	O5-C48-O6	129.1(13)
O5-C48-C47	103.3(13)	O6-C48-C47	125.9(13)
C19-Ir1-C31	86.7(3)	C19-Ir1-N4	93.6(3)
C31-Ir1-N4	80.2(3)	C19-Ir1-N3	80.0(3)
C31-Ir1-N3	95.5(3)	N4-Ir1-N3	172.6(2)
C19-Ir1-N1	99.1(2)	C31-Ir1-N1	173.5(2)
N4-Ir1-N1	96.4(2)	N3-Ir1-N1	88.5(2)
C19-Ir1-N2	174.2(3)	C31-Ir1-N2	97.6(2)
N4-Ir1-N2	90.9(2)	N3-Ir1-N2	95.6(2)
N1-Ir1-N2	76.8(2)	C1-N1-C5	119.2(6)
C1-N1-Ir1	124.8(5)	C5-N1-Ir1	116.0(5)
C10-N2-C6	119.1(6)	C10-N2-Ir1	124.3(5)
C6-N2-Ir1	116.6(5)	C29-N3-C25	120.5(6)
C29-N3-Ir1	123.8(5)	C25-N3-Ir1	115.7(5)
C41-N4-C37	120.0(6)	C41-N4-Ir1	123.7(5)
C37-N4-Ir1	116.1(5)		

Table S18 Anisotropic displacement parameters (\AA^2) for **1**. Refer to Fig S4†.

Atom	U ₁₁	U ₂₂	U ₃₃	U ₂₃	U ₁₃	U ₁₂
C1	0.027(4)	0.025(4)	0.042(4)	-0.003(3)	-0.007(3)	0.003(3)
C2	0.029(4)	0.030(4)	0.048(4)	-0.004(3)	0.000(3)	-0.002(3)
C3	0.033(4)	0.036(4)	0.042(4)	0.007(3)	0.008(3)	0.010(3)
C4	0.027(4)	0.041(4)	0.037(4)	0.007(3)	0.003(3)	0.006(3)
C5	0.019(3)	0.033(4)	0.034(4)	0.004(3)	0.003(3)	0.003(3)
C6	0.024(4)	0.035(4)	0.027(3)	-0.001(3)	0.002(3)	-0.003(3)
C7	0.027(4)	0.047(4)	0.029(4)	0.011(3)	-0.001(3)	0.007(3)
C8	0.026(4)	0.062(6)	0.027(4)	0.000(3)	0.001(3)	-0.005(4)
C9	0.031(4)	0.054(5)	0.038(4)	-0.008(4)	-0.004(3)	-0.010(4)
C10	0.029(4)	0.037(4)	0.037(4)	-0.005(3)	-0.001(3)	-0.007(3)
C11	0.026(4)	0.071(6)	0.030(4)	0.001(4)	-0.010(3)	-0.002(4)
C12	0.041(5)	0.098(8)	0.047(5)	0.017(5)	-0.022(4)	-0.021(6)
C13	0.040(5)	0.120(10)	0.045(5)	-0.010(5)	-0.006(4)	0.029(6)
C14	0.051(6)	0.087(8)	0.038(5)	0.014(5)	-0.011(4)	0.006(5)
C15	0.043(6)	0.028(5)	0.069(6)	0.008(5)	0.001(5)	0.002(5)
C16	0.046(9)	0.034(8)	0.070(8)	0.017(8)	0.002(8)	0.003(8)
C17	0.048(8)	0.022(8)	0.072(9)	0.006(8)	0.001(8)	0.000(8)
C18	0.047(8)	0.027(8)	0.070(9)	0.008(9)	0.000(7)	0.005(7)
C15A	0.041(5)	0.027(5)	0.068(6)	0.007(5)	0.001(5)	0.002(4)
C16A	0.050(7)	0.026(7)	0.071(9)	0.008(8)	0.002(7)	0.007(6)
C17A	0.046(8)	0.039(7)	0.074(7)	0.017(7)	0.000(7)	-0.001(8)
C18A	0.048(7)	0.019(6)	0.076(8)	0.002(7)	0.004(7)	-0.003(6)
C15B	0.041(5)	0.027(5)	0.068(6)	0.006(5)	0.001(5)	0.003(5)
C16B	0.049(7)	0.031(7)	0.071(7)	0.012(7)	0.001(7)	0.005(7)

C17B	0.045(7)	0.020(6)	0.074(7)	0.005(6)	0.001(6)	0.008(6)
C18B	0.050(7)	0.032(7)	0.079(8)	0.014(7)	0.004(7)	-0.002(7)
C19	0.032(4)	0.025(4)	0.036(4)	-0.003(3)	-0.008(3)	0.002(3)
C20	0.026(4)	0.037(4)	0.042(4)	-0.009(3)	-0.007(3)	0.004(3)
C21	0.023(4)	0.033(4)	0.065(5)	-0.010(4)	-0.012(4)	0.004(3)
C22	0.048(5)	0.039(4)	0.042(5)	-0.008(4)	-0.014(4)	0.008(4)
C23	0.034(5)	0.045(5)	0.041(4)	-0.003(4)	-0.012(3)	-0.001(4)
C24	0.032(4)	0.029(4)	0.035(4)	-0.004(3)	-0.007(3)	0.002(3)
C25	0.034(4)	0.033(4)	0.036(4)	-0.003(3)	-0.006(3)	0.000(3)
C26	0.044(5)	0.074(6)	0.030(4)	-0.011(4)	-0.006(3)	0.007(5)
C27	0.042(5)	0.072(6)	0.035(4)	-0.013(4)	0.008(4)	0.004(4)
C28	0.029(4)	0.037(4)	0.042(4)	-0.009(3)	0.001(3)	0.003(3)
C29	0.025(4)	0.025(3)	0.034(4)	-0.004(3)	0.001(3)	0.002(3)
C30	0.030(4)	0.047(5)	0.046(5)	-0.009(4)	0.006(4)	0.007(4)
C31	0.026(3)	0.024(3)	0.036(4)	-0.002(3)	-0.008(3)	-0.001(3)
C32	0.033(4)	0.026(4)	0.051(5)	0.006(3)	0.001(4)	0.000(3)
C33	0.048(5)	0.033(4)	0.055(5)	0.009(4)	-0.009(4)	-0.003(4)
C34	0.044(5)	0.026(4)	0.069(6)	-0.002(4)	-0.018(4)	0.002(4)
C35	0.048(5)	0.039(5)	0.053(5)	-0.012(4)	-0.007(4)	0.005(4)
C36	0.037(4)	0.032(4)	0.042(4)	-0.013(3)	-0.007(3)	0.010(3)
C37	0.031(4)	0.032(4)	0.040(4)	-0.006(3)	-0.004(3)	0.001(3)
C38	0.039(5)	0.052(5)	0.054(5)	-0.011(4)	0.009(4)	-0.002(4)
C39	0.035(5)	0.069(6)	0.054(5)	-0.010(5)	0.018(4)	-0.001(4)
C40	0.039(5)	0.059(6)	0.045(5)	-0.006(4)	0.009(4)	-0.009(4)
C41	0.022(4)	0.041(5)	0.048(5)	-0.003(4)	-0.003(3)	-0.006(3)
C42	0.057(7)	0.076(8)	0.066(7)	-0.005(6)	0.030(5)	-0.016(6)

C43	0.055(6)	0.123(10)	0.063(7)	0.050(7)	0.015(5)	0.010(7)
C44	0.046(5)	0.052(5)	0.043(5)	0.009(4)	0.013(4)	0.015(4)
O1	0.047(4)	0.115(6)	0.049(4)	0.032(4)	0.012(3)	0.015(4)
O2	0.054(4)	0.086(5)	0.047(4)	0.033(3)	0.010(3)	0.020(4)
C45	0.091(16)	0.062(10)	0.041(7)	-0.003(9)	-0.001(8)	-0.042(15)
C46	0.075(10)	0.054(9)	0.036(6)	-0.013(11)	0.006(11)	-0.008(7)
O3	0.035(8)	0.049(9)	0.035(8)	0.001(7)	-0.009(6)	0.007(5)
O4	0.064(16)	0.077(17)	0.050(10)	-0.011(10)	0.005(10)	-0.022(12)
C49	0.062(7)	0.061(7)	0.068(7)	0.001(6)	-0.005(7)	-0.007(6)
C11	0.048(4)	0.056(4)	0.059(4)	-0.012(3)	0.003(3)	-0.006(3)
C12	0.068(3)	0.067(3)	0.066(3)	0.009(2)	0.014(2)	0.008(2)
C49A	0.060(7)	0.058(8)	0.064(8)	0.006(7)	-0.009(7)	-0.003(7)
C11A	0.062(6)	0.076(9)	0.080(6)	0.003(6)	-0.017(6)	-0.001(5)
C12A	0.051(3)	0.066(4)	0.093(4)	0.013(3)	-0.004(3)	0.003(3)
C50	0.078(13)	0.027(10)	0.056(12)	0.021(11)	0.012(11)	0.016(12)
C13	0.081(6)	0.052(5)	0.058(5)	0.026(4)	0.030(5)	0.038(5)
C14	0.085(6)	0.024(4)	0.046(4)	0.003(3)	-0.007(4)	0.005(4)
C47	0.053(7)	0.059(7)	0.043(7)	0.010(6)	0.009(6)	0.024(6)
C48	0.051(5)	0.049(5)	0.046(5)	0.009(4)	-0.002(4)	-0.004(4)
O5	0.064(6)	0.055(6)	0.027(5)	0.005(4)	-0.003(4)	-0.022(5)
O6	0.054(6)	0.022(4)	0.059(5)	0.023(4)	-0.024(5)	-0.003(4)
F1	0.027(3)	0.073(4)	0.078(4)	-0.008(3)	-0.016(2)	0.011(2)
F2	0.057(3)	0.090(4)	0.039(3)	0.004(3)	-0.015(2)	0.001(3)
F3	0.031(3)	0.068(3)	0.051(3)	-0.007(2)	0.001(2)	0.010(2)
F4	0.027(3)	0.085(4)	0.080(4)	0.018(3)	0.007(3)	-0.009(3)
F5	0.043(3)	0.078(4)	0.082(4)	-0.040(3)	0.003(3)	0.019(3)

F6	0.053(3)	0.036(3)	0.094(4)	0.017(3)	0.001(3)	-0.009(2)
F7	0.069(4)	0.042(3)	0.078(4)	-0.018(3)	0.015(3)	0.011(3)
F8	0.102(5)	0.061(4)	0.124(6)	0.023(4)	0.064(5)	-0.005(4)
F9	0.113(6)	0.116(6)	0.066(4)	0.007(4)	0.039(4)	-0.030(5)
F10	0.054(4)	0.111(6)	0.118(5)	0.003(4)	0.023(4)	-0.044(4)
Ir1	0.01967(14)	0.02529(14)	0.03042(15)	- 0.00219(11)	- 0.00216(11)	0.00025(11)
N1	0.021(3)	0.025(3)	0.032(3)	0.000(2)	0.002(2)	0.000(2)
N2	0.020(3)	0.037(4)	0.032(3)	-0.001(3)	-0.007(2)	0.000(2)
N3	0.023(3)	0.030(3)	0.029(3)	-0.001(2)	-0.002(2)	0.001(3)
N4	0.019(3)	0.031(3)	0.034(3)	-0.002(2)	-0.001(2)	-0.001(2)

The anisotropic atomic displacement factor exponent takes the form: $-2\pi^2 [h^2 a^{*2} U_{11} + \dots + 2 h k a^* b^* U_{12}]$

Table S19 Hydrogen atomic coordinates and isotropic atomic displacement parameters (\AA^2) for **1**.

Refer to Fig S4†.

H-Atom	x/a	y/b	z/c	U(eq)
H1	0.5140	0.4823	0.2599	0.038
H2	0.5202	0.3810	0.2719	0.043
H4	0.6846	0.4066	0.3809	0.042
H7	0.7637	0.4733	0.4137	0.041
H9	0.8071	0.6488	0.4273	0.049
H10	0.7068	0.6678	0.3716	0.041
H12A	0.8756	0.6261	0.4987	0.093
H12B	0.9250	0.6205	0.4457	0.093
H12C	0.9512	0.5881	0.4995	0.093
H13A	0.9603	0.4951	0.4535	0.102
H13B	0.9313	0.5224	0.3982	0.102
H13C	0.8906	0.4656	0.4235	0.102
H14A	0.8083	0.4777	0.5028	0.088
H14B	0.8057	0.5407	0.5325	0.088
H14C	0.8803	0.5016	0.5339	0.088
H16A	0.5910	0.3208	0.4203	0.075
H16B	0.5441	0.2661	0.3970	0.075
H16C	0.5125	0.3325	0.3916	0.075
H17A	0.5717	0.2925	0.2585	0.071
H17B	0.5012	0.2878	0.2975	0.071
H17C	0.5639	0.2370	0.2983	0.071
H18A	0.6751	0.2454	0.3451	0.072
H18B	0.7038	0.3062	0.3715	0.072

H18C	0.7051	0.2983	0.3080	0.072
H16D	0.6811	0.2471	0.3279	0.073
H16E	0.7184	0.3089	0.3454	0.073
H16F	0.6900	0.2998	0.2854	0.073
H17D	0.5443	0.3246	0.4105	0.08
H17E	0.6325	0.3190	0.4192	0.08
H17F	0.5841	0.2610	0.4057	0.08
H18D	0.4921	0.2920	0.3204	0.071
H18E	0.5486	0.2376	0.3120	0.071
H18F	0.5455	0.2904	0.2692	0.071
H16G	0.7058	0.3131	0.3833	0.076
H16H	0.6590	0.2528	0.3893	0.076
H16I	0.6342	0.3111	0.4214	0.076
H17G	0.6832	0.3065	0.2789	0.07
H17H	0.5998	0.2922	0.2599	0.07
H17I	0.6453	0.2444	0.2945	0.07
H18G	0.5046	0.3088	0.3819	0.08
H18H	0.5273	0.2477	0.3532	0.08
H18I	0.4945	0.3017	0.3187	0.08
H20	0.4093	0.6068	0.2934	0.042
H22	0.3740	0.6230	0.1336	0.052
H26	0.6301	0.6084	0.1106	0.059
H27	0.7579	0.5882	0.1111	0.059
H29	0.7482	0.5731	0.2714	0.034
H32	0.6691	0.7114	0.2560	0.044
H34	0.5746	0.8544	0.3277	0.056

H38	0.4167	0.7196	0.4176	0.058
H39	0.3664	0.6416	0.4674	0.063
H41	0.5014	0.5271	0.3906	0.045
H43A	0.0815	0.6567	0.5318	0.12
H43B	0.1069	0.6488	0.4709	0.12
H43C	0.1115	0.7129	0.4988	0.12
H1A	0.2294	0.6985	0.4687	0.105
H45A	0.2396	0.7932	0.3066	0.097
H45B	0.1729	0.7474	0.3176	0.097
H45C	0.2540	0.7231	0.3020	0.097
H49A	0.1898	0.5565	0.3897	0.076
H49B	0.1595	0.6222	0.3771	0.076
H49C	0.1507	0.6471	0.3519	0.073
H49D	0.1631	0.6083	0.2990	0.073
H50A	0.7270	0.7174	0.0807	0.064
H50B	0.7339	0.7875	0.0917	0.064
H47A	0.6005	0.8753	-0.0248	0.077
H47B	0.5934	0.8643	0.0381	0.077
H47C	0.5594	0.8169	-0.0030	0.077